DOCUMENTATION OF A TORNADIC SUPERCELL THUNDERSTORM IN THE SAN JOAQUIN VALLEY, CALIFORNIA

A thesis submitted to the faculty of
San Francisco State University
In partial fulfillment of the
Requirements for the Degree

Master of Science

In

Applied Geosciences

by

Theodore B. Schlaepfer

San Francisco, California

June, 2004

CERTIFICATION OF APPROVAL

I certify that I have read Documentation of a Tornadic Supercell Thunderstorm in the San Joaquin Valley, California by Theodore B. Schlaepfer, and that in my opinion this work meets the criteria for approving a thesis submitted in partial fulfillment of the requirements for the degree: Master of Science in Applied Geosciences at San Francisco State University.

John P. Monteverdi
Professor of Meteorology

Oswaldo Garcia
Professor of Meteorology

Erwin Seibel
Professor of Oceanography

DOCUMENTATION OF A TORNADIC SUPERCELL

THUNDERSTORM IN THE SAN JOAQUIN VALLEY, CALIFORNIA

Theodore B. Schlaepfer
San Francisco State University
2004

This study documents a right-moving supercell thunderstorm that occurred on November 22, 1996. A mesocyclone-induced F0 and a subsequent F1 tornado were observed at the Lemoore Naval Air Station in the San Joaquin Valley of California that caused significant wind and hail damage. This study is the first to document a classic, right-moving supercell for which WSR-88D, high-resolution satellite and photographic evidence were available. The development of this tornadic supercell highlighted the significance of topographically induced low-level wind shear in contributing toward the development of F1 and stronger mesocyclone-induced tornadoes in California's Central Valley. The magnitude of the wind shear was within range of observed California tornadic thunderstorms. A modified hodograph of the actual storm environment just prior to the first tornado showed a slight anti-cyclonic veering of the low-level wind shear vector. (KHNX) Doppler radar reflectivity and radial velocity analyses of the supercell showed the presence of a hook, a BWER, and detected embedded low-level and mid-level storm-scale circulations just prior the development of the tornado episodes.

I certify that the Abstract is a correct representation of the content of this thesis.

_____ _____

John P. Monteverdi (Date)
(Chair, Thesis Committee)

ACKNOWLEDGEMENTS

I am indebted to Dr. John P. Monteverdi for his encouragement, dedication, knowledge, and perspectives during the course of this work. I also extend thanks to Dr. Oswaldo Garcia and Erwin Siebel for their unfailing patience. The author also gratefully acknowledges Steven Mendenhall, MIC and Dan Gudgel, WCM, WFO Hanford for their steadfast cooperation in this project. All of the radar plots, photographs of the tornado and parent cumulonimbus, damage track, and official storm reports obtained for this study were provided by Mr. Gudgel. The authors also thank SOO Larry Greiss and all of the Lead Forecasters at WFO Hanford for their encouragement and help in this endeavor. Thanks to Mr. Tom Lee and Kim Richardson at the Marine Meteorology Division of the Naval Research Laboratory (NRL) in Monterey California for graciously supplying high-resolution visible satellite imagery. Thanks to Chi-Fan Shih for the ETA grib data and Jaqueline Lord for help putting that data into PCGRIDDS. Finally, thanks to Jan Null (sounding data) and Bryon Marler (project development).

TABLE OF CONTENTS

LIST OF TABLES

LIST OF FIGURES

LIST OF APPENDICES

Appendix Page

1. Introduction

At 1505 PST 22 November 1996 a tornadic thunderstorm (Fig. 1–1) struck Lemoore Naval Air Station in the San Joaquin Valley of California (see Fig. 1–2 for locations). Two tornadoes were associated with the storm, the first (Fig. 1–3) occurred near the runway complex at Lemoore Naval Air Station at 1427 PST. It caused no structural damage (USDC, 1996) and was rated F0 (see Appendix 1 for the Fujita Scale of tornado damage intensity). The F1 tornado caused substantial destruction to electrical utility lines, building roofs, and fixed structures as it tracked through the administration portion of the base (see Fig. 1–4). In addition, hail up to 2 1/2 inches in diameter caused vehicular damage, yet no fatalities or injuries were associated with the storm.

This storm (hereafter referred to as "the Lemoore storm") may be the best-documented California tornadic storm to date. Since the tornadoes occurred very near the Weather Surveillance Radar-1988 Doppler (WSR-88D) radar at Hanford (KHNX) (see Fig. 1–2), the evolution of the radar structure of the parent storm can be deduced easily. Previous studies of such storms that included analyses of WSR-88D information (Staudenmaier and Cunningham, 1995--Walnut Grove mini-supercell 1995; Kudzlo, 1998--the Lemoore storm 1996), while valuable contributions, were unrefereed and preliminary in nature. They did not attempt a detailed study of satellite, radar, or synoptic-scale surface and

Fig. 1–1. Southeast view of the Lemoore storm at approximately 2230 UTC 22 November 1996. Photo courtesy NWS Hanford.

upper air information. Nor did they attempt to put the buoyancy and shear controls of the respective storms into a context based upon results of current modeling and observational studies. This present study will be the first to document a tornadic thunderstorm in California based upon a careful and detailed analysis of all available information.

Prior to the implementation of the WSR-88D network in the middle 1990s, studies on California supercellular tornadic storms in the refereed literature were

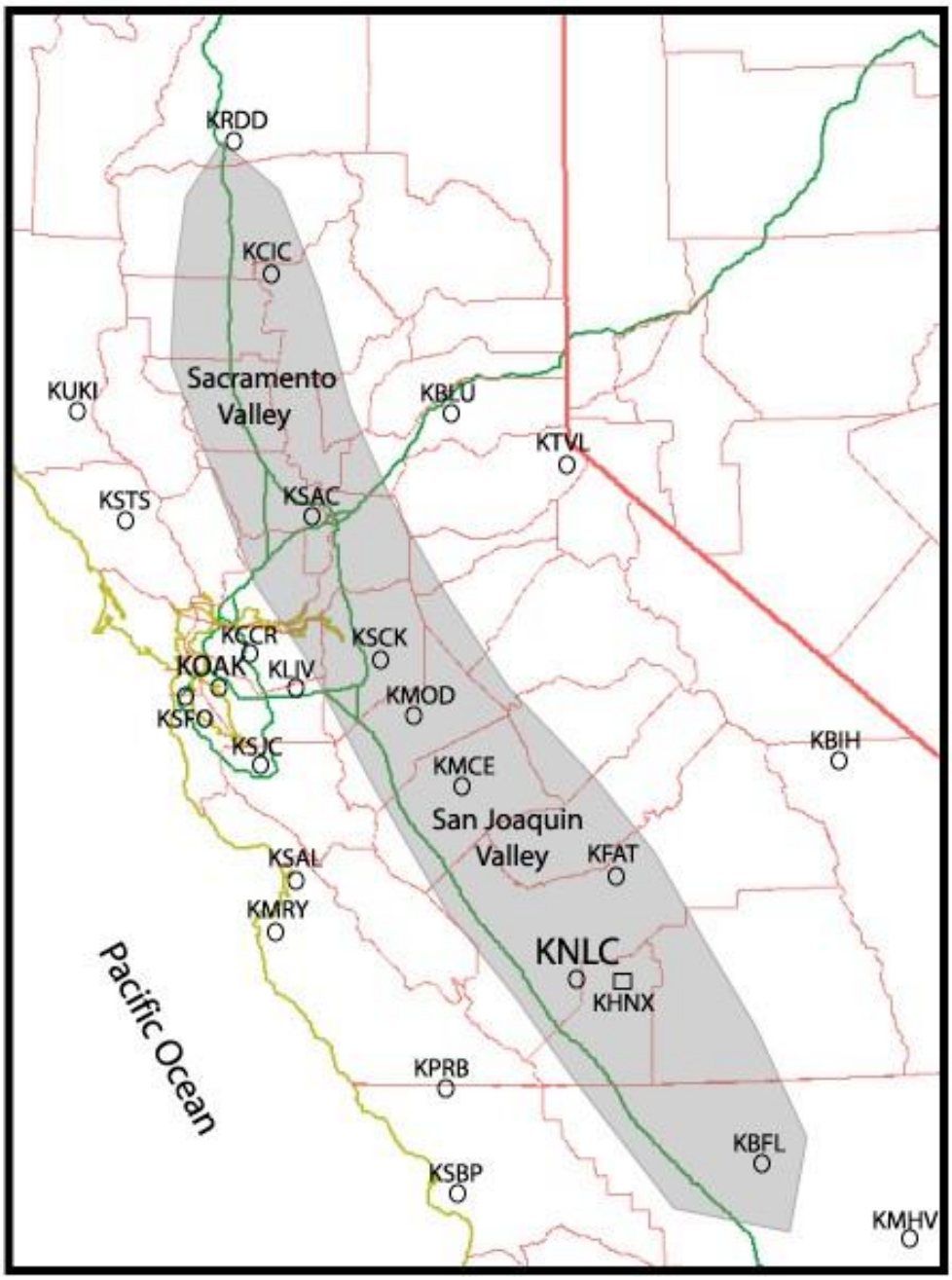

Fig. 1–2. Location map of Central California meteorological stations. Shaded areas correspond to Central Valley locations. The F1 tornado occurred at Lemoore Naval Air Station (KNLC).

largely inferential. Although detailed subsynoptic and synoptic analyses were included (e.g., Braun and Monteverdi, 1991), conclusions about storm type and evolution were made on the bases of thermodynamic and shear considerations and supported by minimal analyses of WSR-57 radar information [with the exception of Monteverdi and Johnson, (1996)].

Through the 1970s and early 1980s, the understanding of California tornadic storms was constrained by what was known about the controls of

Fig. 1–3. Photograph of F0 Lemoore tornado looking toward the southwest taken from the runway complex at Lemoore Naval Air Station at approximately 2230 UTC 22 November 1996. Photo courtesy NWS Hanford.

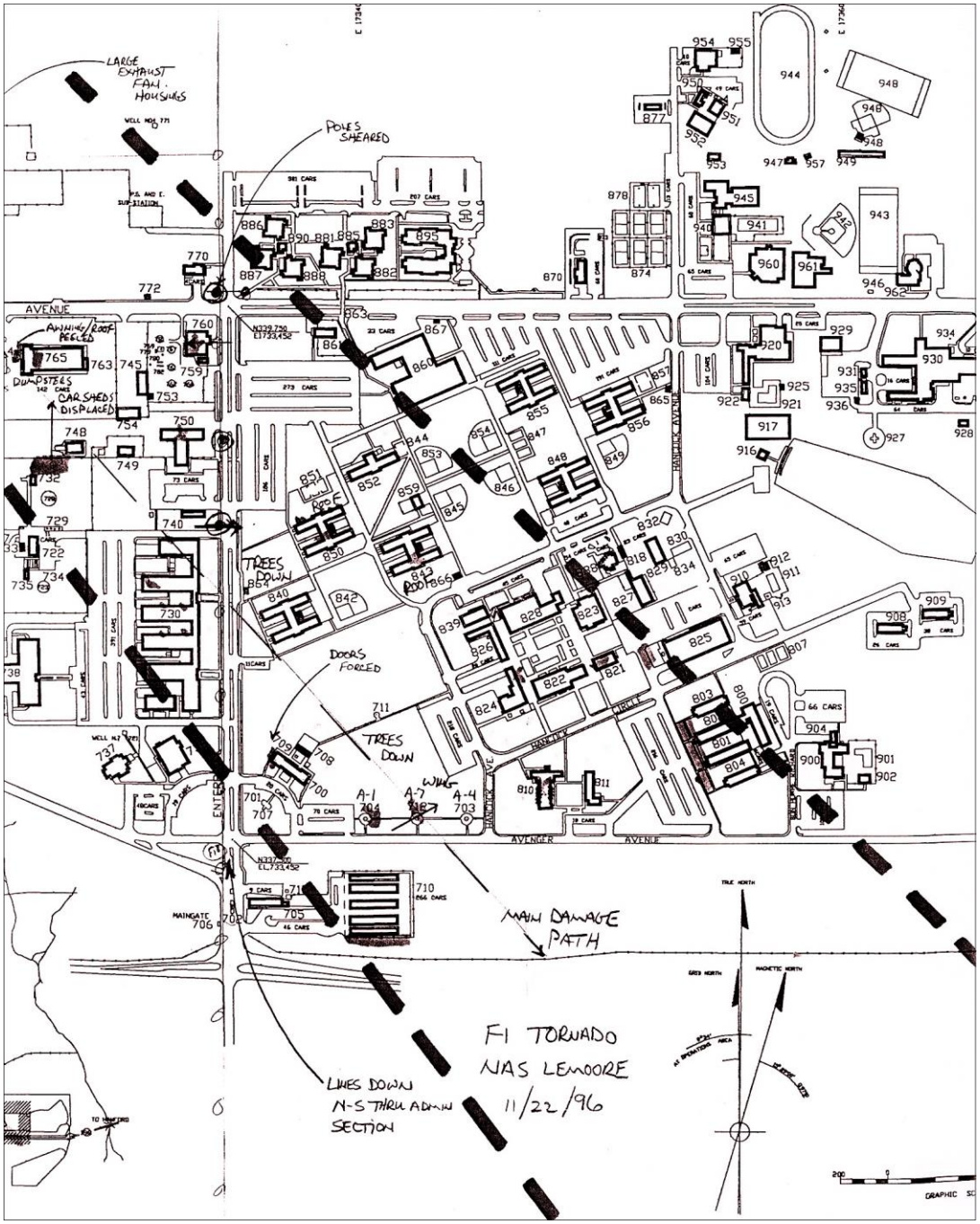

Fig. 1–4. Map of the damage path through the main administration section of Lemoore Naval Air Station of the F1 tornado on November 26 1996. The tornado tracked southeastward with wind damage confined between the bold dashed lines and with the main damage path along the light dashed line.

tornadic storms in general. Most notably, early understanding of such storms was biased by an over-reliance on the impact of buoyancy and very little, if any, understanding of the contribution of shear.

For example, it was known early on that most California severe thunderstorms tended to evolve in the low buoyancy environment within the conditionally unstable maritime air masses behind cold fronts [often referred to as a "Miller Type 3 Profile" (Miller, 1972)]. Later this concept was refined on the basis of operational case studies (e.g., Hales, 1985; Reed and Blier, 1986; Braun and Monteverdi, 1991) in which it was shown that such thunderstorms generally develop in a ‘cold sector’ environment rather than the ‘warm sector’ of wave cyclones that is typical of Midwest tornadic events. Moreover, through the early 1980s, cold sector convection was thought to produce thunderstorms without radar signatures (i.e. hook echoes, weak echo regions, deviant movement, etc.) generally associated with tornadoes found elsewhere and this fact was usually attributed to the low buoyancy associated with such environments (Cooley, 1978). This notion prevailed until a damaging tornado associated with a deep mesocyclone occurred in a cold sector environment between Redding and Chico, California (Braun and Monteverdi, 1991).

The notion that mesocyclones are associated with convective updrafts in northern California synoptic environments was first documented by Carbone (1982, 1983). Using analyses of high-resolution radar reflectivity and radar-

derived velocity fields, these two pioneering studies showed that brief deep rotation along a squall line/cold front was associated with a tornado near Sacramento, CA. Subsequent studies (e.g., Staudenmaier, 1995) showed that similar tornado spin-ups occur along bowed-segments of Central Valley squall lines.

Hales (1985) first suggested that the high incidence of tornadoes in the Los Angeles basin coastal plain is associated with favorable wind fields generated by topographically influenced low level flow. Reed and Blier (1986) documented such effects in the damaging Long Beach tornado of 1982. Blier and Batten (1994) also postulated that deep storm scale rotation often develops in portions of the Los Angeles Basin and southern California coastal valleys due to boundary-layer channeling effects both by the coastal mountains and mountainous offshore islands.

Monteverdi et al. (1988) first examined in detail the synoptic scale environment associated with a Miller Type III sounding that resulted in isolated storms in the Central Valley of California. These storms were associated with funnel cloud and large hail development. In that case, the favorable convective environment lay north of a southward moving cold front and east of the main mid and upper tropospheric trough that lagged off the coast.

Later, a more refined view of the role of topographic effects in generating a shear-environment favorable for tornadic convection emerged. Braun and

Monteverdi (1991) first showed that ahead (east of) the passage of the mid and upper tropospheric trough, lower mid-tropospheric cross-mountain flow against the Coast Range creates a surface lee-side trough in the Central Valley that augments low-level wind shear by increasing surface and low level southerly pressure gradients. The resulting vertical wind profile remarkably resembled that often observed with tornadic supercells in the Great Plains and Midwest.

These results were verified by Monteverdi and Quadros (1994), and Monteverdi and Johnson (1996), in which topographically influenced wind fields in the Central Valley created a veering wind shear and wind shear vector environment favorable for supercell development. The topographic influences not only included the impact of the lee-side trough mentioned above, but a low level jet caused by the "damming" of the lower and mid-tropospheric flow by the Sierra Nevada (Parish, 1982), channeling by local topography (e.g., Sutter Buttes and coastal valleys) (Blier and Batten, 1994) and "gap" effects near the break in the Coast Range marked by the Carquinez Strait (Monteverdi and Quadros, 1994).

The relationship of the position of the mid and upper tropospheric jet to such lower level wind fields suggested to Monteverdi and Johnson (1996) that large low level (e.g., 0-1 km and 0-2 km) shear magnitudes should occur in combination with strong deeper layer shear associated with the jet (0-6 km shear). This would produce very favorable hodographs for tornadic supercells in

such synoptic environments. This notion was corroborated in a much more extensive study of 70 tornadic and non-tornadic thunderstorms during the period 1990-94 (Monteverdi et al., 2000).

Shear-induced pressure forces associated with such hodographs could augment the "low" buoyancy forces to such a degree that rotating updrafts could be of a large enough magnitude to support large hail, deviate motion and storm scale rotation of precipitation to the rear flank (hook echoes) (Monteverdi and Johnson, 1996). This conclusion was consistent with the evolving literature on mini- or low-topped tornadic supercells for low buoyancy environments in other parts of the country (e.g. McCaul, 1990, 1991; Markowski, 2000; and others).

The present study has two purposes. First, the intent is to provide a complete case study of the Lemoore storm, including a detailed analysis of the synoptic, subsynoptic and dynamic controls of the Lemoore storm environment. In addition, evolution of the satellite and radar structure of the Lemoore storm will be examined by analyzing high-resolution visible satellite imagery and Doppler radar information from KHNX respectively.

Second, the controls on the Lemoore storm will be examined in the light of what is now known about the role of buoyancy and shear in the development of tornadic storms in general. The degree to which the buoyancy and shear associated with the Lemoore storm either differs or agrees with that observed with such storms elsewhere will be a key focus of the study. In addition, the

study will show whether the storm fits the characteristic schematic pattern for Central Valley tornadic storms.

The study is organized conventionally into sections. In Section 2, the general dynamic and thermodynamic environment associated with severe weather in the Central Valley of California is discussed. The synoptic scale dynamics, the thermodynamic controls, and wind shear parameters are given in Section 3. High-resolution visible satellite images and surface subsynoptic charts for the afternoon of 22 November 1996 are used to examine the evolution of the controls on the subsynoptic environment are presented in Section 4. Section 5 discusses the radar evolution and structure of the Lemoore Storm using analyses of WSR-88D radar scans. A summary is presented in Section 6 and concluding remarks are given in Section 7.

2. Tornadic Storms in the Central Valley of California

2.1 Overview of California Tornadic Thunderstorms

That tornadoes are a part of the climatology of California has long been recognized in the literature (i.e. Hales, 1985; Blier and Batten, 1994; Monteverdi and Quadros, 1994). Certain regions of the state, however, are at a higher risk for tornadic thunderstorms (Blier and Batten, 1994). For example, on the basis of an analysis of 242 California tornado occurrences from the period 1950–1992, Blier and Batten (1994) identified the Central Valley (comprised of the Sacramento on the north and San Joaquin Valley on the south) and the Los Angeles Basin as regions with unusually high tornado frequencies in comparison to other areas statewide. The tendency for tornadic storms to occur in the Central Valley has been noted in other recent studies—Lipari and Monteverdi (2000) and Monteverdi et al. (2000). In those studies, 70 thunderstorm cases in northern and central California during the period 1990-94 were intensively investigated. Of the 30 tornadic storms (Fig. 2–1) in the data set, 20 occurred in the Central Valley.

The climatology of Central Valley tornado occurrences is both similar and different from those observed in other more tornado-prone areas of the United States, such as the Midwest. For example, tornadic thunderstorm outbreaks in the Central Valley are limited to the seasonal rainfall period— September through

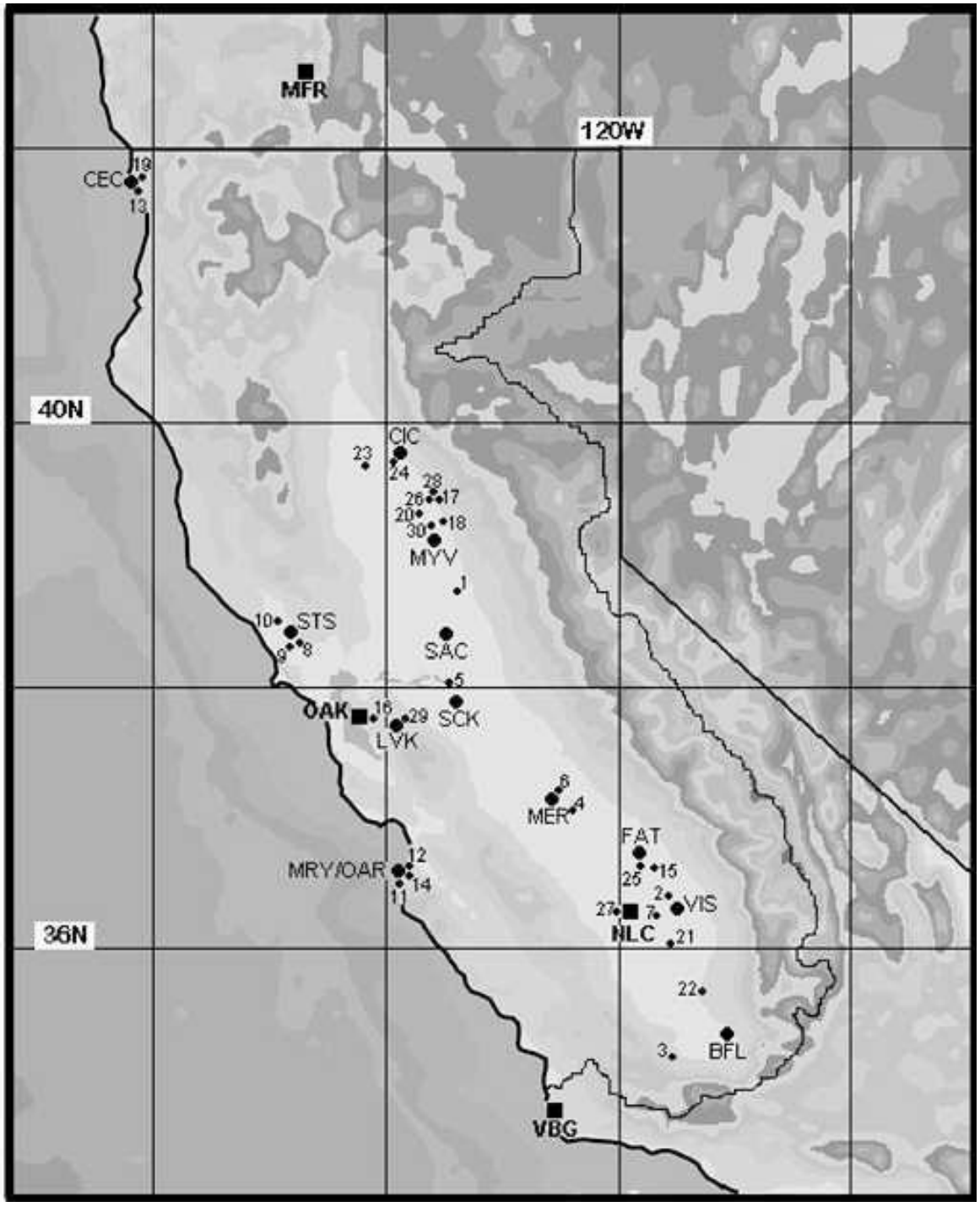

Fig. 2–1. The locations of 30 California tornadoes for the period 1990-94 (from Lipari and Monteverdi, 2000).

the following June (Blier and Batten, 1994). Furthermore, the majority of these Central Valley tornado outbreaks occur in the cool season between December and May. The tendency for Central Valley tornadoes to occur in the cool season is a marked contrast to the seasonal pattern found in the Midwest where the majority of tornadic events occur during the warm season (May and June). Yet the tornado climatology of both regions has a similar aspect as well—tornadogenesis usually occurs in the afternoon hours. Consequently, the increase in surface buoyancy through diurnal heating is often associated with the initiation and the evolution of tornadic thunderstorms in both the Midwest and the Central Valley (Blier and Batten, 1994; Johns and Doswell, 1992).

There are distinct differences between the size and duration of tornadoes in California and those observed in the more tornado-prone Midwest. The average California tornado usually has a smaller mean path width, shorter mean path length, and a life span that is generally not as long as their Midwest cousins (see Table 2–1; from Blier and Batten, 1994). That is consistent with historical

Table 2–1. Mean path length and width of California and Midwest tornadoes. Data from Smith and Mirabella (1972).

Location	Mean Path Length	Mean Path Width
F0 California tornadoes	0.6 mile (~1.0 km)	43 yards (39.3 m)
>F1 California tornadoes	1.9 miles (3.1 km)	91.4 yards (83.6 m)
Midwest Tornadoes	4.0 miles (6.4 km)	170 yards (155.4 m)

records that show that California tornadoes are generally less damaging than tornadoes in the Midwest. Hence, the majority of California tornadoes are rated F0 or F1 for damage; F2 cases are uncommon; F3 intensity events are extremely rare, and no cases have historically been rated higher than F3.

California severe storms can still cause significant damage. A supercell thunderstorm in California's San Joaquin Valley near Fresno on 5 March 1994 caused an estimated $12 million dollars in damage from large hail (Monteverdi and Quadros, 1996). Monteverdi and Quadros (1994) documented several tornadoes that produced substantial destruction in Northern and Central California during December 1992. In addition, minor residential damage and an injury were associated with a pair of tornadoes on 4 May 1998 in the cities of Sunnyvale (F2) and Los Altos (F1) in the San Francisco Bay Area (Monteverdi et al., 2000).

2.2 Synoptic overview of Central Valley Severe Weather

The synoptic and subsynoptic features associated with Central Valley tornado events have been identified in a number of studies (Braun and Monteverdi, 1991; Monteverdi and Quadros, 1994; Monteverdi and Johnson, 1996). The important features associated with the typical or prototype pattern (shown schematically in Fig. 2–2) will be discussed in this section.

California Central Valley severe weather events often occur after a synoptic-scale high-latitude wave cyclone (Weaver, 1962) moves southeastward through California (Fig. 2–2). The wave cyclone is often associated with a mid- and upper-tropospheric short-wave trough progressing through an upper-tropospheric long-wave trough (Fig 2–2, solid-black line) situated along the coastline.

A surface cold front (Fig. 2–2, traditional cold front symbols) is almost always linked with the progressive upper air short-wave trough. Differential cold temperature advection in the lower and middle troposphere is commonly observed as the front passes through Central California (Monteverdi and Quadros, 1994). The cold advection destabilizes middle tropospheric layers that decrease static stabilities and increase the efficiency of quasigeostrophic forcing for upward motions. Thunderstorms that develop in this unstable environment are often referred as “cold sector” thunderstorms.

The onset of moderate to strong cold sector convection in the Central Valley is usually linked with a progressive synoptic-scale mid-tropospheric and surface trough along the West Coast. This trough is usually associated with upward motions and decreased atmospheric stability evidence by an area of enhanced open-cellular cumulus approaching the coast. (Reed and Blier, 1986; Monteverdi et al., 1988).

These migratory short-wave troughs are also often associated with so-called “jet streaks” in the upper-level isotach pattern. In the typical scenario, a jet streak’s (Fig. 2–2; solid black line and shaded region) left-front quadrant (Fig. 2–2; location A) usually moves through Central California during the progression

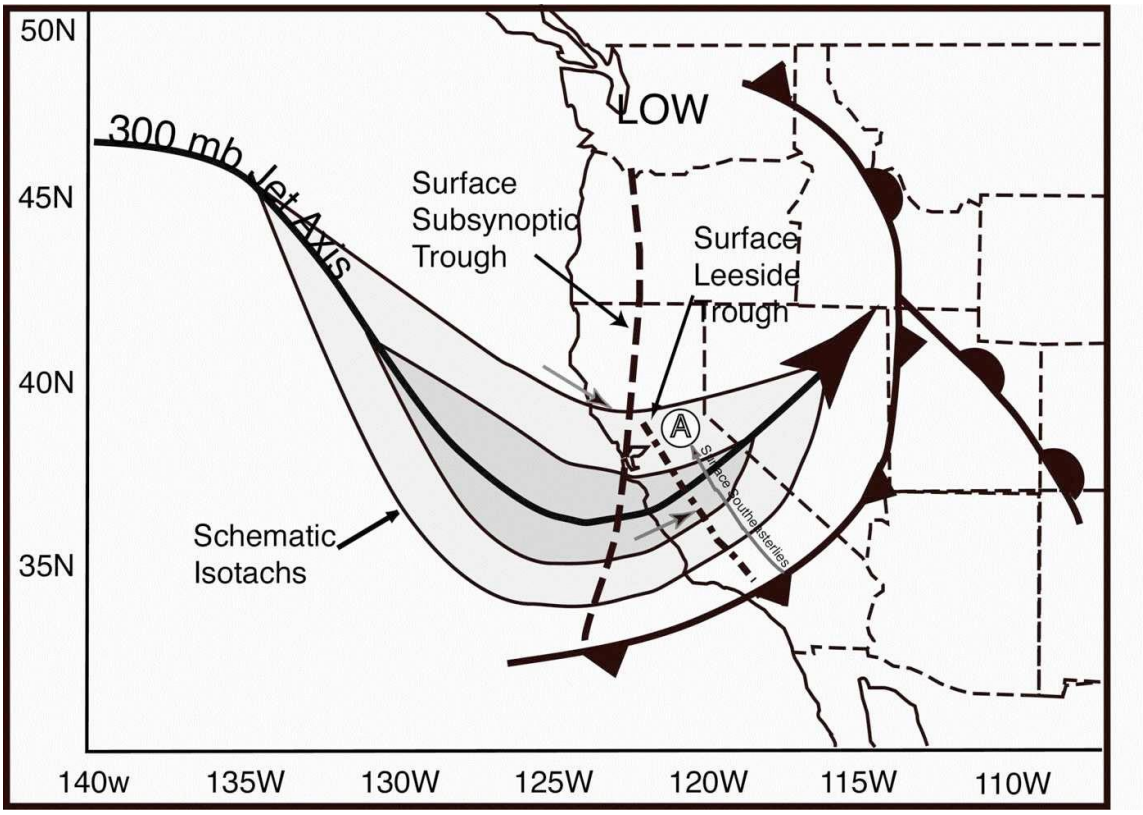

Fig. 2–2. Schematic diagram showing the locations of major upper air and surface features associated with a typical severe weather outbreak in the Central Valley of California. The solid black line is the upper tropospheric jet axis; 70 knot and 90 knot shading shows the location of an upper tropospheric jet streak; bold dashed-line is the location of the progressive surface subsynoptic trough; dashed-dot-line is the location of the surface lee-side trough; light solid arrow shows the location of surface southeasterly winds. Location A is the most favored area for severe weather near the left-front quadrant of the jet streak.

of a short-wave trough. This short-wave trough is also typically linked with mid-tropospheric differential cyclonic vorticity advection (CVA), divergence aloft, and upward vertical velocities in the mid-troposphere (Reed and Blier, 1986; Monteverdi et al., 1988; Braun and Monteverdi, 1991; Monteverdi and Quadros, 1994; Monteverdi and Johnson, 1996).

These middle and upper air features can be loosely thought of as “trigger” mechanisms for the initiation of convection in the post-frontal unstable atmosphere (Monteverdi and Quadros, 1994). This occurs when tropospheric layer-lifting destabilizes the environment, a process that in turn, lowers the level of free convection (LFC) for buoyant air parcels. Convection usually develops along a surface subsynoptic trough (Fig. 2–2, dashed-line) observed near the region of strongest upward vertical motions and surface convergence.

2.3 Overview of Subsynoptic Features

Many observational studies have shown that severe thunderstorms often develop and intensify at the intersections of boundary-layer features (i.e. dry-line, outflow boundaries, etc). In the Central Valley, a boundary-layer feature commonly observed during a severe weather outbreak is a mountain lee-side quasi-stationary mesoscale trough (Fig. 2–2, dashed-dot-line. This convergence

zone often is a focus for the genesis of severe storms, including the parent storm of the 1986 F2 Vina tornado (Braun and Monteverdi, 1991).

The lee-side trough develops when there is significant cross-mountain flow against the Coast Range and Sierra Nevada in the middle and lower third of the troposphere (Braun and Monteverdi, 1991; Monteverdi and Quadros, 1994). The trough is usually linked with synoptically forced progressive upward vertical motion fields associated with short-wave troughs that rotate around the base of a long-wave trough off the California coast (Braun and Monteverdi, 1991; Monteverdi and Quadros, 1994; Monteverdi et al., 2003).

The strongest low-level convergence in the boundary-layer wind field, including moisture convergence, often develops near the axis of the lee-side trough (Braun and Monteverdi, 1991; Monteverdi and Quadros, 1994). In the western portions of the trough, down-slope adiabatic warming east of the Coast Range often results in subsident, westerly boundary-layer flow and a low-level environment having low dewpoint temperatures. But the eastern areas of the lee-side trough are characterized by southeasterly winds (Fig. 2–2, long thin gray arrow) that often advect moisture pooled in the southern portions of the Central Valley northward and locally raise surface dewpoint temperatures in the areas of moisture convergence (Monteverdi and Quadros, 1994). Strong surface moisture convergence leads to boundary-layer destabilization and an increase in surface-based parcel buoyancy.

The lee-side trough also affects boundary-layer wind shear in the Central Valley. Southeast surface winds are related to stronger low-level (0–1-km, 0–2-km) wind shear in areas east of the trough in comparison to weaker shear at the same levels in regions where synoptic-scale southwesterly winds predominate. A wind shear vector of great length with a veer in the 0–2-km layer is often evident on simulated hodographs for tornado cases from stations east of the trough axis, features usually missing on hodographs from stations west of the trough axis and near coastal locations (i.e. KOAK) (Monteverdi and Quadros, 1994). In the study of thirty California tornadoes events between 1990–94, Lipari and Monteverdi (2000) found the sample average mean 0–1-km and 0–2-km positive shear values for the F1/F2 cases were 18.9 X $10^{-3}s^{-1}$ and 10.1 X $10^{-3}s^{-1}$ respectively—the latter in the range of positive shear values associated with strong or violent cold season mesocyclone-induced tornadoes observed elsewhere (Johns et al., 1993).

Another subsynoptic feature in the Central Valley that alters the profile of the wind field in the boundary layer and is also an important detail associated with some severe weather events is a low-level jet stream. Parish (1982) used observational findings and a two-dimensional primitive equation model to show that a 100-km wide low-level mountain-parallel jets is common in the eastern Central Valley during the passage of a middle- and upper-tropospheric trough. This jet is found in a 600 – 1500-m layer AGL and develops in response to a

pressure field created by the damming of synoptically forced, rising stable air against the Sierra Nevada (Parish, 1982). Anecdotal evidence suggests this low-level jet is more commonly observed in the Sacramento Valley and not in the San Joaquin Valley. Southeasterly wind speeds exceeding 50 knots at 1500-m AGL are often observed with this low-level jet stream (Monteverdi et al, 2000).

The combination of southeast surface winds and a southeasterly low-level jet increase the speed shear in the 0–3-km layer. This transforms a Central Valley low-level wind field characterized by strong veering of the wind in the lowest layers, but minimal speed shear [mean tropospheric wind southwesterly (250°) at 13.5 m/s], into an environment that can support rotating storms (Monteverdi et al., 2000). This modification of the wind shear environment (evidenced as a wind shear vector of even longer length in the lowest 3-km on a hodograph) can lead to mesocyclonic thunderstorms (i.e. supercells and bow-echo mesocyclones) to evolve from pulse-type convection (Monteverdi and Quadros, 1994).

2.4 Overview of buoyancy and wind shear

Severe weather events in the Central Valley, including almost all mesocyclone-induced tornadoes, occur in a cold sector environment. This environment is characterized by weak buoyancy, low tropopause heights, and low equilibrium levels (Braun and Monteverdi, 1991; Monteverdi and Quadros, 1994; Monteverdi and Johnson, 1996). Cold sector storms usually have Convective Available Potential Energy (CAPE) values typically less than 500 J/kg (Table 2–2) (Monteverdi and Quadros, 1994).

Most of the positive buoyancy area on soundings associated with cold sector storms is found in the lower troposphere due to stronger cold advection beneath the 500-mb level (Braun and Monteverdi, 1991). Monteverdi and Quadros (1994) and Monteverdi and Johnson (1996) found that the 500-mb LI underestimated the low- to mid-level positive buoyancy in the analyses of five simulated soundings from four tornado cases and one severe thunderstorm event (Table 2–2). In addition, in the Oroville case, a positive 500-mb LI suggested no risk of severe thunderstorms, but the negative 700-mb LI is evidence of the actual low- to mid-level convective nature associated with that tornado event. Monteverdi (1994) thus suggests that the 700-mb level lifted index (LI) is a better indicator of the weak to moderate low- to mid-level California buoyancy than the traditional 500-mb level LI, although CAPE is the best

Table 2–2. The lifted index (LI) for the 500-mb and 700-mb layers from an analyses of estimated soundings for five severe weather events including four tornado occurrences in north-central California (from Monteverdi and Quadros,1994; Monteverdi and Johnson, 1996).

EVENT/DATE	Severe Weather	500-mb LI (℃)	700-mb LI (℃)	C.A.P.E. (J/kg)
Vina 24 Sept. 1986	F2 tornado	-3	-5	1806
Sebastopol 2 Dec. 1992	F1 tornado	-1	-2.5	393
Carmel 6 Dec. 1992	F1 tornado	-1	-3	446
Oroville 17 Dec. 1992	F1 tornado	3	-3.5	552
Fresno 5 March 1994	Hail/Funnel Clouds	-8	-6	1961

measure of the buoyancy.

A low buoyancy environment (CAPE < 1000 J/kg) is usually identified with developing convective updrafts that contain small vertical velocities. However, wind shear-induced vertical perturbation pressure gradients can augment the strength of these weakly buoyant updrafts (Weisman and Klemp, 1982; Rotunno

and Klemp, 1982; Weisman and Klemp, 1984). In moderate- to strongly-sheared environments in the lower and middle troposphere with no veer of the wind shear vector (long straight hodograph), non-hydrostatic dynamic vertical pressure gradients significantly boost vertical accelerations on the flanks of the updraft, creating a cyclonic and anticyclonic couplet on the right and left flank of the storm, respectively. New updrafts develop on the flanks of these cyclonic and anticyclonic rotational couplets as the original updraft divides into two storms—right and left moving supercells.

In an environment with a veering wind shear vector in the low- to mid-level wind field (curved hodograph of great length), non-hydrostatic perturbation pressure gradients augment the strength of developing updrafts only on the right flank of the cyclonic member of the original couplet (Rotunno and Klemp, 1982). The growth of the updraft on the left flank of the original cell's midlevel rotational couplet (anticyclonic member) is inhibited by non-hydrostatic downward pressure forces. A potential left-moving supercell is thus suppressed while dynamic upward pressure gradients augment updraft accelerations on the cyclonic member. The end result is often a mature supercell with deviate storm motions (right-mover).

The role of shear-induced vertical perturbation forces in significantly augmenting updrafts in low buoyancy environments has been underscored by several recent studies on tornadic supercells in other parts of the country. For

example, McCaul (1990, 1991) has shown that the shear profiles in low buoyancy hurricane environments that spawn tornadic supercells produce non-hydrostatic vertical pressure gradients that can boost updraft strength significantly. These deep thunderstorms, including supercells, developed with CAPE and shear magnitudes comparable to buoyancy and shear values observed with typical Central Valley cold sector storms (McCaul 1990, 1991; Monteverdi and Quadros, 1994). Therefore, in other low buoyancy environments, deep convection can develop with minimal instability if favorable low-level wind shear is also present.

Several recent studies of California severe storms also have emphasized the importance of environmental wind shear in the evolution of tornadic thunderstorms. Strong low-level shear is usually observed during severe weather outbreaks (i.e. large hail, straight-line winds, etc.) and always during tornadic events. Braun and Monteverdi (1991) were the first to document the convective and rotational parameters associated with a mesocyclone-induced tornadic thunderstorm in a strongly sheared low-level environment in Northern California. The study emphasized the significance of topographically influenced low-level wind shear in the development of mesocyclonic thunderstorms in the low buoyancy, moderate deep-layer shear environment of California.

Monteverdi and Quadros (1994) and Monteverdi and Johnson (1996) also investigated the connection between strong environmental wind shear and

tornadogenesis during severe weather patterns in California. Four severe weather events studied by Monteverdi and Quadros (1994) and one by Monteverdi and Johnson (1996) yielded a diagnosis of low-level (0–2-km) positive shear values similar to findings associated with mesocyclones and at least weak tornadoes elsewhere (Table 2–3). Furthermore, the F1 tornado in Oroville on 17 December 1992 had a positive shear value comparable to those observed with strong and violent cold season tornadoes in the southern Plains and Gulf coastal regions (Johns et al., 1993).

The minimal role of buoyancy, and the important role of shear, as a distinguishing characteristic between tornadic and non-tornadic thunderstorms in California was most recently documented in Lipari and Monteverdi (2000) and Monteverdi et al. (2000). It was shown that there were no statistically-significant differences observed in the buoyancy values obtained from 30 proximity soundings near F0, F1, and F2 tornadic thunderstorms, mostly in the Central Valley, during the period 1990-94 (Fig. 2–3). When the 1990-94 data set was expanded to include 40 non-tornadic thunderstorms that occurred during the same period, Monteverdi et al. (2000) likewise found no statistically significant difference in the observed buoyancy values between the non-tornadic and the tornadic data sets. However, there were highly statistically significant differences between the shear values for the 0–1 km and 0–6 km layers between the F1/F2events and the F0/null events (Fig. 2–3 and Fig. 2–4). Conclusions were

Table 2–3. The 0–2-km positive shear, 0–3-km storm relative helicity, and the Bulk Richardson Number (BRN) from an analyses of estimated soundings for five severe weather events including four tornado occurrences in north-central California (from Monteverdi and Quadros,1994; Monteverdi and Johnson, 1996).

EVENT/DATE	Severe Weather	Pos. Shear (0-2 km) $(10^{-3}s^{-1})$	0–3-km s-r helicity $(ms^{-1})^2$	Bulk Richardson Num. (BRN)
Vina 24 Sept. 1986	F2 Tornado	9.7	342	15
Sebastopol 2 Dec. 1992	F1 Tornado	9.4	284	3
Carmel 6 Dec. 1992	F1 tornado	8.6	254	5
Oroville 17 Dec.1992	F1 tornado	12.5	454	3
Fresno 5 March 1994	Large Hail Funnel Clouds	3.4	143	40

that buoyancy is modest for most California convection, including tornadic and non-tornadic events alike, but larger values of shear increase the risk that a thunderstorm will produce a tornado. Finally, the shear profile for the F1/F2 cases had shear values and hodographs that compared favorably to those observed for tornadic supercells elsewhere in the country. Based on these

statistical differences of low-level and deep-layer shear, forecast shear thresholds were established which separate the potentially strong tornado environments from weak tornadic/non-tornadic ones.

A useful index of the combined effects of buoyancy and shear in the determination of thunderstorm type is the Bulk Richardson Number (BRN). The BRN is basically a ratio of buoyancy (CAPE) to the shear that was developed as a constraint in modeling studies of convective storms (Weisman and Klemp,

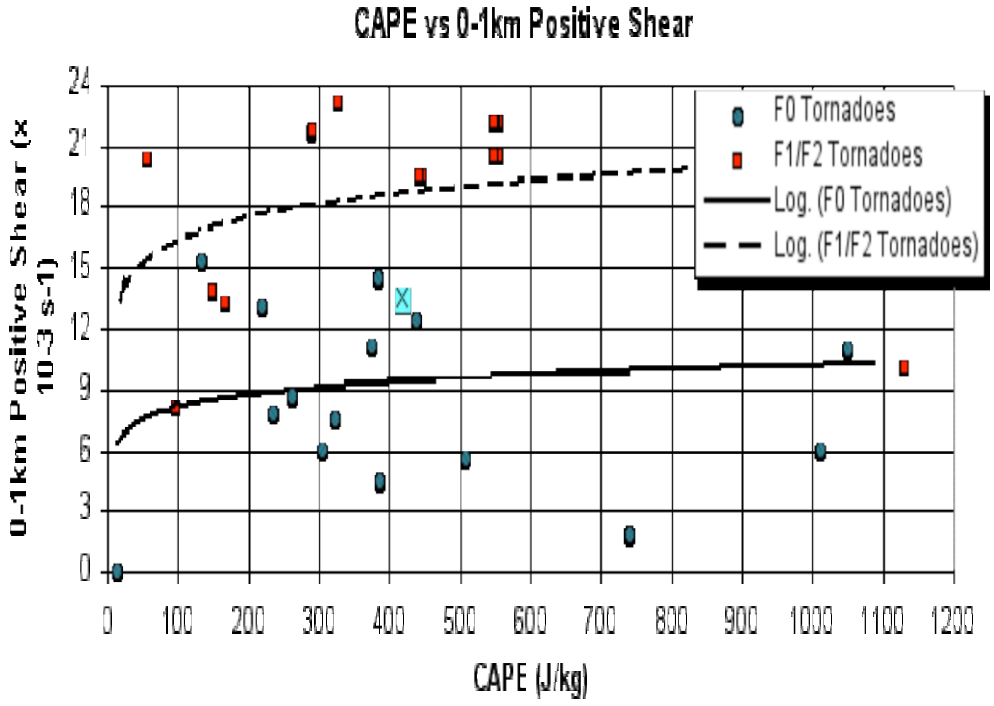

Fig. 2–3. Plot of CAPE versus 0–1-km positive shear for California tornado events, 1990-94. Best fit curves for F0 and F1/F2 data sets show stratification based upon statistically significant differences in the 0–1-km positive shear values for F0 and F1/F2 tornadoes. Highlighted “X’ is the sample average (from Lipari and Monteverdi, 2000).

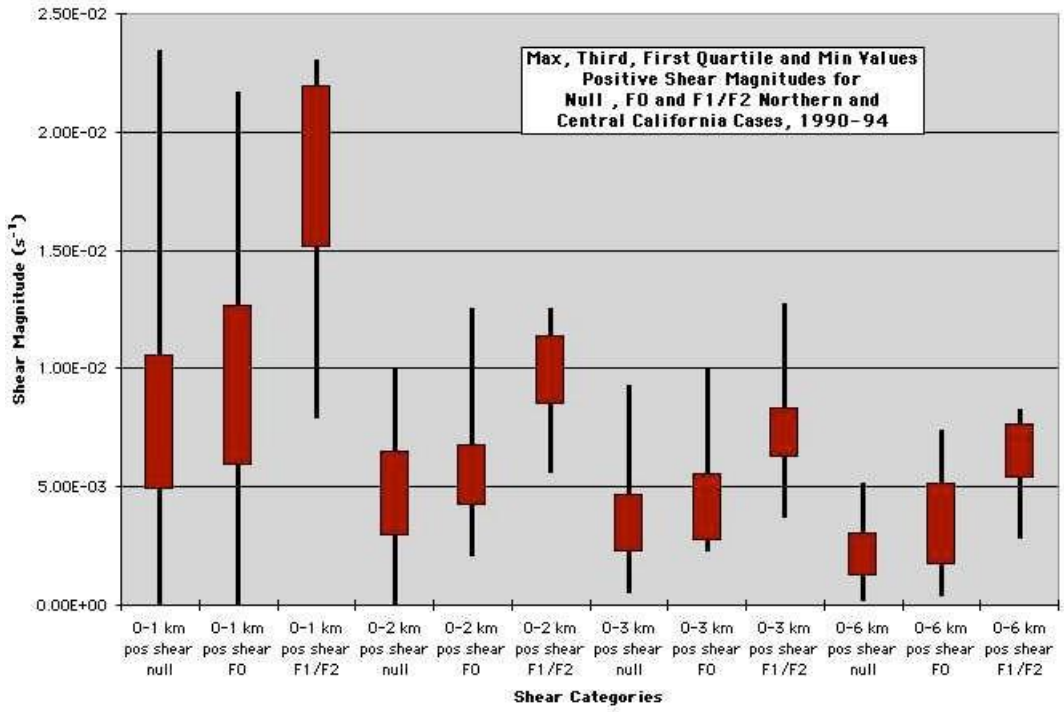

Fig. 2–4. Box and whisker plots of positive shear values for various layers for null, F0, and F1/F2 tornado cases (from Monteverdi et al., 2000).

1986). The BRN shear, in the denominator, is defined on the basis of the value of 0–6-km bulk shear that would generate sufficient streamwise vorticity upon tilt to produce a mesocyclone.

In environments dominated by buoyancy and weak vertical wind shear, the BRN values are large (>50) and the associated convection is often multicellular (Weisman and Klemp, 1986). BRN's between (15 – 40) have combinations of buoyancy to shear that are best linked with supercell development. In the low CAPE and strong shear environment that characterizes

most California severe storms, the BRN is usually quite low (2 – 14), and the buoyancy accelerations alone are too weak to develop sustained convective updrafts. However, the growth of long-lived thunderstorms is not completely inhibited since perturbation forces can significantly increase updraft accelerations (Weisman and Klemp, 1986). Other researchers have noted this in other similar low BRN environments where rotating updrafts and/or mini-supercells were documented (Johns et al., 1993, Markowski and Straka, 2000).

Updraft rotational potential can be assessed using storm-relative environmental helicity (SREH)—an estimate of a thunderstorm's potential to acquire a rotating updraft given an environmental vertical wind shear profile. The documentation of tornadic thunderstorm events, especially supercell thunderstorms, often use observations of SREH to assess the rotational magnitude of the parent storm since the storm motion vector is known or can be accurately estimated. Johns and Doswell (1992) found most strong and violent tornadoes occurred in environments where 0 – 3 km layer SREH values are greater than 300 $(ms^{-1})^2$. Even including cases with limited buoyancy, high values of SREH are associated with tornadic supercells occurrences (Johns et al., 1993, Johns and Doswell, 1992).

Monteverdi and Quadros (1994) found that California tornadic storms have 0–3-km SREH values comparable to those associated with tornadic thunderstorms observed elsewhere. Values of SREH (Table 2–3) for the four

cases documented by Monteverdi and Quadros (1994) and the one by Monteverdi and Johnson (1996) were consistent to known parameters. Davies-Jones et al. (1990) advise that values of SREH up to 151 $(ms^{-1})^2$ support mesocyclone development, 151–299 $(ms^{-1})^2$ weak tornadoes, 300–449 $(ms^{-1})^2$ strong tornadoes, and values greater than 450 $(ms^{-1})^2$ violent tornadoes. Severe storms in California rarely have values of SREH that exceed 400 $(ms^{-1})^2$, the only documented exception was the F1 tornado event near Oroville on 17 December 1992 (see Table 2–3) (Monteverdi and Quadros, 1994).

3. Synoptic and Thermodynamic Controls on the Lemoore Storm

Previous studies of severe weather events in California (i.e. Carbone, 1982; Braun and Monteverdi, 1991; Monteverdi and Johnson, 1996; and Staudenmaier and Cunningham, 1995) have shown that shear and buoyancy profiles favorable for the development of supercells and tornadic storms in the Central Valley usually have been associated with the schematic pattern depicted in Fig. 2–2, hereafter referred to as SP (schematic pattern). While it is important for meteorologists to remain focused on the factors that might contribute to severe weather, recognition of patterns that seem climatologically favorable for simultaneous occurrence of such favorable factors is obviously helpful to the forecasting process.

In the context of the present study, the author had no preconceived notion regarding the synoptic pattern that occurred in association with the Lemoore storm on 22 November 1996. However, since a cluster of multicells and at least one tornadic supercell did occur that day, there was an expectation that the shear and buoyancy parameters observed in the Valley would correspond to what would be expected for the development of such storms. To the extent that the environment controls shear and buoyancy, the author hoped that the synoptic and mesoscale patterns on 22 November 1996 would be consistent with what would be expected given the outbreak of convection that developed.

3.1 Large-scale Setting

3.1.1 Sources of Information

National Meteorological Center (NMC)[1] mandatory level and surface charts, and satellite imagery obtained from the National Climatic Data Center (NCDC) were used to discuss the evolution of the weather pattern (sections 3.1.2 and 3.1.3). The gridded Eta data for 1200 UTC 22 November and 0000 UTC 23 November 1996 were obtained from the National Center for Atmospheric Research (NCAR) in order to construct and analyze diagnostic fields using the public domain software known as Personal Computer based Gridded Interactive Display and Diagnostic System (PCGRIDDS) (National Oceanic and Atmospheric Administration, 1997).

PCGRIDDS is software that analyzes gridded model data and produces charts that can be used to infer the sign and relative magnitude of quasigeostrophic (QG) -forcing for vertical motion. The vertical motion fields are very important in understanding the buoyancy setting for a severe weather outbreak since they can contribute layer-lifting that destabilizes the environment. In the present case, the author chose charts used routinely by forecasters in an

[1] Currently known as the National Centers for Environmental Prediction (NCEP)

operational setting to illustrate the extent to which the inferred forcing corresponded to the actual vertical motion patterns.

3.1.2 Quasigeostrophic Diagnosis

The controls on the mid-tropospheric vertical motion patterns in the atmosphere are complex. As explained in Holton (Holton, pp. 166-175, 1992) and Bluestein (Bluestein, pp. 14, 27-28, 1992), however, QG analysis allows a forecaster to diagnose the large-scale controls on vertical motion using commonly available charts. In the case of weather systems that develop or evolve over relatively short time frames, e.g., 12h to 24h, the QG “forcing terms” for vertical motion and height/pressure changes relate basically to the vorticity advection and temperature advection patterns at various levels bounding near or in the center of the layer considered. Software such as PCGRIDDS, GemPak or wxp allows such patterns to be analyzed using either observational or gridded model data.

The QG omega equation has two terms that can serve as a basis for diagnosis of synoptic-scale vertical motion patterns. These terms, known as “forcing terms”, are proportional to the differential absolute geostrophic vorticity advection across a layer centered at a given level and the temperature advection at that same level. In the present study, the 1000-500-mb thickness advection is used to infer the general lower to mid-tropospheric advection patterns and the

850-mb and 700-mb height/vorticity pattern is used to assess the sign of the differential vorticity pattern for the layer from the surface upward to 500-mb, centering at 850-mb and 700-mb respectively. Since the two forcing functions have terms in common, it is often useful for forecasters to examine fields of the combined functions. The two forcing functions can be combined to one (if terms small at the synoptic scale are dropped) to obtain the so-called Trenberth approximation. Stated simply, the Trenberth approximation states that QG omega at a given level is proportional to the isothermal vorticity advection, that is, the absolute geostrophic vorticity advection at a given level by the thermal wind centered at the same level. This is also known as Isentropic Potential Vorticity Advection (IPVA). In this study, comparisons of IPVA fields with differential vorticity advection and temperature advection patterns across the same layers are used to assess the relative contributions of the synoptic scale environment to the vertical motion fields that developed on the day of the Lemoore storm.

3.1.3 Overview of the Synoptic Setting

The mid- and upper- tropospheric pattern in the eastern Pacific two days prior to the Lemoore event was characterized by a strong trough associated with the polar jet stream. NMC 500-mb (Fig. 3–1) and 300-mb (Fig. 3–2) analyses for 1200 UTC 21 November 1996 show this major trough centered at approximately 135 °W. Two disturbances were progressing around this trough and were evident

both in the vorticity fields at the two levels (not shown) and as localized 90-knot wind speeds maximums (i.e. jet streaks) in the upper tropospheric wind fields (Fig. 3–2; shown as JS1 and JS2). The systems were located (from east to west) in the diffluent portion (35°N/130°W; in the southwesterly flow into California and Oregon) and the confluent portion (35°N/140°W; upstream region) of the major long wave respectively.

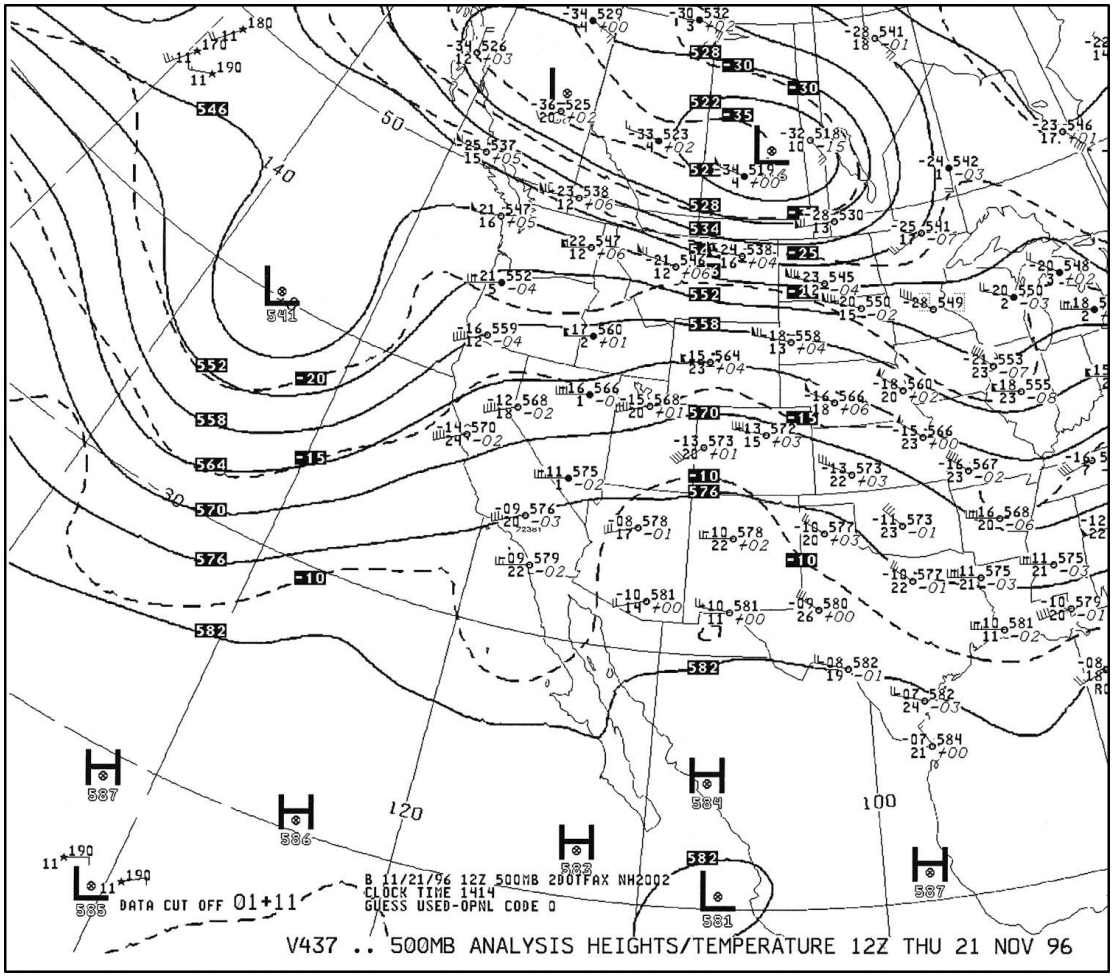

Fig. 3–1. 500-mb NMC analysis for 1200 UTC 21 November 1996.

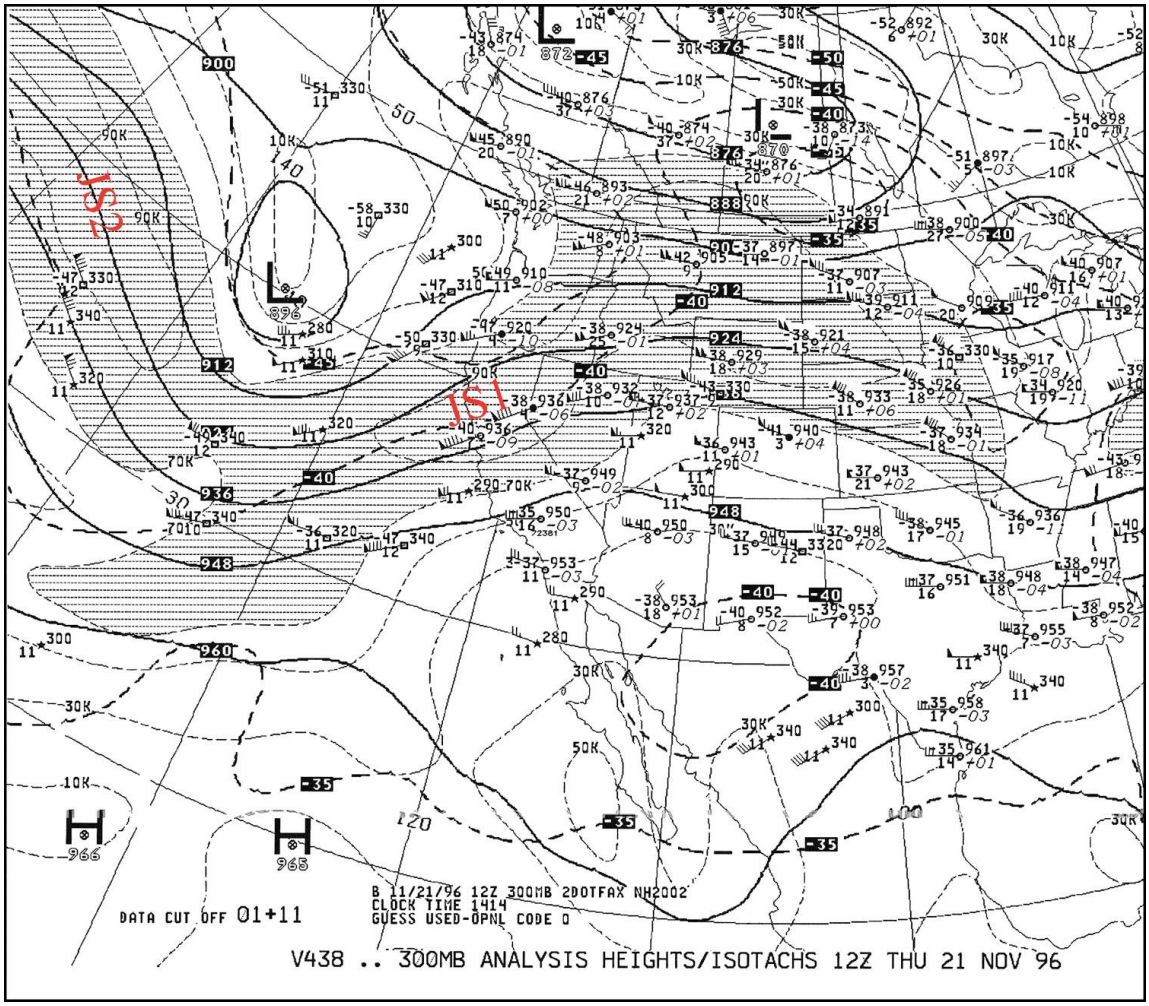

Fig. 3–2. 300-mb NMC analysis for 1200 UTC 21 November 1996.

The first upper-tropospheric disturbance was associated with a synoptic scale cold front at the surface (Fig. 3–3) and lower troposphere (Fig. 3–4, cold front symbols) positioned off the California coast at 1200 UTC 22 November 1996. The 850-mb (Fig. 3–4) analysis shows warm air temperature advection in the warm sector of this advancing cold front (Fig 3–3) was phased with the

location of the divergent right-rear quadrant of JS1 at 300-mb (Fig 3–1) and 500-mb differential vorticity advection (not shown). These factors contributed to upward omega that resulted in differential layer-lifting upstream of

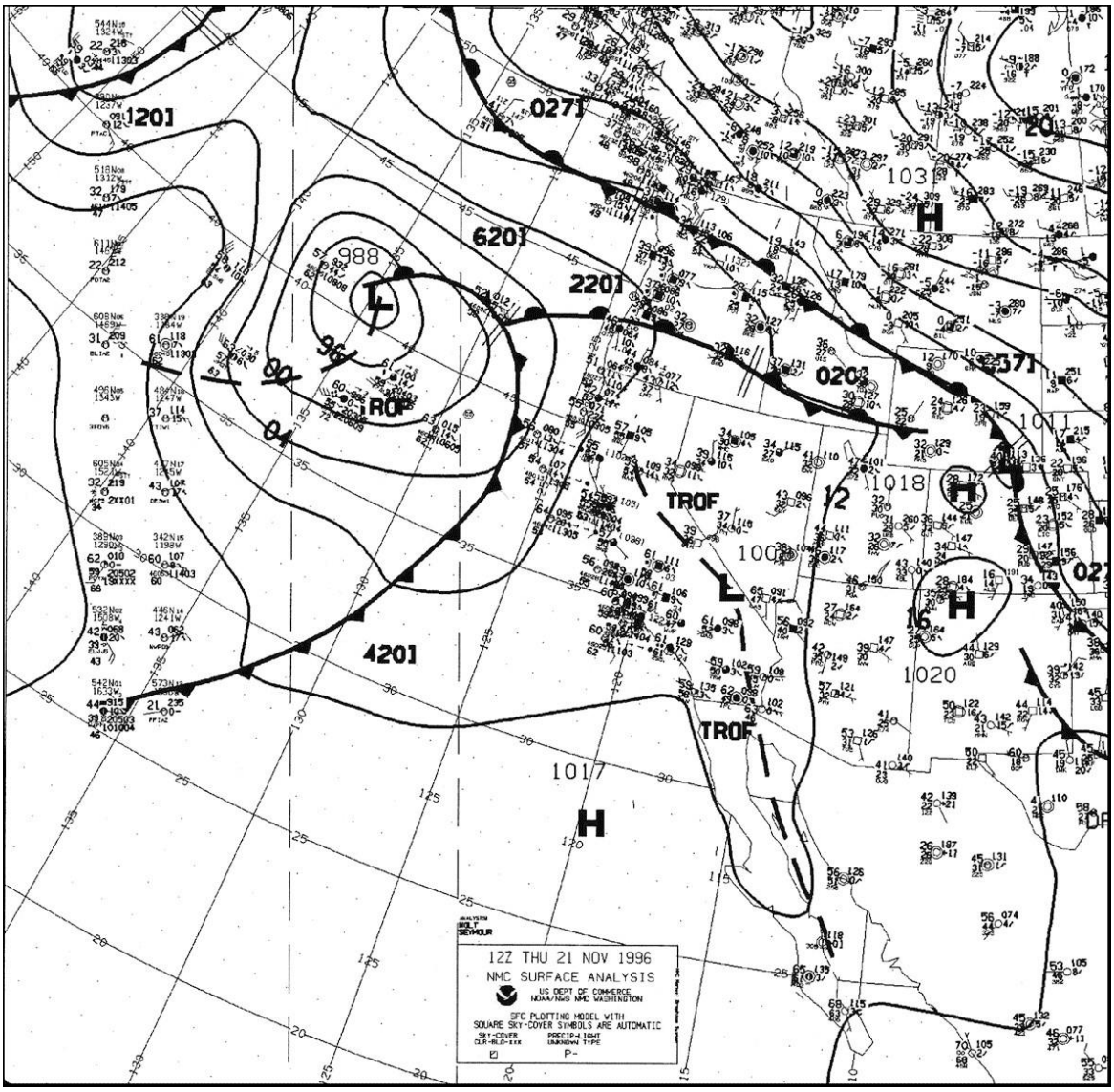

Fig. 3–3. NMC surface analysis for 1200 UTC 21 November 1996.

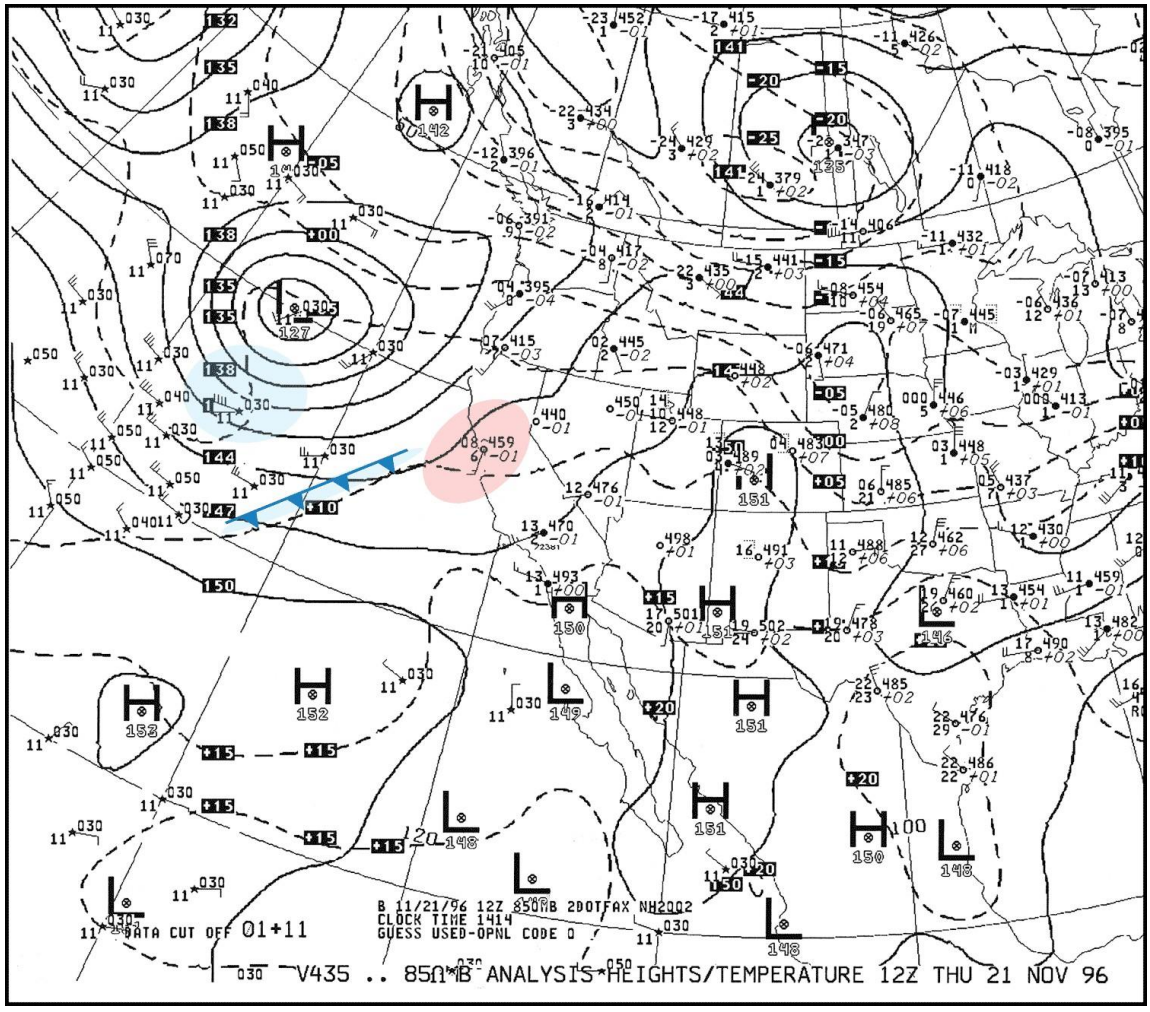

Fig. 3–4. 850-mb NMC analysis for 1200 UTC 21 November 1996. Red shading indicates warm air advection and blue shading cold air advection.

the frontal boundary. Satellite imagery (Fig 3–5; area 1) depicted a broad area of cloudiness along the California coast in the same location.

The upstream disturbance (35 °N/140 °W) was associated with a surface subsynoptic trough (37.5 °N/137.5 °W) (Fig. 3–3) and low-pressure area (988-mb) (41 °N/135 °W) (Fig. 3–3), the parent long-wave upper-tropospheric trough

(40°N/135°W) (Fig. 3–1; Fig. 3–2), and the other upper-level 90-knot jet streak (Fig. 3–2; JS2). The 850-mb and 700-mb analyses (Fig. 3–4; Fig. 3–6) show that this disturbance was also associated with lower and middle tropospheric cold air advection (blue shading) in the vicinity of the surface subsynoptic trough. The synoptic-scale mid-tropospheric downward forcing related to the lower tropospheric cold air advection was likely negated by stronger contributions toward upward omega from upper-tropospheric jet-streak divergence linked to

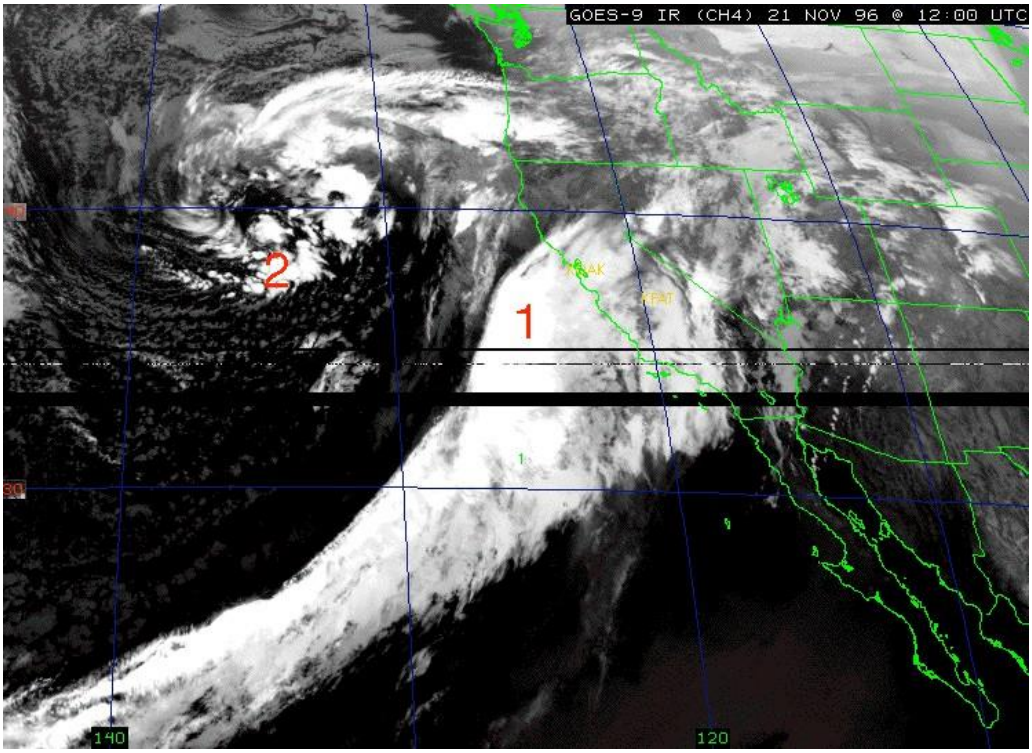

Fig. 3–5. GOES-9 infrared satellite imagery for 1200 UTC 21 November 1996. The numbers refer to cloud features discussed in the text.

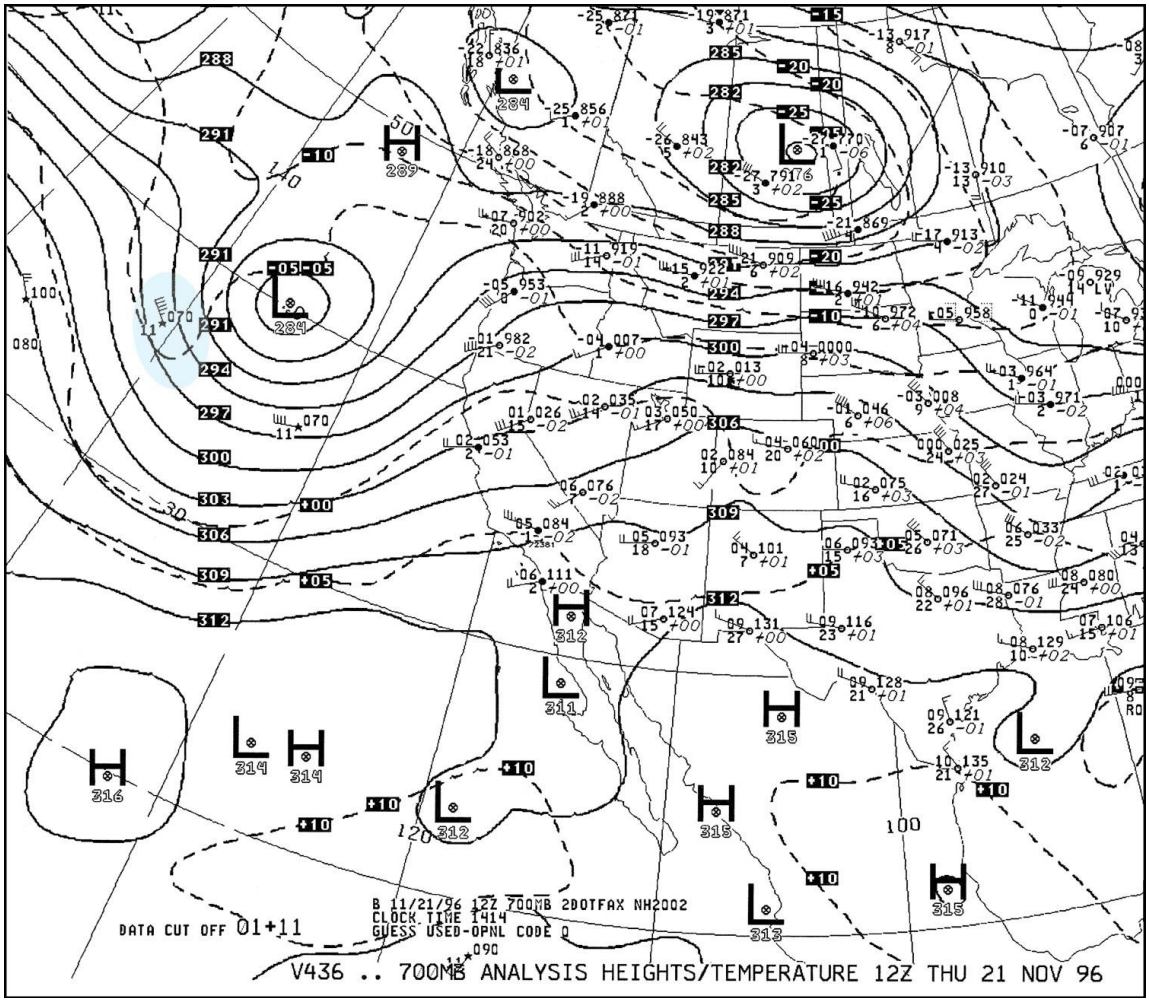

Fig. 3–6. 700-mb NMC analysis for 1200 UTC 21 November 1996. Blue shading indicates cold air advection.

the left-front quadrant of JS2 (Fig. 3–2) and 500-mb differential CVA (not shown). The resulting upward vertical motion field caused layer-lifting (and destabilization) near the same location as the localized low-level convergence zone that marked the position of the surface subsynoptic trough (Fig. 3–3) and developing comma-cloud on infrared satellite imagery (Fig. 3–5, area 2). The

open-cellular nature of the cloudiness in the vicinity of the upper-tropospheric low-pressure (Fig. 3–5, area 2) area also suggests the presence of cold pool of air aloft (< 5 ℃ at 850-mb; ~ -5 ℃ at 700-mb; < -20 ℃ at 500-mb; ~ -45 ℃ at 300-mb). Enhancement of the cloudiness in that same region is consistent with

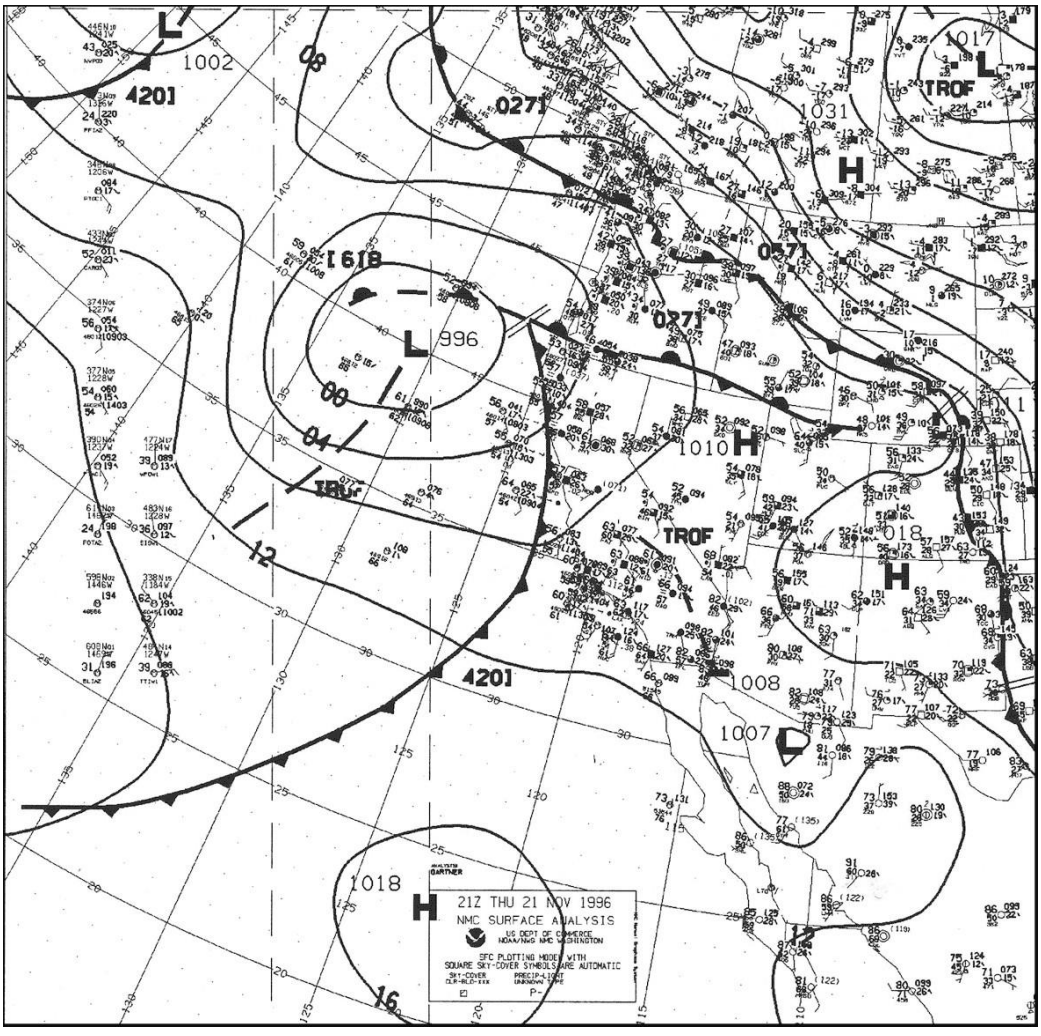

Fig. 3–7. NMC surface analysis for 2100 UTC 21 November 1996.

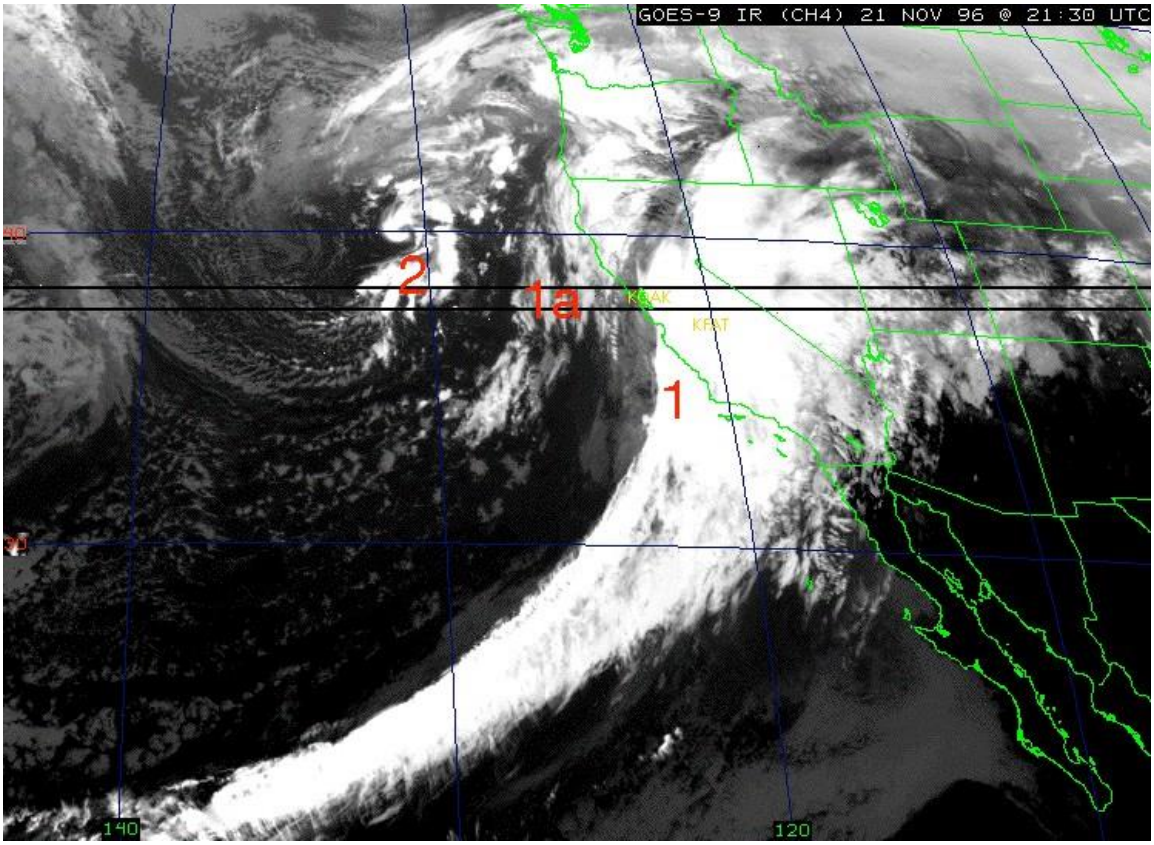

Fig. 3–8. Same as Fig. 3–5, except for 2130 UTC 21 November 1996.

air mass destabilization related to that cold pool of air in the middle and upper troposphere and to heat transfer from the relatively warmer ocean water that increased lower-tropospheric instability.

These surface and upper-air features advanced eastward over the next nine hours (2100 UTC 21 November 1996). The cold front made landfall in California (Fig. 3–7; Fig. 3–8, area 1), the parent surface low-pressure area now at 40 °N /131 °W weakened (988-mb to 996-mb) (Fig. 3–7; Fig. 3–8, area 2), and satellite imagery showed a decrease in cellular cloudiness near the center of the

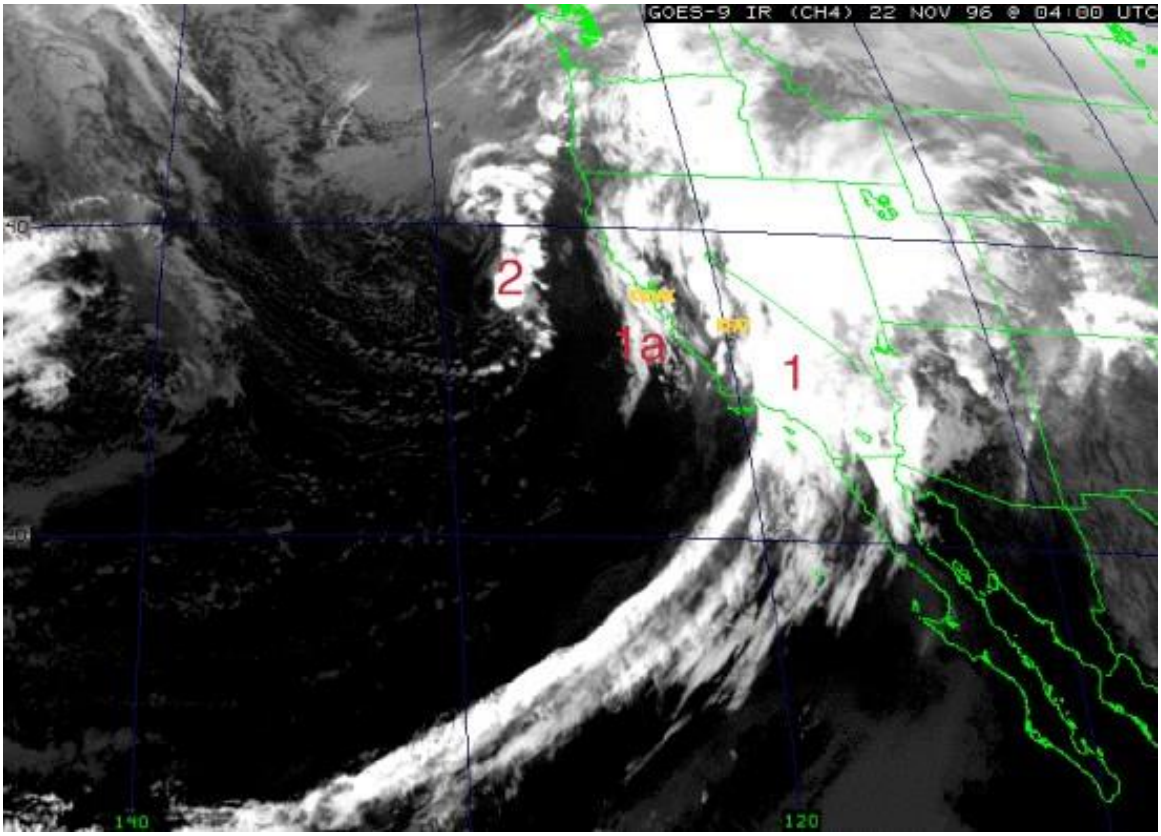

Fig. 3–9. Same as Fig. 3–5, except for 0400 UTC 22 November 1996.

low (Fig. 3–8, area 2). A weak post-frontal trough (Fig. 3–8, area 1a) also trailed the eastward progression of the cold front into Central/Northern California and satellite imagery suggested convective rain showers might have been embedded in this cloud band (Fig. 3–9; area 1a).

Middle and upper tropospheric analyses for three hours later at 0000 UTC 22 November show the long-wave trough axis remained off the California coast (Fig. 3–10; Fig. 3–11) as the surface (Fig 3–12) and lower tropospheric (Fig. 3-13) cold front moved south along the California coast. The nose of the second 90-knot 300-mb jet streak (Fig. 3–11, JS2) had moved into the base of the upper-

level circulation at 30°N/125°W. Cold air advection at 850-mb was located in the upstream portion of the re-strengthening parent surface low at 40°/130°W (996-mb to 994-mb) (Fig. 3–13) and a cold pool of air in the mid-troposphere was located in the leading edge (Fig 3–14). Infrared satellite imagery shows a well-defined comma-cloud residing in the same region (interpolation of Fig. 3–8 and Fig. 3–9, area 2). Progressive movement of these surface and upper-air features into Northern and Central California occurred over the next twenty-four hours.

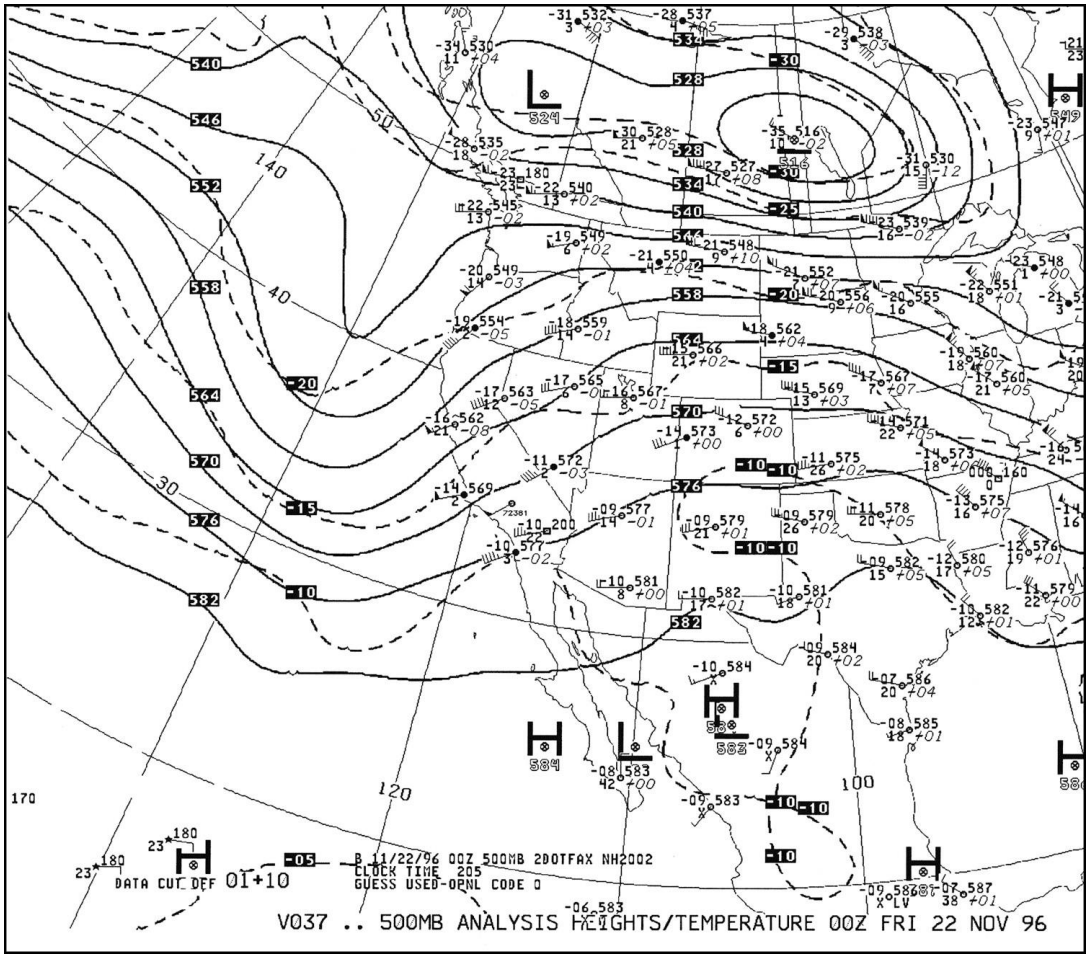

Fig. 3–10. 500-mb NMC analysis for 0000 UTC 22 November 1996.

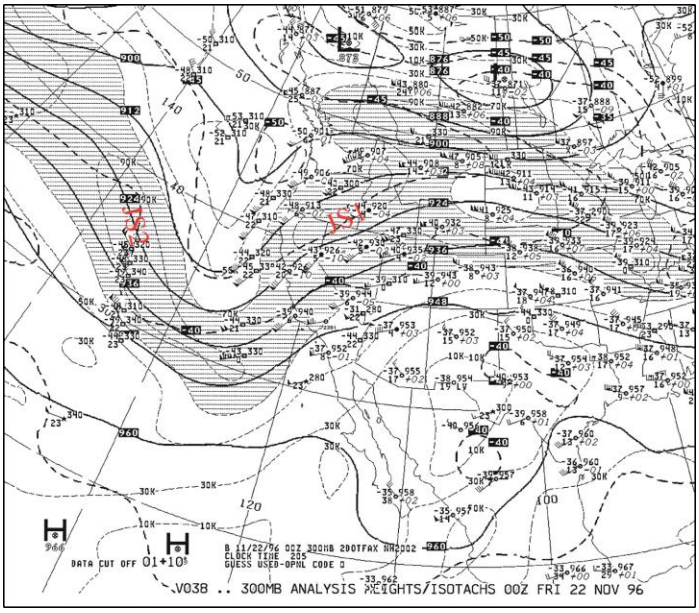

Fig. 3–11. 300-mb NMC analysis for 0000 UTC 22 November 1996.

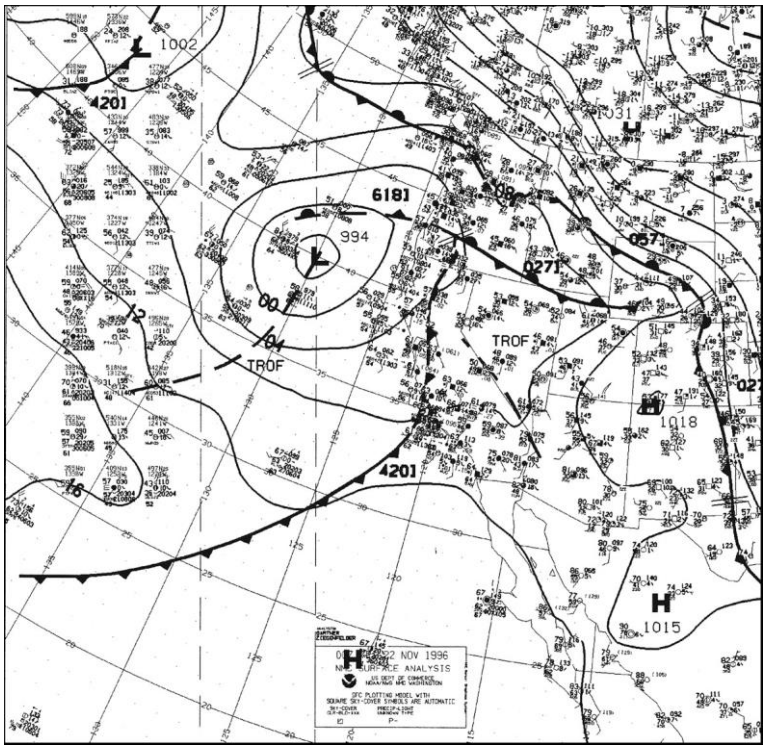

Fig. 3–12. NMC surface analysis for 0000 UTC 22 November 1996.

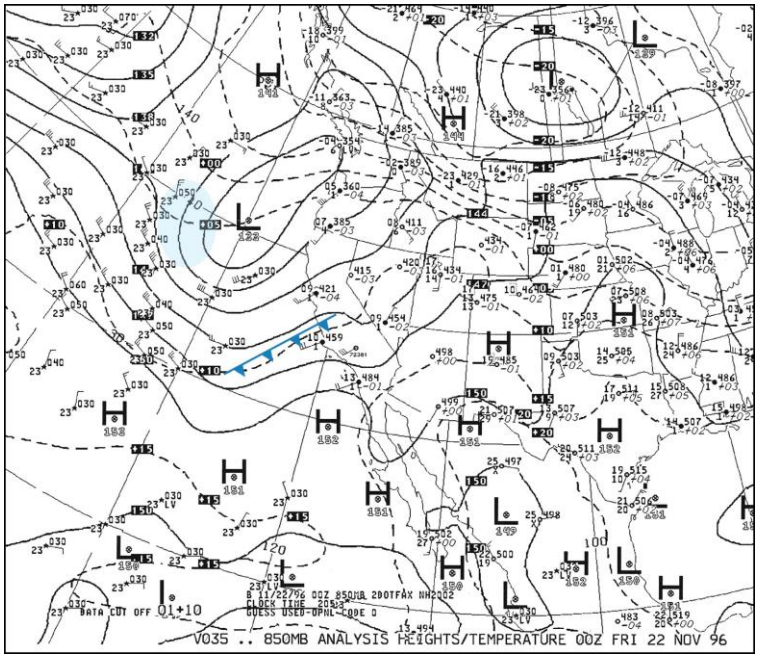

Fig. 3–13. 850-mb NMC analysis for 0000 UTC 22 November 1996. Blue shading indicates cold air advection.

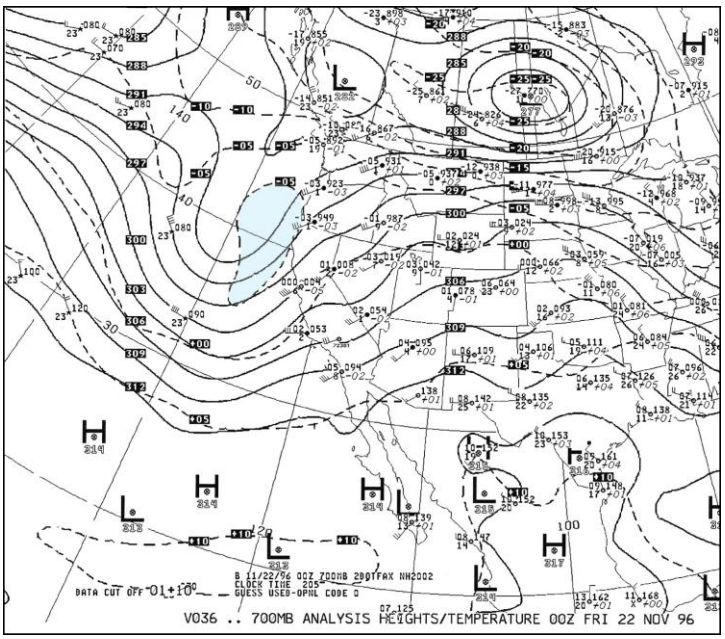

Fig. 3–14. 700-mb NMC analysis for 0000 UTC 22 November 1996. Blue shading indicates location of the cold air pool.

3.1.4 The Landfall of the Post-frontal Trough

The surface post-frontal trough and low-pressure area (Fig. 3–15) moved into the Northern and Central California with the eastward progression of the

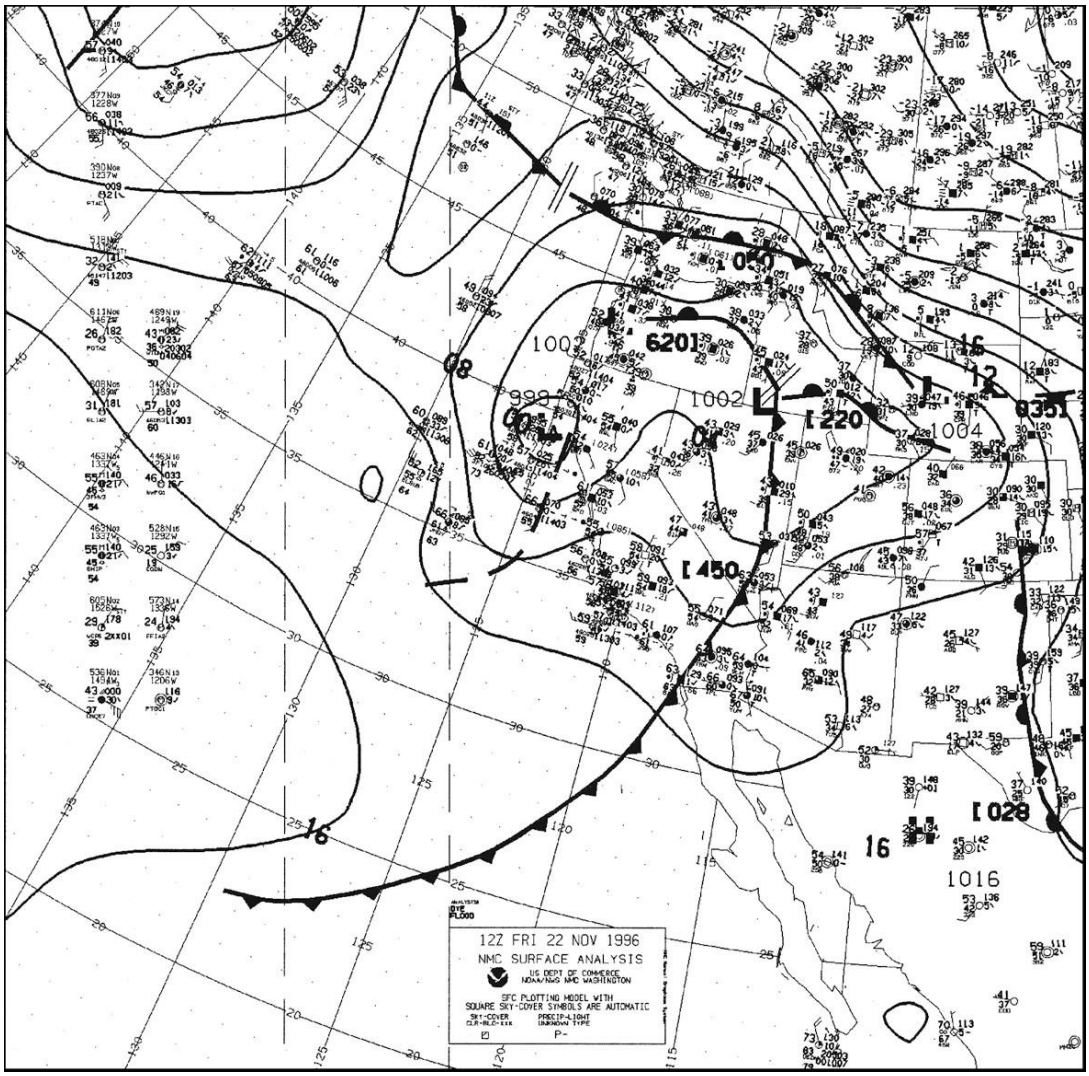

Fig. 3–15. NMC surface analysis for 1200 UTC 22 November 1996.

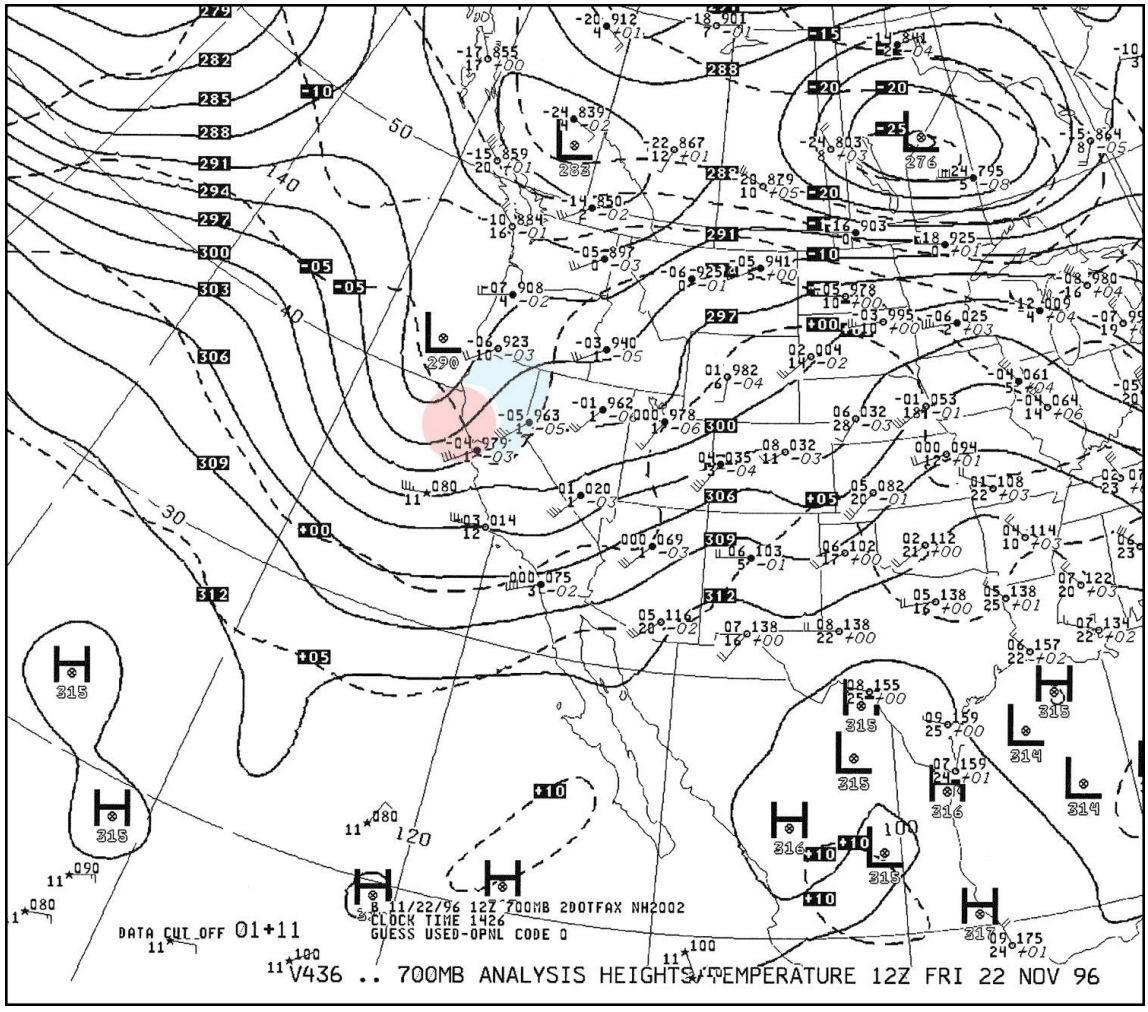

Fig. 3–16. 700-mb NMC analysis for 1200 UTC 22 November 1996. Red shading indicates warm air advection and blue shading cold air advection.

middle and upper-tropospheric trough at 1200 UTC 22 November 1996 (Fig. 3–16, Fig. 3–17, Fig. 3–18). Cold cloud tops on infrared satellite imagery suggested of a line of convection (area 2) along the Central California and Oregon coastlines was the remnants of the comma cloud associated with the post-frontal trough (Fig. 3–19). The 500-mb analysis showed that a cold pool of

air was also located in the same region as this cloud band (Fig 3–17, blue shading). The cold pool likely developed from adiabatic cooling of dry 700-mb air caused by layer-lifting associated with lower tropospheric warm air advection (Fig 3– 16, red shading).

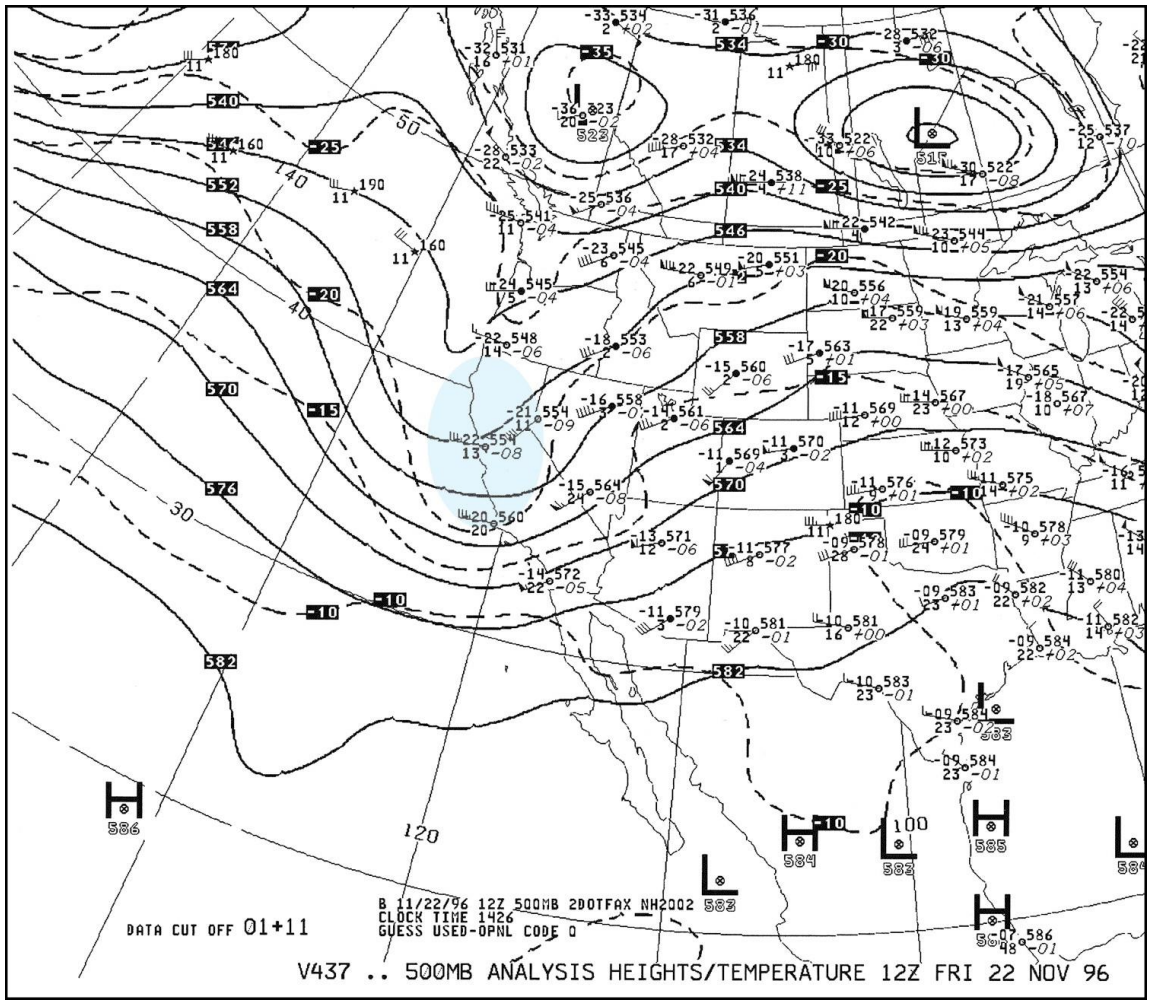

Fig. 3–17. 500-mb NMC analysis for 1200 UTC 22 November 1996. Blue shading indicates location of the cold air pool.

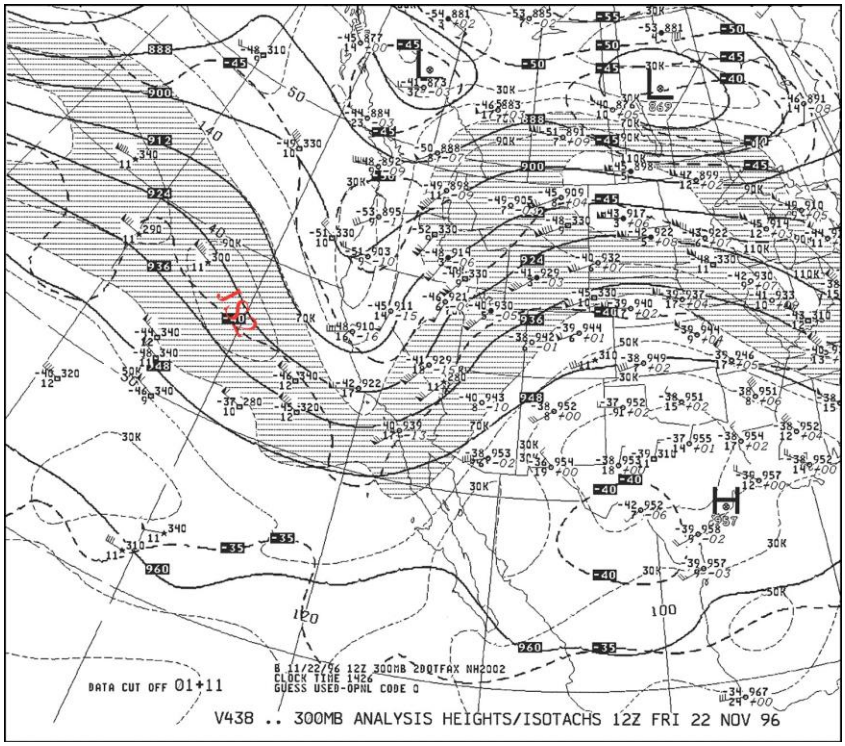

Fig. 3–18. 300-mb NMC analysis for 1200 UTC 22 November 1996.

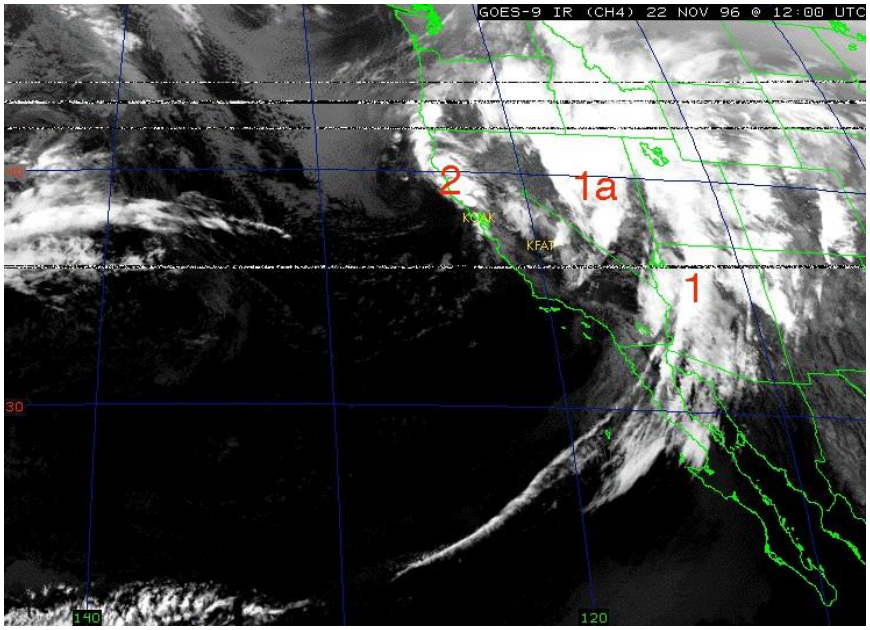

Fig. 3–19. Same as Fig. 3–5, except for 1200 UTC 22 November 1996.

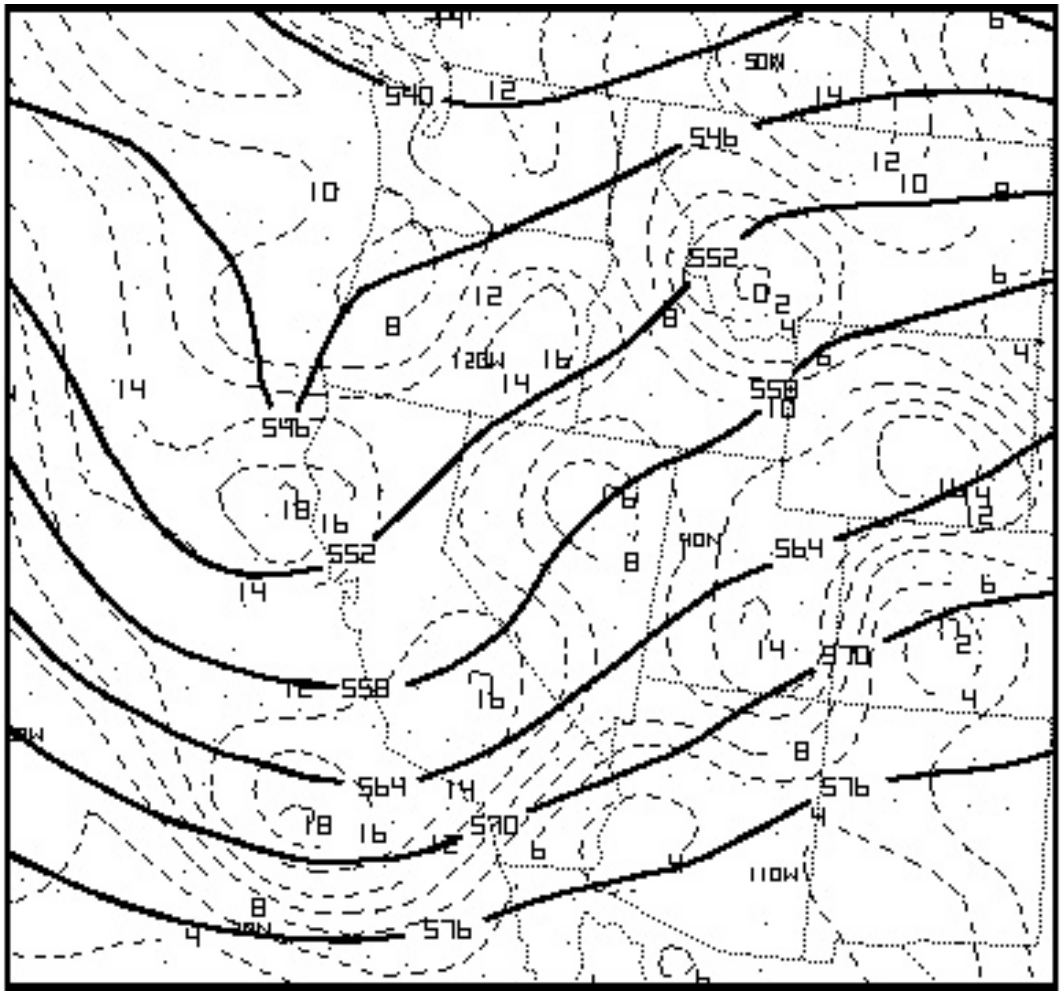

Fig. 3–20. PC-Grids analysis of Eta model 500-mb heights (dam, solid) and absolute vorticity (10^{-5} s^{-1}, dashed) for 1200 UTC 22 November 1996.

Quasi-geostrophic omega forcing for mid-tropospheric upward motions associated with the post-frontal trough at 1200 UTC 22 November 1996 was diagnosed by equal contributions from 500-mb CVA and 1000-500-mb warm advection (Fig. 3–20; Fig. 3–21). Closer examination shows an augmentation of the large-scale upward omega fields at the 700-mb and 850-mb levels (Fig.

3–22; Fig. 3–23, shaded regions) can be linked to CIVA in those layers (Fig. 3- – 24; Fig. 3–25). Overlays of the shaded areas show upward vertical velocity maxima of -6 μb s^{-1} at 700-mb and 850-mb located near the regions of strongest CIVA in Central California. The result was dynamic layer-lifting and a saturated lower troposphere that marked the axis of low-level moisture convergence (Fig. 3–26). The location of the surface subsynoptic trough (Fig. 3–15) and a line of

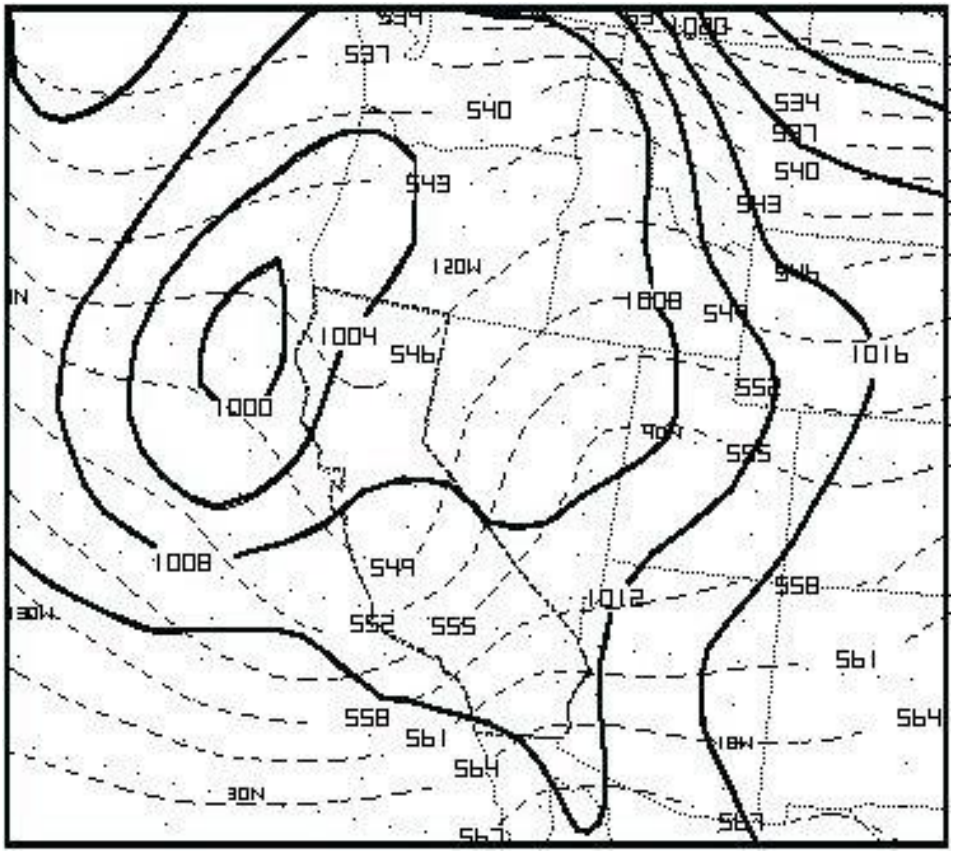

Fig. 3–21. PC-Grids analysis of Eta model mean sea level pressure (mb; solid) and 1000-500-mb thickness (dam; dashed) for 1200 UTC 22 November 1996.

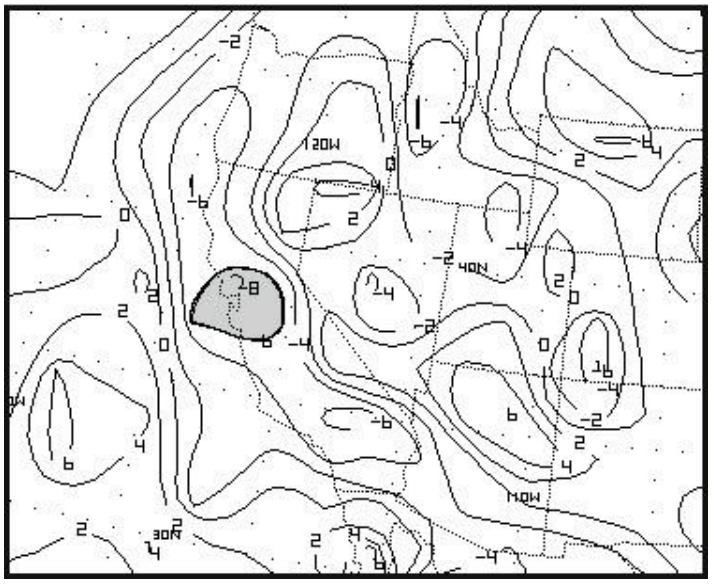

Fig. 3–22. PC-Grids analysis of Eta model 700-mb vertical velocities (μbs^{-1} ; negative–rising motion, positive–sinking motion) for 1200 UTC 22 November 1996.

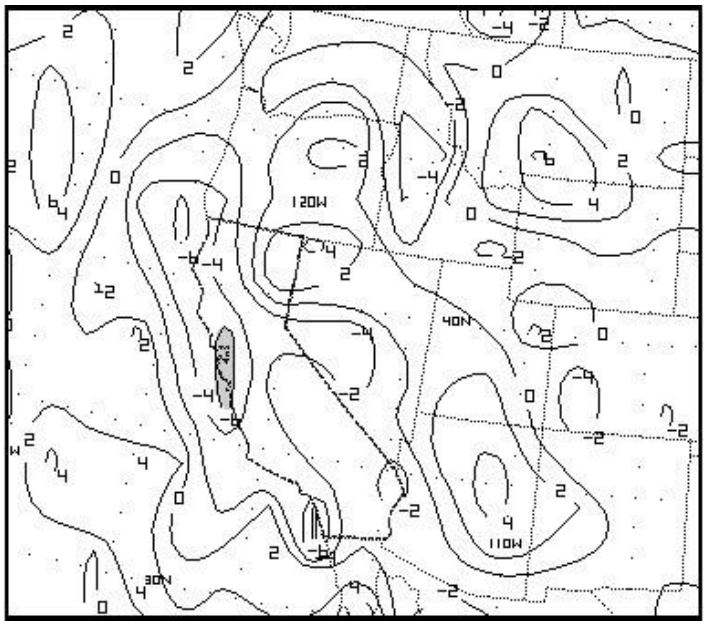

Fig. 3–23. PC-Grids analysis of Eta model 850-mb vertical velocities (μbs^{-1}; negative–rising motion, positive–sinking motion) for 1200 UTC 22 November 1996.

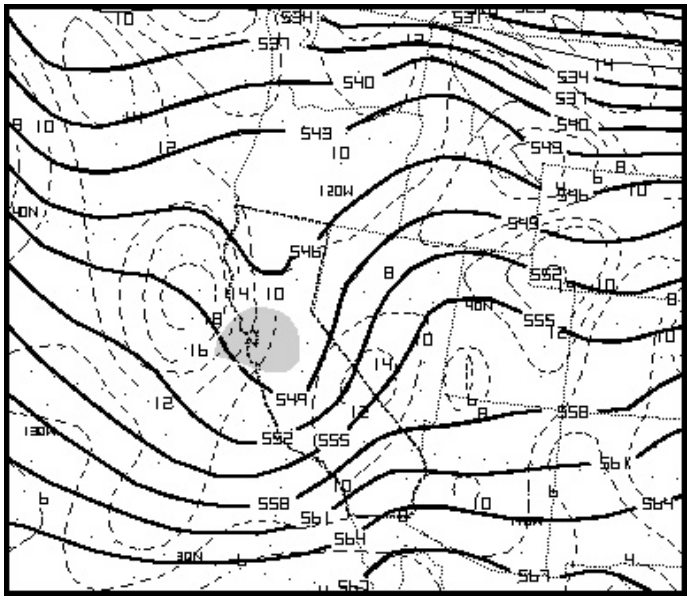

Fig. 3–24. PC-Grids analysis of Eta model 1000-500-mb thickness (dam; solid) and 700-mb absolute vorticity (10^{-5} s^{-1}, dashed) for 1200 UTC 22 November 1996.

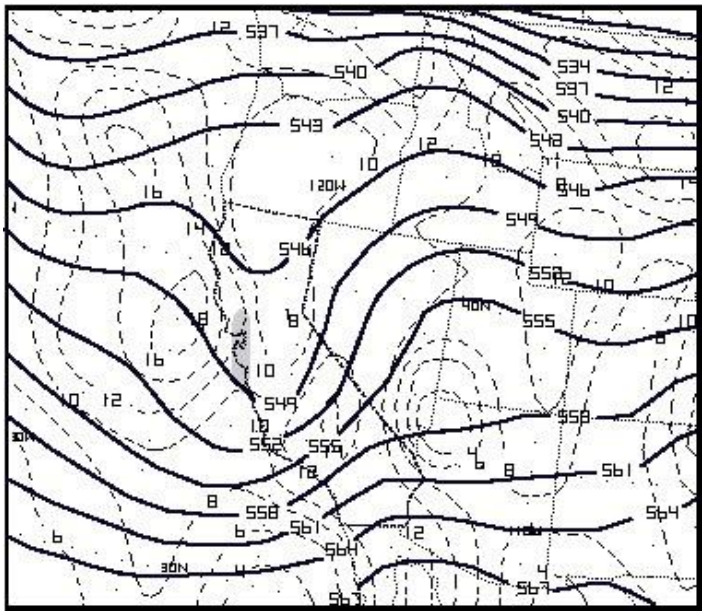

Fig. 3–25. PC-Grids analysis of Eta model 1000-500-mb thickness (dam; solid) and 850-mb absolute vorticity (10^{-5} s^{-1}, dashed) for 1200 UTC 22 November 1996.

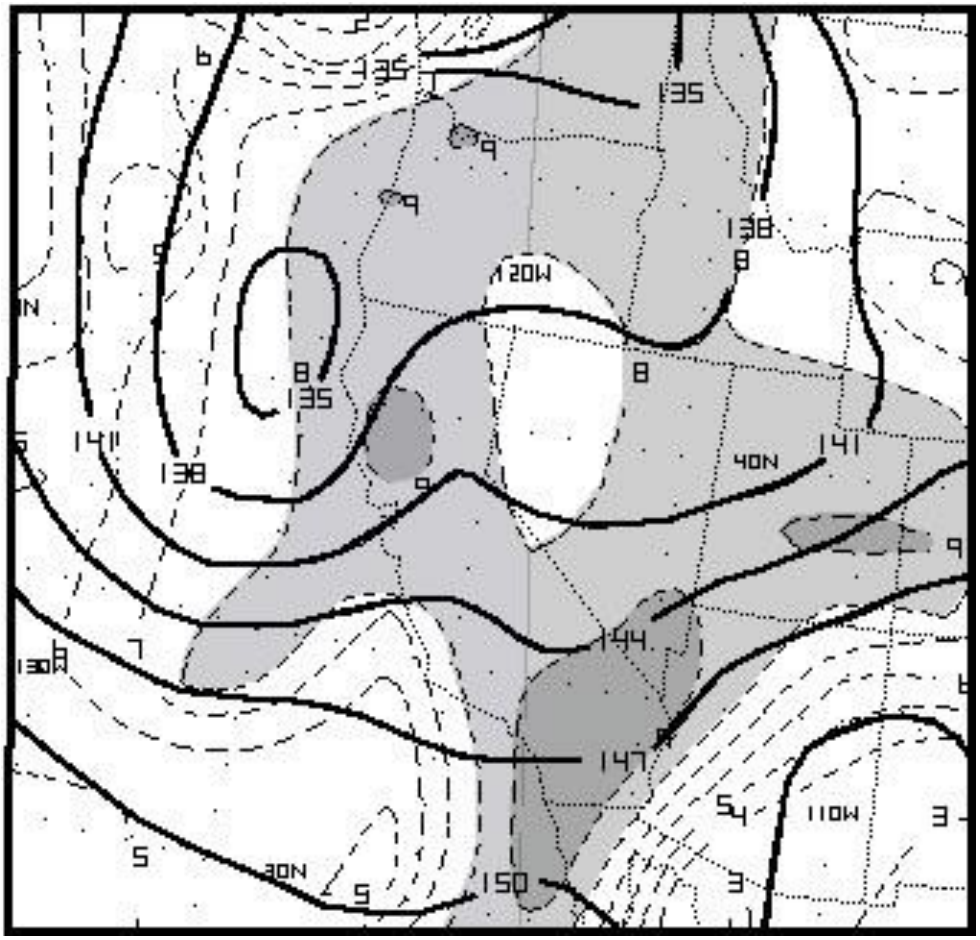

Fig. 3–26. PC-Grids analysis of Eta model 850-mb heights (dam, bold solid) and relative humidity (x 10%, dashed) for 1200 UTC 22 November 1996. Dark shading indicates areas of greater than 90% R.H. and light shading 80%.

convection on infrared satellite imagery (Fig. 3–19; area 2) coincided with the region of strongest upward motions as well.

The vertically-stacked trough, associated upward motion field, and the mid-tropospheric cold pool of air progressed eastward during the early afternoon into the Central Valley. The dynamically induced layer-lifting lowered the Level of

Free Convection (LFC) and increased the efficiency of vertical air parcel accelerations during the hours of maximum sensible heating. This likely initiated the widespread convective outbreak in the Central Valley that included the Lemoore storm at 2300 UTC 22 November 1996 (Fig. 3–27, area 2). Other mechanisms to induce synoptic and/or mesoscale tropospheric lift in Central and Northern California during the afternoon of 22 November included 850-mb CVA, a 850-mb weak warm/cold air advection couplet in Central California (Fig. 3–28;

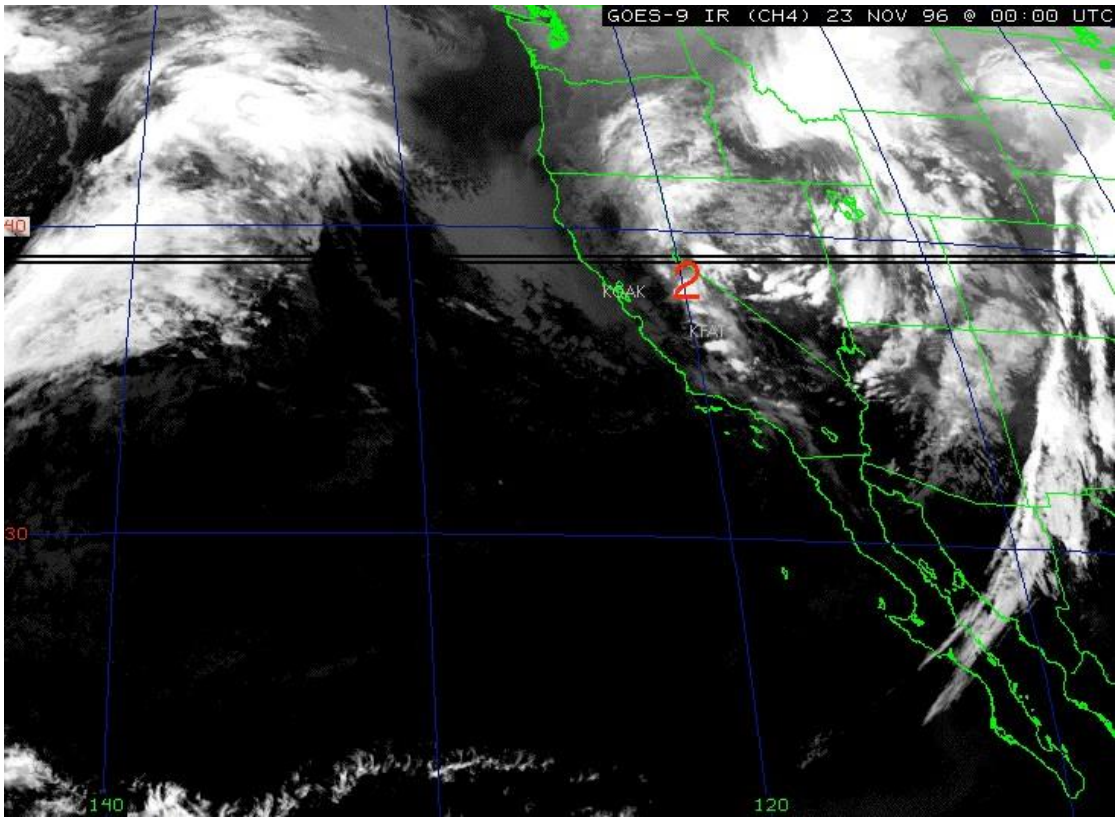

Fig. 3–27. Same as Fig. 3–5, except for 0000 UTC 23 November 1996.

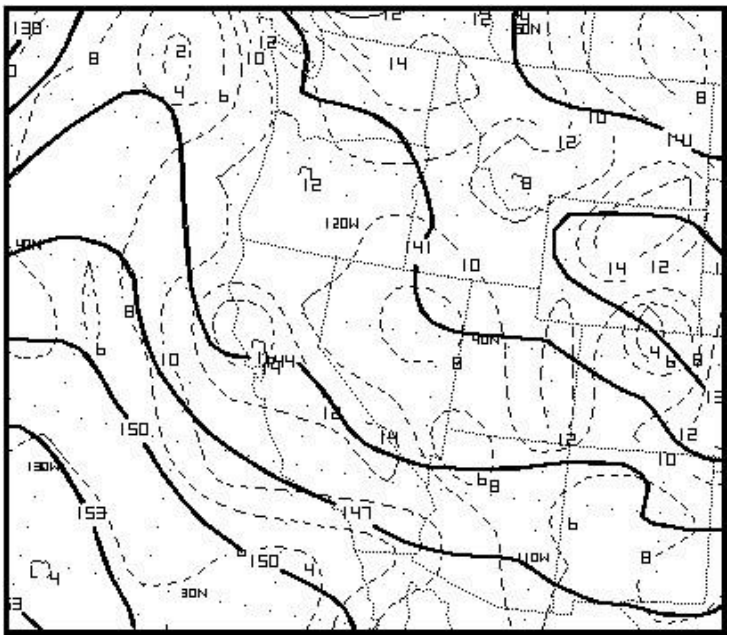

Fig. 3–28. PC-Grids analysis of Eta model 850-mb heights (dam, solid) and absolute vorticity (10^{-5} s^{-1}, dashed) for 0000 UTC 23 November 1996.

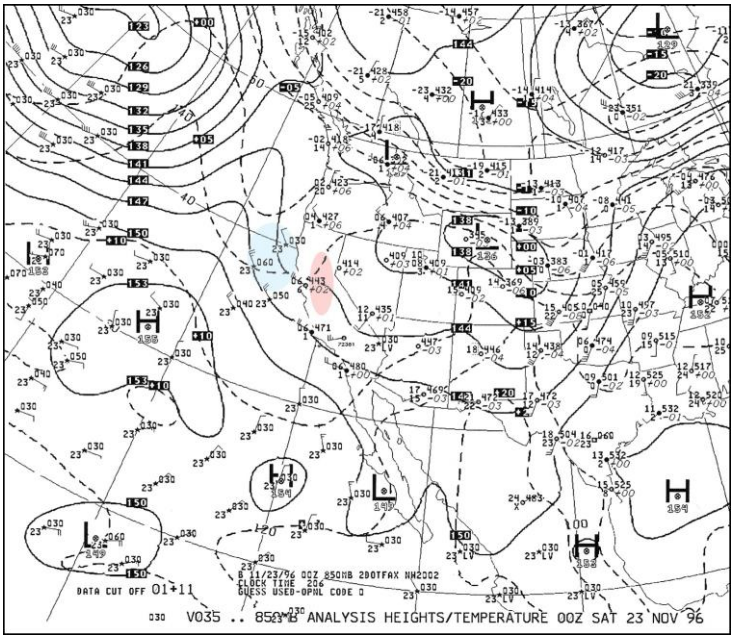

Fig. 3–29. 850-mb NMC analysis for 0000 UTC 23 November 1996. Red shading indicates warm air advection and blue shading cold air advection.

Fig. 3–29, red/blue shading), and in the San Joaquin Valley, possible divergence aloft associated with the left-front quadrant of a 90-knot jet-streak rounding the base of the long-wave trough (Fig. 3–30, JS2).

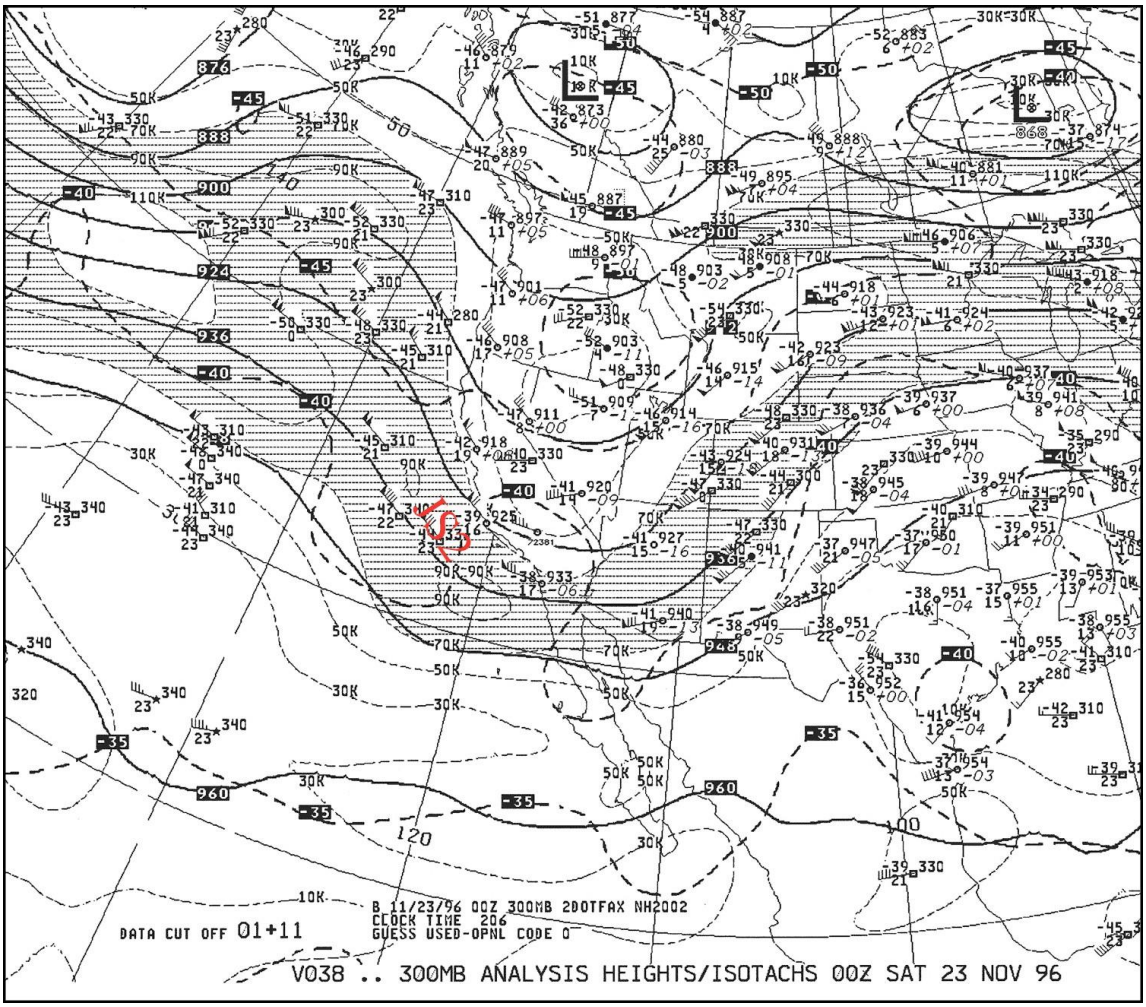

Fig. 3–30. NMC analysis of 300-mb heights (dam, solid), temperature (Celsius, dashed) and winds (x 10 knots, dashed and shaded) for 0000 UTC 23 November 1996. Shading locates winds over 70 knots.

3.2 Buoyancy and Wind Shear Parameters

3.2.1 Sources of Information and Methods

The Skew-T/Hodograph Analysis and Research Program (SHARP) (Hart and Korotky, 1991) was used to construct proximity soundings and hodographs. The “parent” sounding was taken as the 1200 UTC 22 November 1996 Oakland (KOAK) radiosonde. A simulated proximity sounding/hodograph then was created by inserting the observed vector storm motion, data from the Vertical Azimuth Display (VAD) obtained from the Hanford (KHNX) WSR-88D radar, and surface data (T, T_d, vector wind) from Lemoore Naval Air Station (KNLC) at 2227 UTC, the time immediately preceding that of the development of the first tornado

Brooks et al. (1994) summarize the perils associated with trying to define the convective "environment" with a simulated sounding. The pre-convective "environment" is not homogeneous, and once convection gets going, it alters its surroundings significantly. Brooks at al. (1994) make it clear that there are essentially two paths that can legitimately be followed: (1) use the nearest sounding in space and time, subject to some set of criteria about the time-space distance (usually within 6 h and 200 km or so of the event studied), or (2) interpolate upper-air data to the time and space location of the event. Both methodologies merely attempt to estimate the environmental conditions that arise from the synoptic-scale environment rather than attempting to recreate the actual

buoyancy and shear characteristics for the ever-varying microscale environment around the developing storm. Option (1) was utilized this study, as it has in many others in the study of tornadic storms in general (e.g., Davies-Jones et al., 1990; Brooks et al., 1994) and in the study of California tornadic storms in particular (Monteverdi et al., 2003).

There was a dual purpose for using the 1200 UTC OAK sounding rather than that of 0000 UTC 23 November 1996. By 0000 UTC, the major synoptic scale trough had passed Oakland, bringing the San Francisco Bay Area into a different synoptic and thermodynamic environment than existed east of the trough axis. The 1200 UTC sounding sampled the synoptic and thermodynamic environment prior to the passage of the trough and, given the speed of motion of the trough, that pre-storm synoptic environment would have been over the San Joaquin Valley by mid afternoon.

In addition, the author was attempting to verify the utility of simple modification of the morning radiosonde in assessing potential for afternoon convection downstream as a forecasting tool at the time of the event. This methodology has been shown to be very effective in anticipating the nature of Central Valley convection in several studies (Monteverdi and Braun, 1991; Monteverdi and Quadros, 1994; and, Monteverdi et al., 2003). The author also recognizes that other methodologies exist currently, including creating spot soundings using gridded data.

Buoyancy was calculated on the basis of the CAPE of a surface lifted parcel (SBCAPE) and wind shear parameters were calculated from the hodographs. Surface-based superadiabatic layers that appeared were eliminated by assuming dry adiabatic conditions from the surface temperature to the intersection with the original sounding.

Wind shear parameters calculated included storm relative environmental helicity (SREH), bulk Richardson number (BRN) and positive shear for various layers. Positive shear was used in this study instead of other shear measures because of the relationship of positive shear to the vertical perturbation pressure gradient forces, as explained in Section 2.4.

3.2.2 Observed Oakland (KOAK) Sounding

Steep lapse rates in the lower troposphere and an absence of a significant stable layer, consistent with a Miller “Type III” sounding, characterized the 1200 UTC 22 November KOAK sounding (Fig. 3–31). The relatively unstable layer was probably partially linked with the cold air advection related to the passage of the cold front (Fig. 3–12) and subsequent weak post-frontal trough (Fig. 3–9, area 1a). Lapse rates were probably further steepened by the warming that occurred in the lower troposphere due to warm advection, as surface winds backed to southerly. This warm advection is indicated in the hodograph by winds

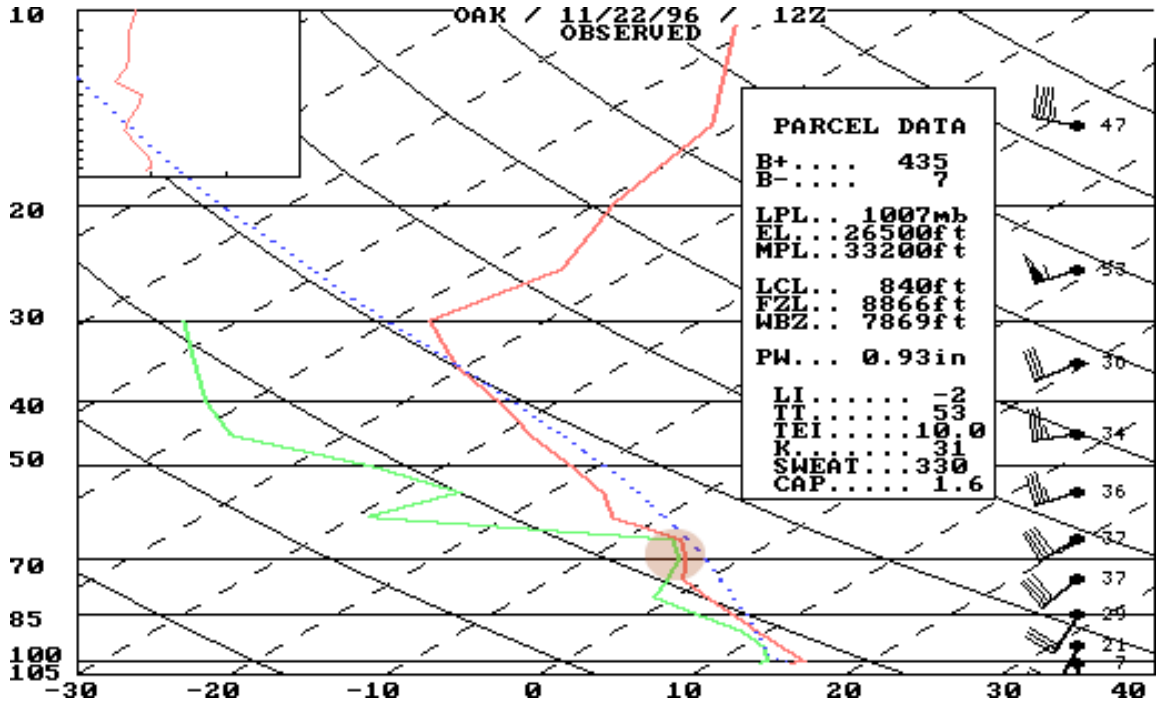

Fig. 3–31. Observed KOAK sounding for 1200 UTC 22 November 1996 produced on SHARP. Dashed blue line shows surface lifted parcel. Numbers next to plotted winds are actual wind speed observations (kts.). Information left of the plotted winds relates to various parameters calculated by SHARP.

veering with height in the layer bounded by the surface and 850 mb. Layer-lifting ahead the second post-frontal trough (Fig. 3–15; Fig 3–19, area 2) associated with this warm advection and differential positive vorticity advection probably accounted for the saturation in that same layer. Additionally, the SBCAPE would have been greater if not for a stable layer (possible frontal layer) between the 750-mb and 650-mb levels (Fig. 3–31, brown shading).

Buoyancy parameters calculated from the KOAK sounding indicate that weak instability was present at 1200 UTC. The 500-mb and 700-mb lifted indices (LI) of –2 ℃ (Table 3–1) were consistent with the SBCAPE of 435 J/kg— a small

buoyancy value, but in the lower to middle range for California storms (Monteverdi et al., 2003). In an environment characterized by such meager buoyancy, thunderstorms would generally be “miniature” in nature. Low topped convection observed elsewhere have been associated with similar CAPE values (Davies, 1993; Stalker et al., 1993; Wicker and Cantrell, 1996; Markowski and Straka, 2000). Furthermore, the equilibrium level (EL) of 8000 meters (26,500 ft) is consistent with the expectation for low-topped storms.

3.2.3 Observed Oakland (KOAK) Hodograph.

The 1200 UTC 22 November Oakland (KOAK) low-level (0–4-km) hodograph (Fig. 3–32) is straight, but is surmounted by a deep layer in which the wind and wind shear vector veers with height. The length of the total wind shear vector was indicative of moderate deep layer shear. Positive shear values for the 0–1-km, 0–3-km, and 0–6-km layers (Table 3–1) are in range with previously observed shear magnitudes in California (Fig. 2–4) for weak tornadic events (F0), but not for F1 or F2 tornadic storms that are usually mesocyclone induced (Monteverdi et al., 2003). According to Monteverdi et al. 2003, even though the (0–6-km) layer positive shear is strong enough for deep mesocyclogenesis, in combination with the low-level shear (0–1-km), the shear in the buoyant inflow

Table 3–1. Convective and rotational parameters on 22 November 1996 for the observed KOAK sounding at 1200 UTC and the proximity sounding for KNLC for 2230 UTC.

Convective/rotational parameter	1200 UTC – KOAK	2230 UTC – KNLC
500-mb LI (°C)	-2	-6
700-mb LI (°C)	-2	-4
CAPE (J/kg)	435	1197
pos. shear (0–1) km ($\times 10^{-3} s^{-1}$)	11.6	14
pos. shear (0–3) km ($\times 10^{-3} s^{-1}$)	6.2	7.8
pos. shear (0–6) km ($\times 10^{-3} s^{-1}$)	3.6	4.3
SREH (0–3) km ($m^2 s^{-2}$)	121	225
BRN	10	15

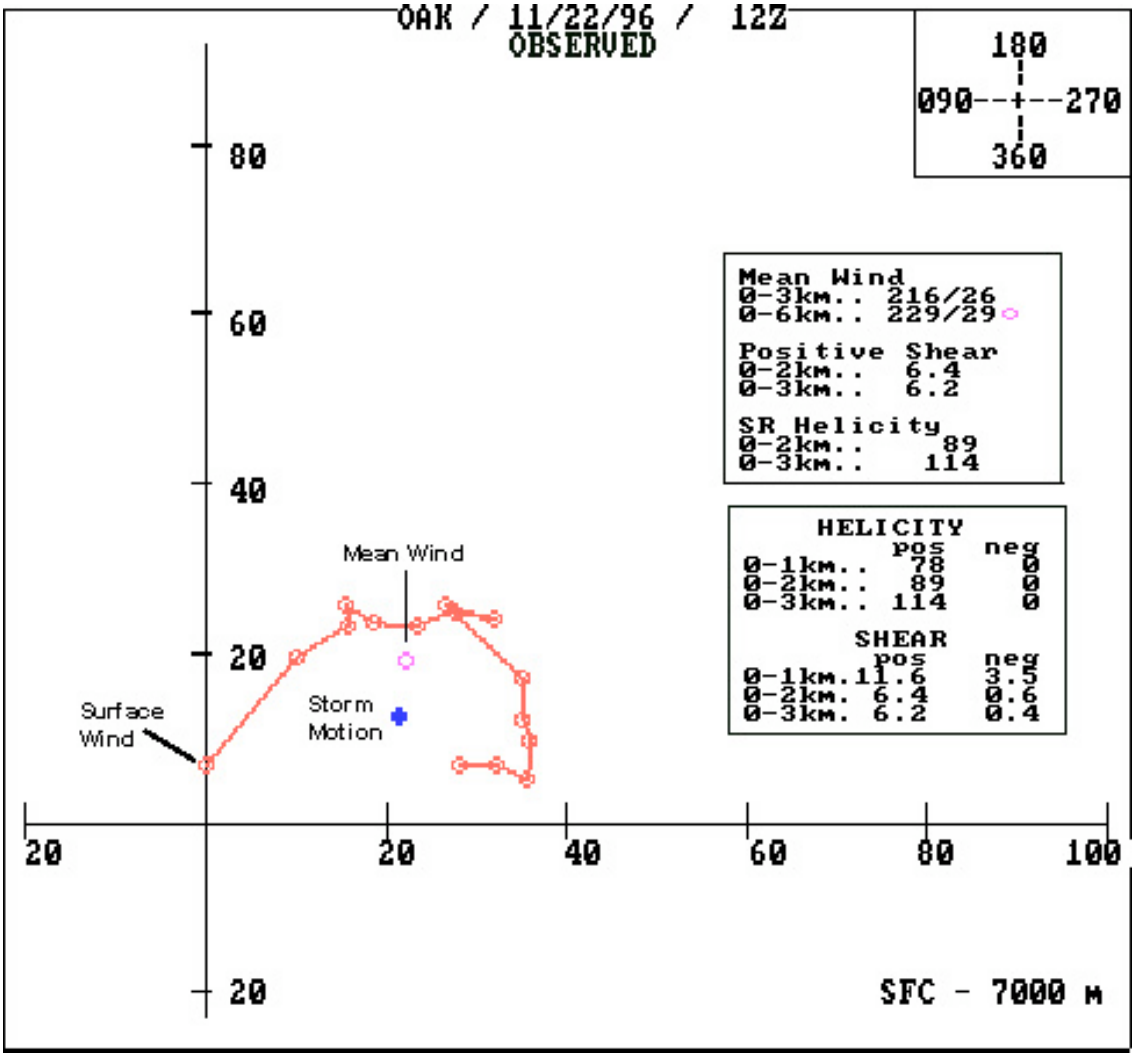

Fig. 3–32. Observed KOAK hodograph (winds plotted at 500-m intervals) for 1200 UTC 22 November 1996 produced on SHARP. Wind shear and helicity information is also shown.

layer is too weak to support a low-level mesocyclone that could produce F1/F2 tornadoes.

The BRN of 10 also suggests that the deep-layer shear is potentially strong enough for supercells (Weisman and Klemp, 1986). More specifically,

modeling and observational studies have shown that convection maturing in such an environment characterized by moderately strong deep-layer shear and a straight low-level wind shear vector is usually associated with left and right moving supercells (splitting storms). In this situation, outflow from neighboring storms often interrupts the supercell cascade process. However, isolated storms could still mature into supercells, but, with the small value of CAPE (435 J/kg) and the low EL [8000 meters (26,500 ft)], the buoyancy and shear combination suggests any deep, persistent mesocyclones would be associated with minisupercells. Tornadoes from such storms would be unlikely since helicity (assuming deviate storm motions) in the lower troposphere (0–3-km = 114 $m^2\ s^{-2}$) and in the inflow layers (0–1-km = 78 $m^2\ s^{-2}$) was small (Davies-Jones et al., 1990; Johns and Doswell, 1992; Davies and Johns, 1993; and Rasmussen and Blanchard, 1998).

The likely mode of organized convection capable of producing a tornado would be multicellular storms that do not contain deep, persistent mesocyclones, but instead, shallow short-lived microscale circulations. These nonsupercellar storms are associated with the majority of the tornadoes observed across California (Blier and Batten, 1994). Storms linked to such tornadoes are often found at the intersection of squall lines containing embedded bowed-segments (Staudenmaier and Cunningham, 1996) and in areas of strong horizontal shear along frontral boundaries (Carbone, 1983). Isolated strong or severe

thunderstorms that ingest pre-existing vertical vorticity fields related to topographic channeling (Blier and Batten, 1994) have also been linked with weak tornado events in California. Cells that intercept and tilt the solenoidal circulations associated with outflow boundaries and/or sea-breeze fronts (Monteverdi et al., 2001) have produced funnel clouds or weak tornadoes as well.

3.2.4 Evolution of Central Valley buoyancy and shear on 22 November 1996

Operational forecasters on the morning of 22 November 1996 examining the thunderstorm probability for the afternoon of 22 November would likely have included a forecast of such storms both at the coast and in the Central Valley based on observations from the 1200 UTC KOAK sounding and hodograph. However, if the meteorologists used the coastal profile as the sole source of data for examining the convective threat for Northern and Central California, the strength of the storms in the interior may have been underestimated.

As shown first by Braun and Monteverdi (1991), the observed KOAK sounding often underestimates buoyancy in the Central Valley because boundary-layer temperatures and dewpoint temperatures often exceed coastal values. The difference is due to greater diurnal heating effects (especially in the warm season) and increased northward transport of low-level moisture from southerly winds that develop in response to a surface trough that often forms on

the lee-side of the Coast Range. Analogously, wind shear in locales east of this quasi-stationary lee-side trough is underestimated by the KOAK wind profile as well since the synoptic scale surface pressure gradient is often more westerly at the coast (Braun and Monteverdi, 1991; Monteverdi and Quadros, 1994; and Monteverdi and Johnson, 1996).

At 1200 UTC 22 November 1996, a synoptic scale trough situated along the West Coast was associated with deep-layer shear profiles that varied little

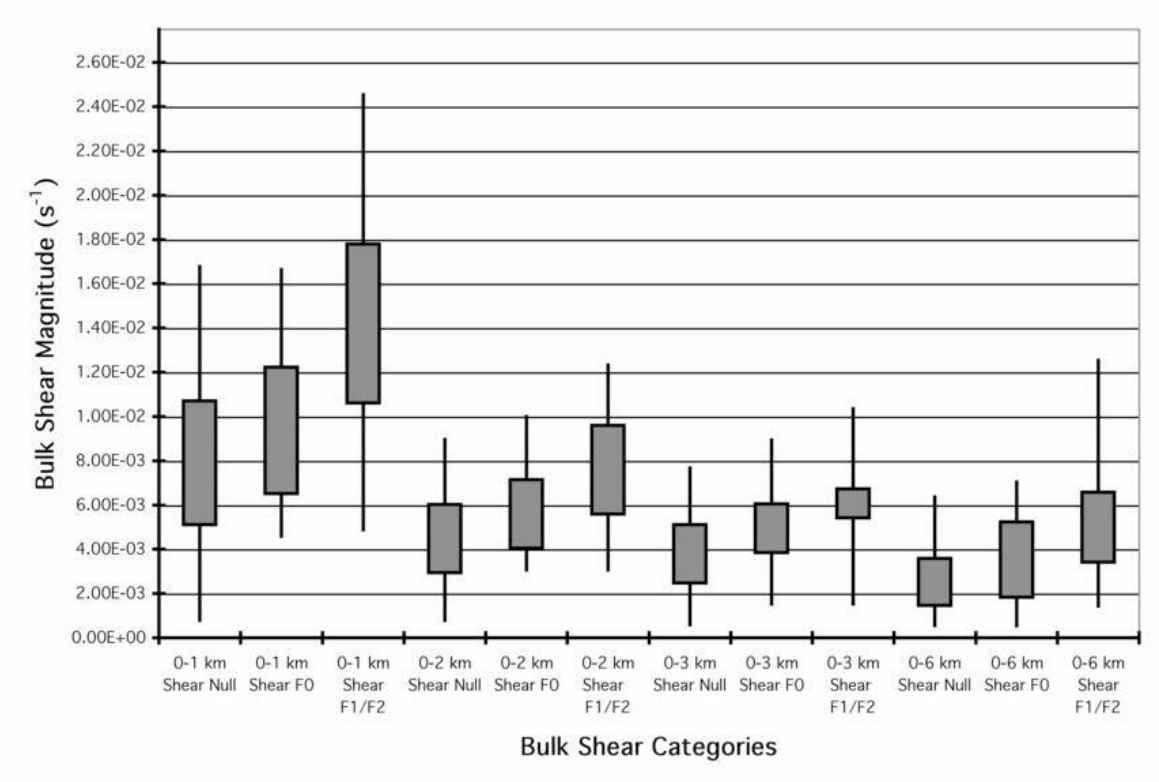

Fig. 3–33. Maximum, 75th and 25th percentile and minimum values of bulk shear observed for the Null, F0 and F1/F2 Bins for various layers (from Monteverdi et. al., 2003).

across the Central Valley. To quickly estimate the strength of the deep-layer shear across the valley, severe weather meteorologists in an operational setting often calculate the magnitude of the shear vector or the bulk shear. This 'back of the envelope' calculation is simply made by subtracting the surface wind from the 500-mb wind (0–6-km layer) to obtain a rough, bulk measure of the shear (Davies and Johns, 1993; Davies, 1996). In the present case, the bulk shear using a 500-mb wind observation (Fig. 3–17) of 35-knots (18 m/s) for both the Sacramento Valley [using Oakland (KOAK)] and the San Joaquin Valley [using Vandenberg (KVGB) or Desert Rock (KDCA)] was 1.9 X $10^{-3}s^{-1}$. According to Monteverdi et al. 2003, this value of bulk shear for California storms is on the low end of the range of observed bulk shear values associated with null tornado cases and on the very low end of the range for cases linked with F0 tornadoes events (Fig. 3–33). Monteverdi et al. 2003 theorized that storms developing in such environments would likely be nonsupercellular due to inadequate deep-layer shear. Even though the observed KOAK 0-6-km positive shear (assuming similar conditions over the valley) is more favorable than the bulk shear regarding the potential for deep persistent mesocyclones, both diagnostic methods indicate the strength of the environmental shear is too weak for the occurrence of supercellular storms to be likely during the morning hours in the Central Valley.

Although there was only minimal variation in the deep-layer shear across the Central Valley, the low-level positive shear was stronger in the Sacramento

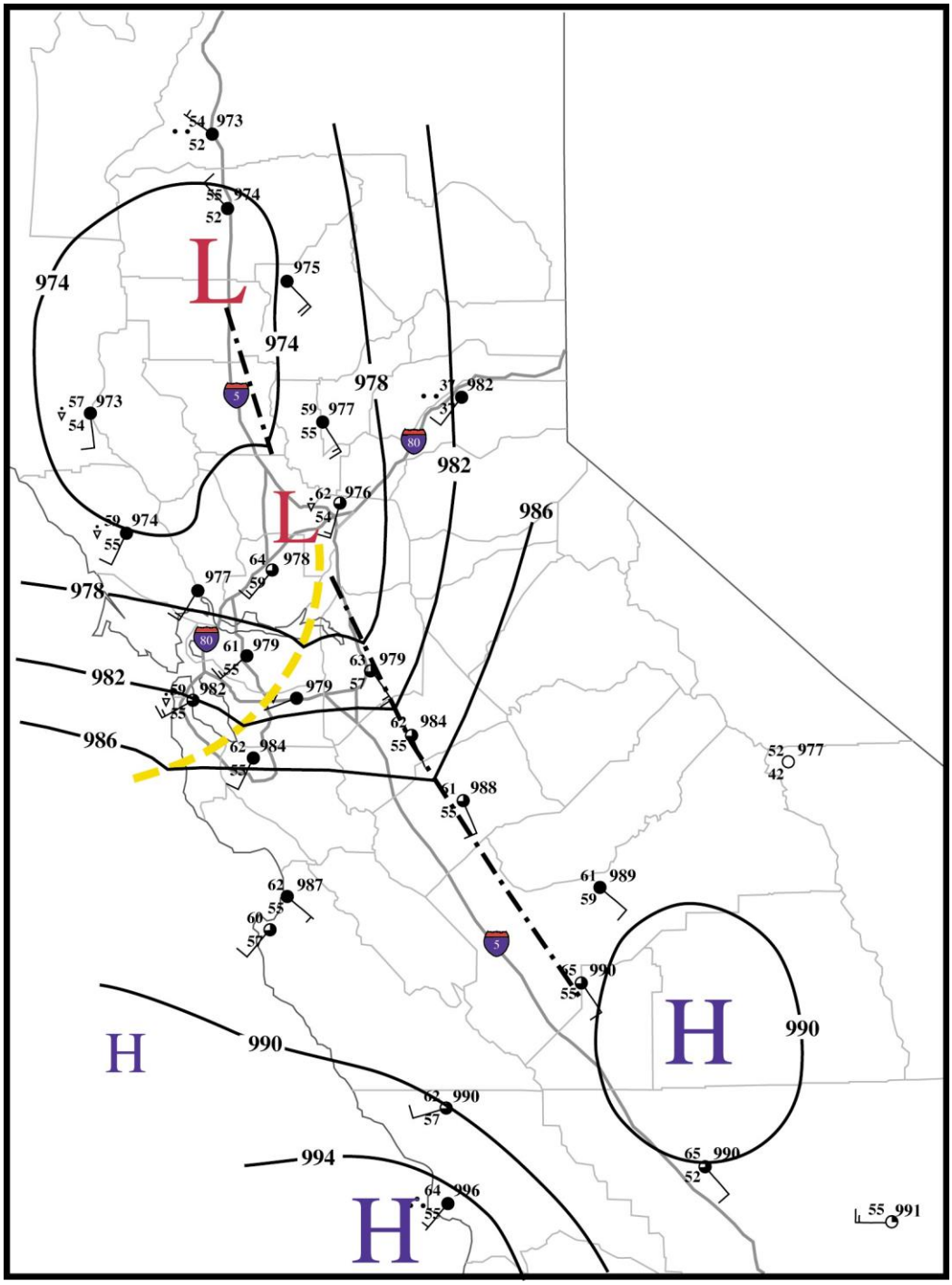

Fig. 3–34. Plot of surface hourly observations for Northern and Central California at 19 UTC (11 PST) 22 November 1996. The position of the lee-side trough/meso-low (hashed) and the post-frontal trough (dashed) is also shown.

Valley due to a synoptic-scale surface low-pressure area along the California coast (Fig. 3–15) and associated north/south surface pressure gradient in Northern California. The combinations of surface south/southeast winds, southwest flow in the lower troposphere (Fig. 3–16), and westerly flow in the middle troposphere (Fig. 3–17) produced a veering vertical wind profile. In the

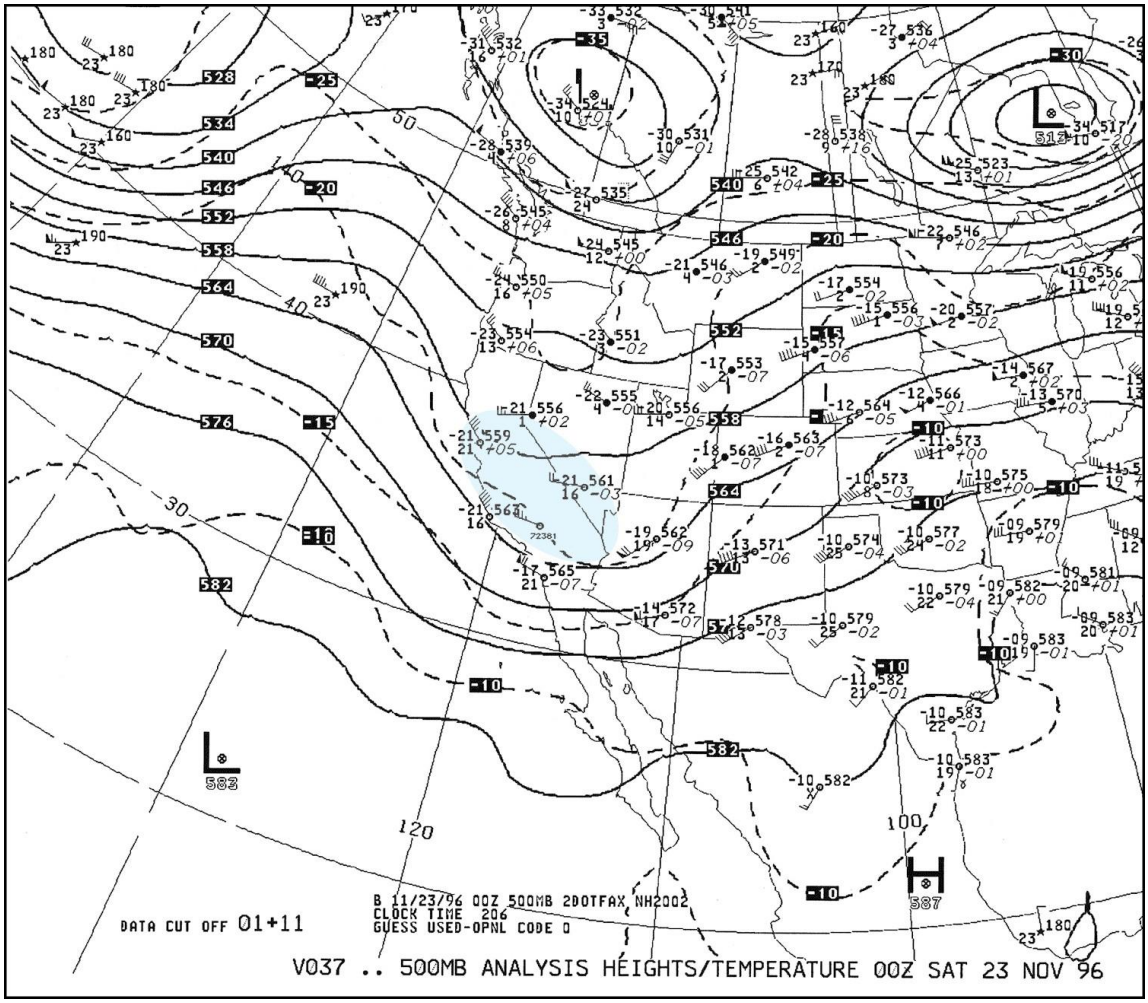

Fig. 3–35. 500-mb NMC analysis for 0000 UTC 23 November 1996. Blue shading indicates position of cold pool.

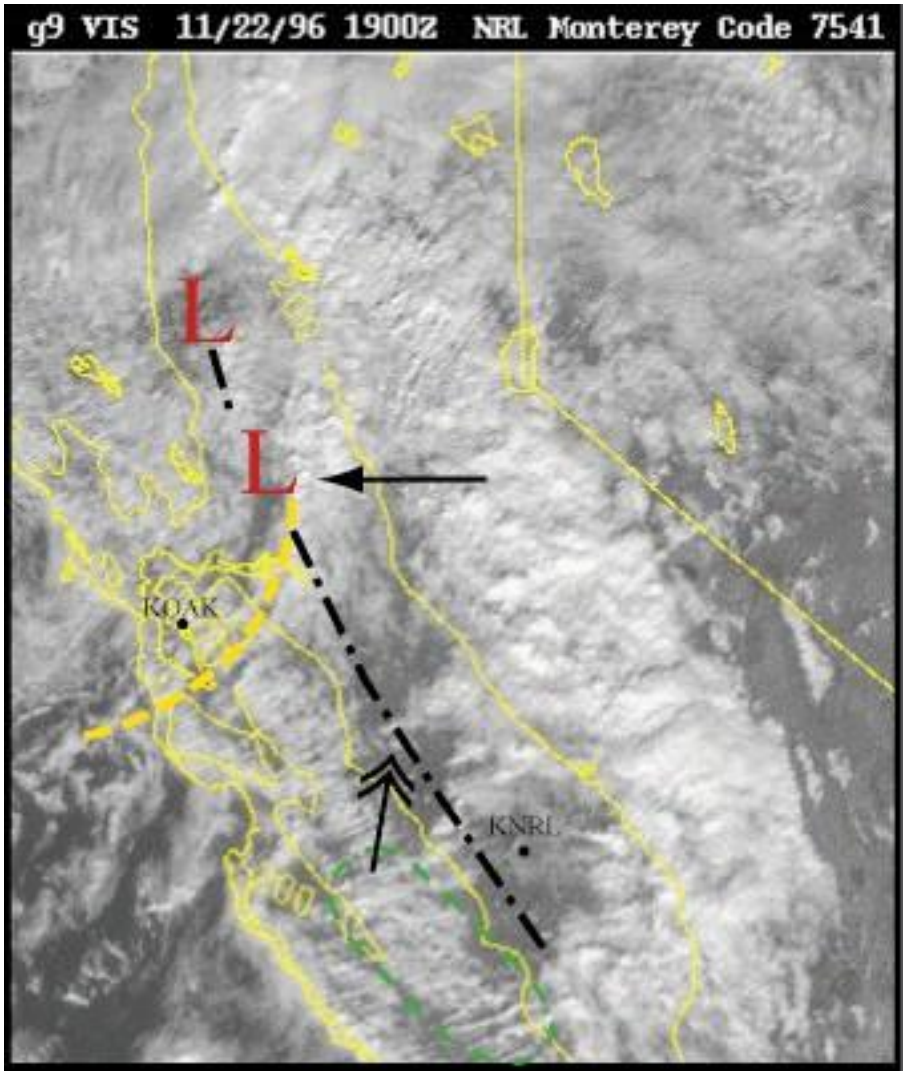

Fig. 3–36. GOES-9 visible satellite image for 1900 UTC 22 November 1996. The position of the lee-side trough/meso-low (black hashed) and the post-frontal trough (yellow dashed) and surface low is also shown. Arrows are discussed in the text.

San Joaquin Valley, the qualitative aspects of the positive shear were less due to the absence of a boundary-layer veer of the wind. Light northerly (not southerly) surface winds (Fig. 3–15) were observed under the influence of a subsidence-

related high-pressure area that developed behind the cold front resulting in a backing vertical wind profile at the lowest levels.

During the late morning and early afternoon hours on 22 November, the buoyancy and vertical shear profiles in the Central Valley evolved under the influence of the approaching trough (Fig. 3–16; Fig. 3–17) and associated upward vertical velocity field (Fig. 3–22, shaded area). Moderate lower and middle tropospheric flow normal to the Coast Range and Sierra Nevada resulted in the formation of a meso-low pressure area in Northern California and a surface lee-side trough that extended into both valleys (Fig. 3–34, black hashed). Areas in the San Joaquin Valley where northerly winds were observed under the influence of the subsynoptic surface high pressure area now reported southerly surface winds. The switch in wind direction was a response to an increasing southerly pressure gradient associated with the deepening terrain-induced meso-low in Northern California (Fig. 3–34) and a low-level convergence zone developing at the intersection of the axes of the lee-side trough and a subsynoptic post-frontal trough entering the valley at 1900 UTC (Fig. 3–34, yellow dashed). Increased moisture convergence focused along this boundary coupled with surface diurnal heating likely lead to decreased static stabilities in the lowest levels of the troposphere. Simultaneously, a cold pool of air in the mid-troposphere (Fig. 3–17, blue shading) advected over the Central Valley (Fig. 3–35, blue shading) that increased lapse rates in those layers and raised the

convective equilibrium level. Additionally, the Central Valley was characterized by strong divergence in the upper troposphere related to the left-front exit region of a jet-streak entering the southern San Joaquin Valley (Fig. 3–30, JS2). The end result was a line of showers and possible thunderstorms (Fig. 3–36, single-headed arrow) that developed in the Sacramento and northern San Joaquin Valley when the lower and middle tropospheric QG related upward motion field associated with the subsynoptic post-frontal trough (Fig. 3–36, yellow dashed) acted on this conditionally unstable environment. In the western areas of the Central San Joaquin Valley near the axis of the lee-side trough, steering flow off the Diablo Range (Fig. 3–36, dashed green circle) likely initiated another line of showers and thunderstorms. One particular thunderstorm on the very southern end of that line of strong convection would eventually become a supercell that caused the Lemoore Storm (Fig. 3–36, double-headed arrow), but it was not a supercell storm yet.

3.2.5 Buoyancy and Shear Environment in the Central Valley

3.2.5.1 Lemoore Naval Air Station (KNLC) Proximity Sounding

A proximity sounding for the Lemoore Naval Air Station (KNLC), shown in Figure 3–37, was created from observations at 2227 UTC 22 November that is near the time of tornado genesis of the Lemoore storm. Operational forecasters

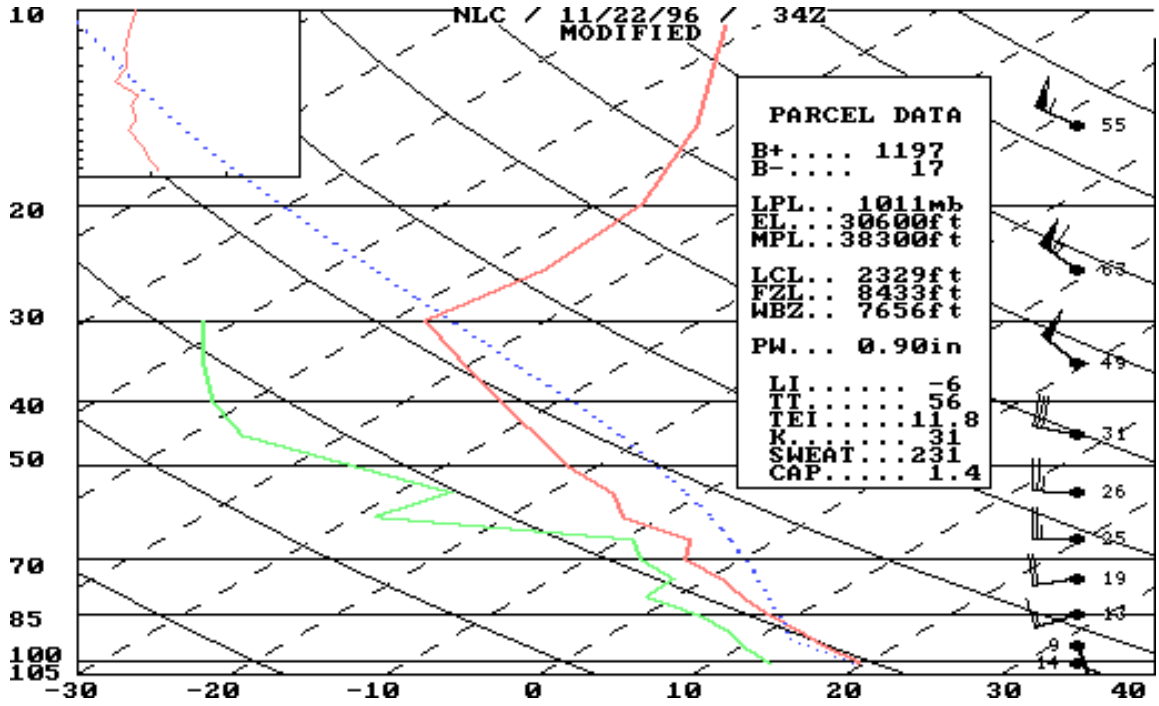

Fig. 3–37. Same as Fig. 3–17, except simulated KNLC sounding.

would likely notice the sounding showed a substantial increase in instability versus the observed KOAK sounding (Table 3–1) from the morning. The increased buoyancy would result in the development of much deeper storms in the San Joaquin Valley than the coastal sounding from the morning would have suggested. Factors related to this increase include efficient sensible heating into the early afternoon due to minimal cloud cover and moisture convergence along the lee-side trough associated with southerly surface winds advecting warm moist air northward. Surface and dewpoint temperatures at 2200 UTC at KNLC increased to 20 ℃ (68 ℉) and 13.8 ℃ (57 ℉) respectively, about 4 ℃ and 1 ℃

warmer than coastal locales. Likewise, CAPE values also increased to 1197 J/kg from 435 J/kg (See Table 3–1 for comparisons with other buoyancy indices as well). This value of CAPE was consistent with those observed with previous severe California thunderstorms cases and was near the upper range for storms in California during the cold season (Braun and Monteverdi, 1991; Monteverdi and Quadros, 1994; Monteverdi and Johnson, 1996).

3.2.5.2 Shear in the Central Valley in the afternoon of 22 November

Supercells, and especially tornadic supercells, occur in environments characterized by moderate to strong deep-layer [i.e. (0-6-km)] shear. Significant deep-layer shear is often indicative of substantial mid- to upper-level winds necessary to sustain a long-lived updraft through the advection of precipitation downstream (prevents “drowning” of the updraft) (Moller et al., 1994). In addition, supercells that mature in such an environment often produce non-hydrostatic vertical perturbation pressure forces that can augment updraft strength and produce a deeper storm, especially in low buoyancy settings.

The evolution of the deep-layer wind shear in the Central Valley on the afternoon of 22 November was influenced by a 90-knot jet-streak (Fig. 3–18, JS2; Fig. 3–30, JS2) entering the base of the long-wave trough about 600-km (400-mi) south of the parent upper-tropospheric low in Northern California. Due

to the southern trajectory of the jet streak, the San Joaquin Valley, but not the Sacramento Valley, was a region characterized by enhanced deep-layer (0-6-km) shear. Deep-layer bulk shear values using 500-mb wind observations from 0000 UTC 23 November (Fig. 3–35) of 25-knot (13 m/s)[for the Sacramento Valley using Reno (KRNO) and Medford (MFR) observations] and 45-knot (23 m/s) winds [for the San Joaquin Valley using Vandenberg (KVBG)] are 1.4 X $10^{-3}s^{-1}$ and 2.5 X $10^{-3}s^{-1}$ respectively. Monteverdi et al. 2003 found that (0-6-km) bulk shear values for California storms under 2.0 X $10^{-3}s^{-1}$ are associated with non-tornadic storms, but a shear of 2.5 X $10^{-3}s^{-1}$, although near the lower end of the threshold bin, has been observed with other F0 tornadic thunderstorms (Fig. 3–33). Observational studies conducted outside of California have identified bulk wind shear values that can be used to forecast the threat of tornadic supercells (Davies, 1996; Stensrud et al., 1997). Shear magnitudes in the 0–6-km layer in a low-buoyancy environment (~1000 J/kg) of 15 m/s (30-knots) and 23 m/s (45-knots) were found to be the minimum necessary and the most optimal velocities at 6-km, respectively, to generate enough deep-layer shear to support supercells with tornadic potential (Davies and Johns, 1993; Davies, 1996; Stensrud et al., 1997). The findings in these studies suggests that in the San Joaquin Valley *only* was there sufficient wind shear for the development of a deep long-lived mesocyclone that could support a F0 or stronger tornado.

With the increase in deep-layer shear during the early afternoon hours, the shear environment in the San Joaquin Valley, not the Sacramento Valley, evolved into a setting where non-severe convection could mature into severe multicellular and/or supercell storms capable of producing damaging straight-line winds, large hail, and weak short-lived tornadoes. However, maturing supercells that develop a near ground mesocyclone and possibly a F0 or stronger tornado need to evolve in an environment of substantial low-level (i.e. 0–1-km) positive shear. As a measure of that, low-level storm relative environmental helicity (SREH) indicates the degree to which ingested air will have large values of streamwise vorticity that could be tilted vertically by a convective updraft to produce low-level rotation. Large values of SREH are associated with a wind shear vector with significant anticyclonic curvature in the lowest layers on the hodograph. Furthermore, for the conditions on this day, a veering low-level wind shear vector would ensure that the cell on the right-flank of the spitting supercell would be favored for further development and more importantly, if that storm was the southernmost cell on a line of storms or simply isolated, the deviate movement of that cell would limit interactions with other convective outflows in the area that could terminate the supercell cascade process.

3.2.5.3 Lemoore Naval Air Station (KNLC) Hodograph

A transformation in the low-level vertical shear profile in the San Joaquin Valley occurred when the meso-low developed in the Northern Sacramento Valley and the associated lee-side trough in the Central Valley. The lower tropospheric wind field in the San Joaquin Valley evolved from a backing to a veering vertical profile when the winds shifted from northerly to southerly in response to surface pressure falls related to the meso-low and lee-side trough.

The change in the near surface wind field was also reflected in the shape of the hodograph for the San Joaquin Valley. The low-level curvature and total length of the vertical wind shear vector was quite different compared to the observed morning KOAK hodograph that operational forecasters would possibly use as a basis for their forecast in the valley in the afternoon. The hodograph (Fig. 3–38) for KNLC (and the Lemoore Storm) created from the KHNX Vertical Azimuth Display (VAD) (Fig. 3–39) wind profile at 2234 UTC (the time of tornado genesis) was still essentially straight, but had longer length and low-amplitude anticyclonic curvature in lowest 2.5-km, although the lack of a significant low-level jet stream (winds < 20 knots below 2.5-km) limited that curvature. The weakly curved hodograph in the lowest layers versus that observed with the Oakland (KOAK) hodograph was related to more southerly surface winds at KHNX. Without the subsynoptic influences (i.e. meso-low and lee-side trough),

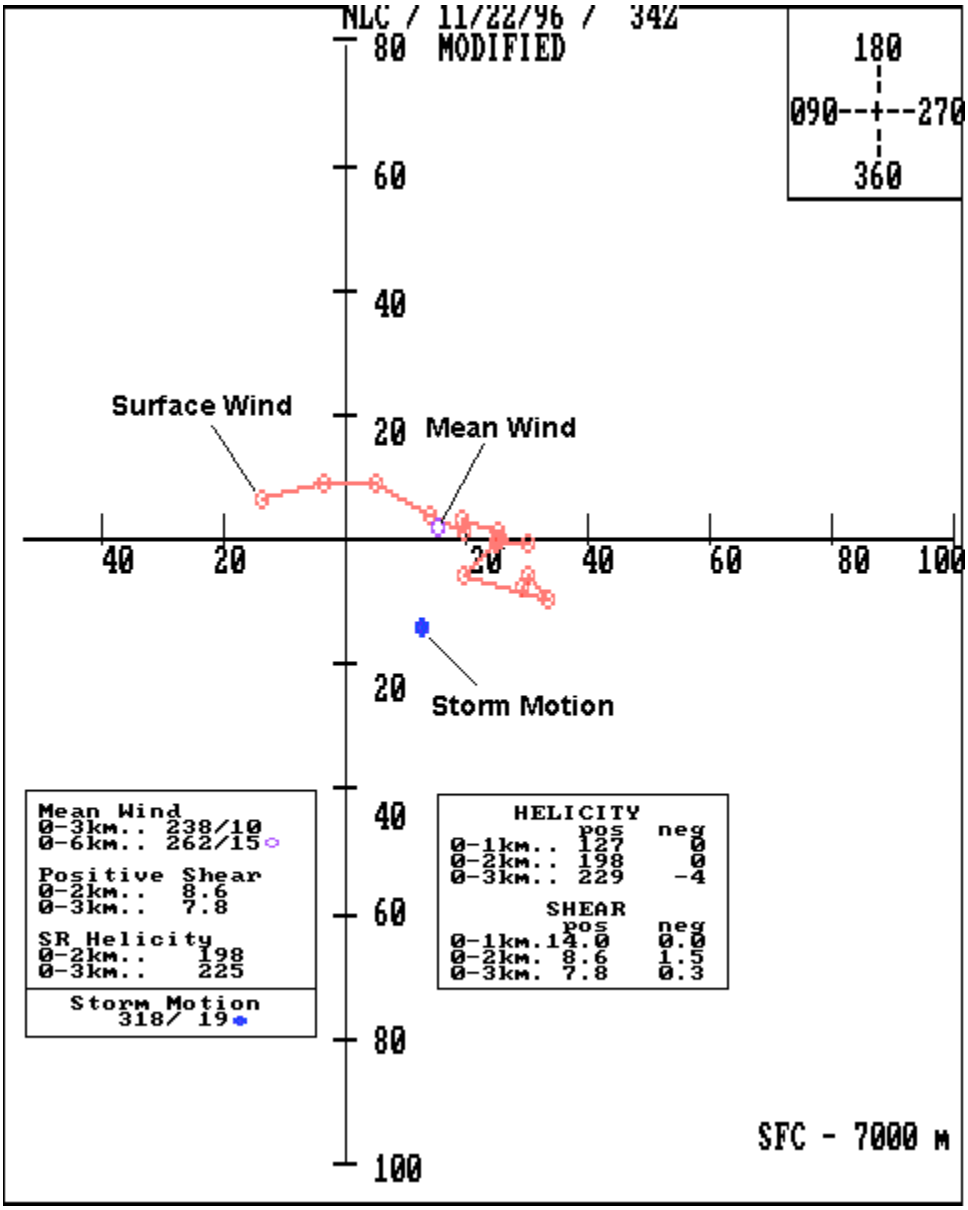

Fig. 3–38. Same as Fig. 3–18, except for KNLC using KHNX VAD wind profile (Fig. 3–39) at 2234 UTC 22 November 1996.

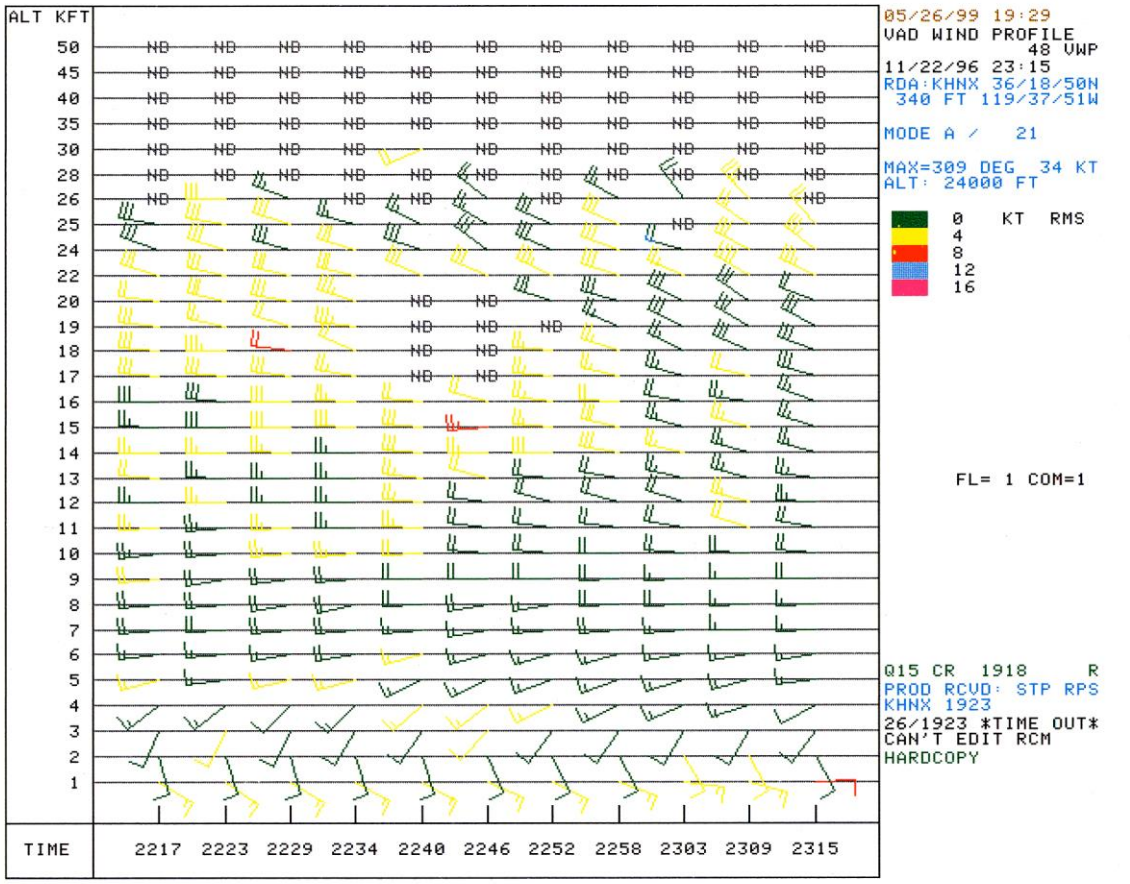

Fig. 3–39. VAD wind profile from KHNX at 23:15 UTC 22 November 1996. Green wind plots indicated high, yellow medium, and red low confidence in accuracy of Doppler wind observations.

the surface winds along the coast were controlled by synoptic-scale pressure gradients that were generally southwesterly.

The convective and rotational parameters associated with the KNLC hodograph suggests a higher supercell potential in the San Joaquin Valley then in the coastal regions. Positive wind shear increased at all levels in comparison

with the rotational indices derived from the 1200 UTC 22 November KOAK wind profile (Table 3–1). The increase in lower-tropospheric shear (0–1-km, 0–2-km, 0–3-km) was related to an increase in the veer of the boundary-layer wind field. The higher value of 0–1-km positive shear was due to a strongly backed surface wind at Lemoore Naval Air station (KNLC). With the strong shear at the lower levels, storms developing in such layers (below 600-mb) are often associated with dynamic perturbation pressure forces that can augment buoyancy in those same layers and increase the potential for a strong convective updraft.

Shear parameters associated with the KNLC wind profile were in range with previously observed mesocyclone-induced tornadic storms in California and elsewhere. According to Johns et al. 1993, observations of other cold-season tornado cases in other parts of the country suggest that 1000 J/Kg CAPE needs to be associated with a 0–2-km positive shear of 10.0 X $10^{-3}s^{-1}$ for the development of a strong mesocyclone. The KNLC shear was near this threshold at 8.6 X $10^{-3}s^{-1}$. Lipari and Monteverdi (2000) and Monteverdi et al. (2000) found a similar relationship between very low-level (0–1-km) shear and CAPE related to tornado intensity in California. The moderate buoyancy and the 0–1-km positive shear associated with KNLC hodograph was above the mean values observed with other F0 tornadoes and at the lower end of the bin for F1 and F2 tornadic storms in California (Fig. 2–3) (Monteverdi et al., 2000). The best fit in the box and whisker plots for 0–1-km positive shear magnitudes (Fig. 2–4) is the F1/F2

bin, although the value was near the low end of the range. This correlates well with the higher potential for the development of a low-level mesocyclone and tornado potential that is suggested from the values of 0–3-km and 0–1-km SREH. SREH in the 0–3-km layer increased to 225 $m^2\ s^{-2}$ and is not only in the range for mesocyclones (~150 $m^2\ s^{-2}$), but also for the genesis of weak mesocyclonic produced tornadoes (151-299 $m^2\ s^{-2}$) (Davies-Jones et al., 1990; Johns and Doswell, 1992; and Davies and Johns, 1993). SREH in the 0–1-km inflow layer increased from 78 to 127 $m^2\ s^{-2}$ as well. An increased threat of tornadic supercells has been associated with 0–1-km SREH values greater than 100 $m^2\ s^{-2}$ (Rasmussen and Blanchard, 1998). However, it should be noted that with SREH, larger is generally better, but there are no clear "signals" between non-tornadic and significant tornadic supercells.

A small increase in the deep-layer (0-6-km) positive shear (Table 3–1) can be attributed to the upper tropospheric jet streak over the San Joaquin Valley (Fig 3–30). Numerical studies and observational cases outside of California suggest 4.3 X $10^{-3}s^{-1}$ positive shear is high enough for the occurrence of deep mesocyclones (Weisman and Klemp, 1982; Johns et al., 1993; Moller et al., 1994). Additionally, the BRN of 15 was in the range (15–45) for documented supercells in a moderately buoyant environment (CAPE ~ 1500 J/kg)(Weisman and Klemp, 1986). In regard to California cases, the deep-layer (0-6-km) positive

shear was near shear magnitudes associated with F0 tornadoes, but less than values observed with F1/F2 cases (Fig. 2–4) (Monteverdi et al., 2003).

Rotational indices associated with the KNLC hodograph strongly suggest that wind shear was sufficient for a mesocyclonic supercell in the San Joaquin Valley and that other short-lived supercells likely occurred on 22 November 1996 as well. Specifically, numerical modeling studies have shown that for the mostly straight 0–6-km wind shear vector on the KNLC hodograph that a splitting convective updraft would likely develop and that neither the cyclonic nor the anticyclonic cell would be favored (Weisman and Klemp, 1986). WSR-88D Doppler radar base reflectivity from KHNX showed this might have been the case north of the Lemoore storm (Fig. 3–40, letters A and B-splitting storms). The end result would likely have been right- and left-moving supercells if the cascade process had not been interrupted possibly due to outflow from the Lemoore storm to the south.

Satellite and radar evidence (shown later) though, indicate that the storm motion of the Lemoore storm was to the right of the mean wind vector. Right-moving supercells with the deepest and strongest mesocyclones are associated both in observational and modeling studies with an anticyclonically curved hodographs coupled with moderate to strong deep-layer environmental shear. In these cases, the cyclonic cell of a splitting convective updraft is favored and the anticyclonic cell subsequently suppressed due to shear-induced vertical

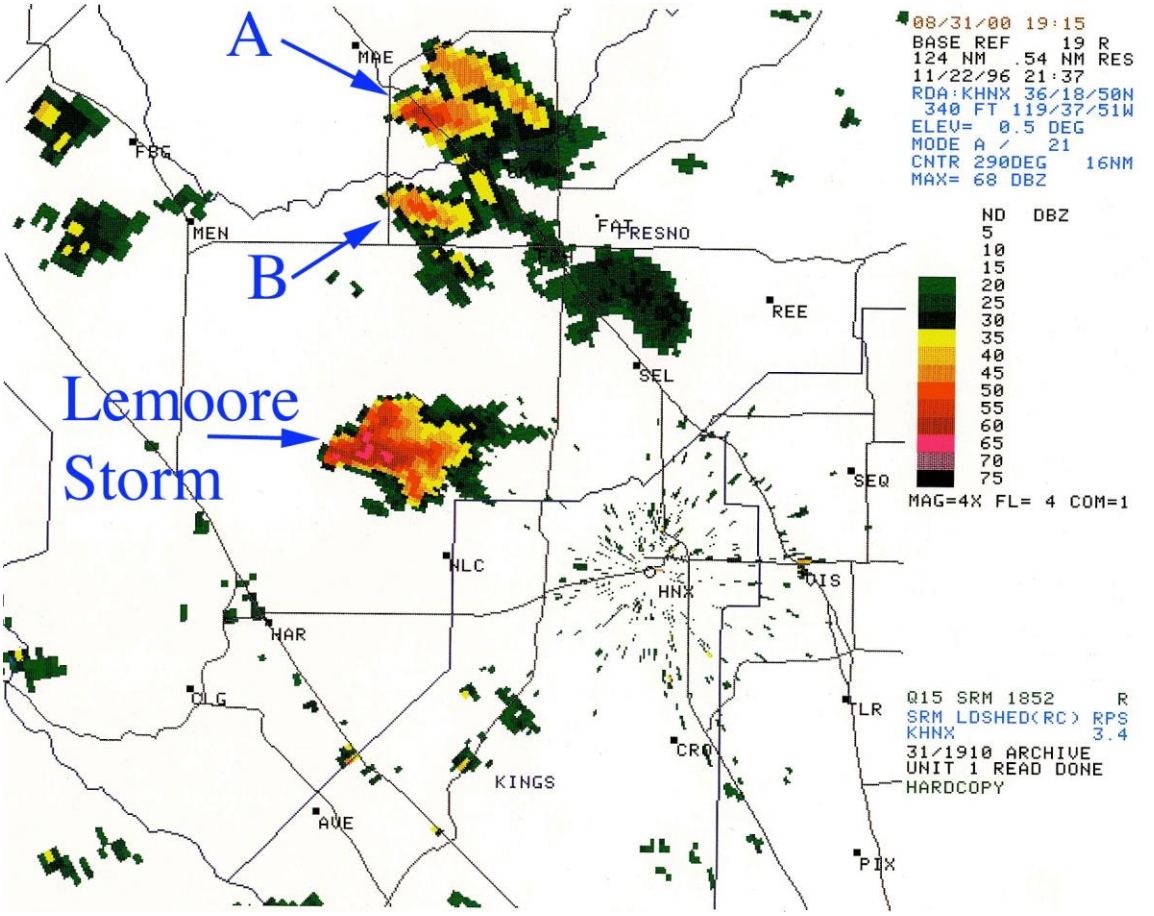

Fig. 3–40. KHNX WSR-88D Doppler base reflectivity for 21:37 UTC 22 November 1996. Letter and labeling refer to items discussed in the text.

perturbation pressure forces. This acts to promote continuous updraft growth on the right flank of the cyclonic cell and leads to deviate storm movement. Although the veer in the low-level wind shear vector was minimal, enough positive shear was present to initiate the process described above and cause the movement of the Lemoore storm to be off the hodograph (Fig. 3–38).

3.2.6 Large-scale Pattern in Comparison to Schematic Pattern (SP)

This evolution of the buoyancy and shear profiles in the Central Valley on 22 November 1996 as related to the synoptic and subsynoptic features was similar to previous patterns that resulted in tornado occurrences in California. Operational forecasters often find synoptic-scale pattern recognition useful as a “first” signal that buoyancy and shear profiles in the Central Valley may progress into a setting that is supportive of severe convection. Important synoptic and subsynoptic features within the schematic pattern (SP) in Fig. 2–2 closely resemble the large-scale pattern on 22 November 1996.

Similar synoptic features with SP include a broad long-wave trough in the middle and upper troposphere associated with a polar branch of the jet stream, multiple lower and middle tropospheric short-wave troughs embedded in that flow, and the initial progressive short wave trough was linked with the passage of a cold front. Subsequent moderate to strong lower and middle tropospheric flow against the Coast Range related to the approach of the parent upper-tropospheric trough and a lower to middle tropospheric short-wave (linked with a mobile post-frontal subsynoptic surface trough) resulted in the formation of a meso-low and lee-side trough in the Central Valley. The surface subsynoptic trough was associated with upward vertical motions in the middle troposphere that resulted in convection in the post-frontal unstable air mass.

However, according to the SP model, supercell thunderstorm formation is most likely at the intersection of the mobile short-wave trough, the lee-side trough, and the divergent quadrant of an upper-tropospheric jet streak that is usually associated with the progressive short-wave trough. At this location, the combination of buoyancy to both low-level and deep-layer shear is the most favorable for supercell thunderstorms. This did not exactly occur in association with the Lemoore Storm on 22 November 1996 since the locations of these focus features were not phased as in the SP archetype. The intersection of the mobile short wave and lee-side trough was farther north (Fig. 3–34) than the location of the strongest deep-layer shear associated with the jet streak (Fig 3–30). Subsequently, the Lemoore supercell developed about 100-km (68 mi) south of that intersection (Fig 3–36. double arrow) in the region of stronger deep-layer shear.

4. The Evolution of the Controls on the Subsynoptic Environment

Subsynoptic analyses using hourly surface observations supplemented with high-resolution satellite and radar images are effective ways to identify meso-scale features that are important for the development or diminution of severe convection (Doswell et al., 2002). These features are often difficult or impossible to discern on larger-scale synoptic surface charts. Progressive subsynoptic-scale surface troughs and low-pressure areas, terrain-induced convergence zones, convective outflows, and meso-scale cloud-free or stratiform overcast regions are a few examples of elements that can be distinguished on the basis of a thorough examination of surface and satellite data.

Detailed subsynoptic analyses combined with thoughtful consideration of buoyancy and shear data by an operational forecaster can be used to suggest a mesoscale or subsynoptic focus for thunderstorm development in the Central Valley of California (Monteverdi and Quadros, 1994). Focus areas often see localized changes in either/both the thermodynamic environment and wind shear profile conducive for the development of supercell structure or mesocyclogenesis in non-supercell storms. For example, the supercell linked with the 1986 F2 Vina tornado event developed at the intersection of a progressive subsynoptic surface trough and a terrain-induced convergence zone (i.e. Coast Range lee-side trough) (Braun and Monteverdi, 1991). This region is usually associated

with increased moisture convergence and stronger deep-layer/low-level wind shear. Moisture convergence leads to increased boundary-layer instability (i.e. higher CAPE), and in combination with the strength of the deep-layer shear, determines storm type (a.k.a. BRN). The stronger low-level shear then increases the possibility for a mature thunderstorm (supercellular or nonsupercellular) to become tornadic. Tornadic supercells are most likely to form in the region with the strongest deep-layer and low-level shear, independent of the SBCAPE, as long as a minimal amount of instability is present. There is no relationship between buoyancy magnitude alone and the potential for thunderstorms to become tornadic in California (Monteverdi et al., 2003).

Observational studies conducted outside of California have found that tornadoes also occur when mature thunderstorms (supercellular and non-supercellular) come into contact with localized shear boundaries and/or solenoidally-induced circulations (Maddox et al., 1980; Markowski et al., 1998; Atkins and Weisman, 1998). For example, subsynoptic or mesoscale low-level baroclinicity generation can be found along the boundaries of convective outflows, sea-breeze fronts, anvil shadows, and areas of localized high-isolation. Such circumstances have lead to the formation of tornadic storms in California as well when updrafts tilt and stretch inflow air latent with solenoidally-generated vorticity (vortex tube stretching) that in turn strengthens low-level updraft rotation (Carbone, 1982, 1983; Staudenmaier, 1995; Monteverdi et al., 2001).

4.1 Sources of Information and methods

For this case study, surface subsynoptic analyses were subjectively completed for the afternoon hours on 22 November 1996 using Meteorological Terminal Aviation Reports (METAR) from sites in Northern and Central California obtained from NCDC. This data was supplemented with WSR-88D radar base-reflectivity data from KHNX for the same times. In addition, high-resolution visible satellite imagery attained from the Marine Meteorology Division of the Naval Research Laboratory (NRL) in Monterey California was also used to identify cloud features and cloud coverage.

4.2 Formation stage of the Lemoore Storm

At approximately 1900 UTC (1100 PST local time), a surface trough (Fig. 3–33) associated with a synoptic-scale upward motion field (Fig 3–22) was entering the southern Sacramento and northern San Joaquin Valleys. The trough was generally moving southeastward and at 2000 UTC (1200 PST) the low-pressure center was near Sacramento (KSAC) with the trough axis aligned northeast to southwest across the northern San Joaquin Valley (Fig. 4–1). Surface pressure falls along the trough axis in combination with a subsynoptic area of high pressure in the southern San Joaquin Valley produced a tight

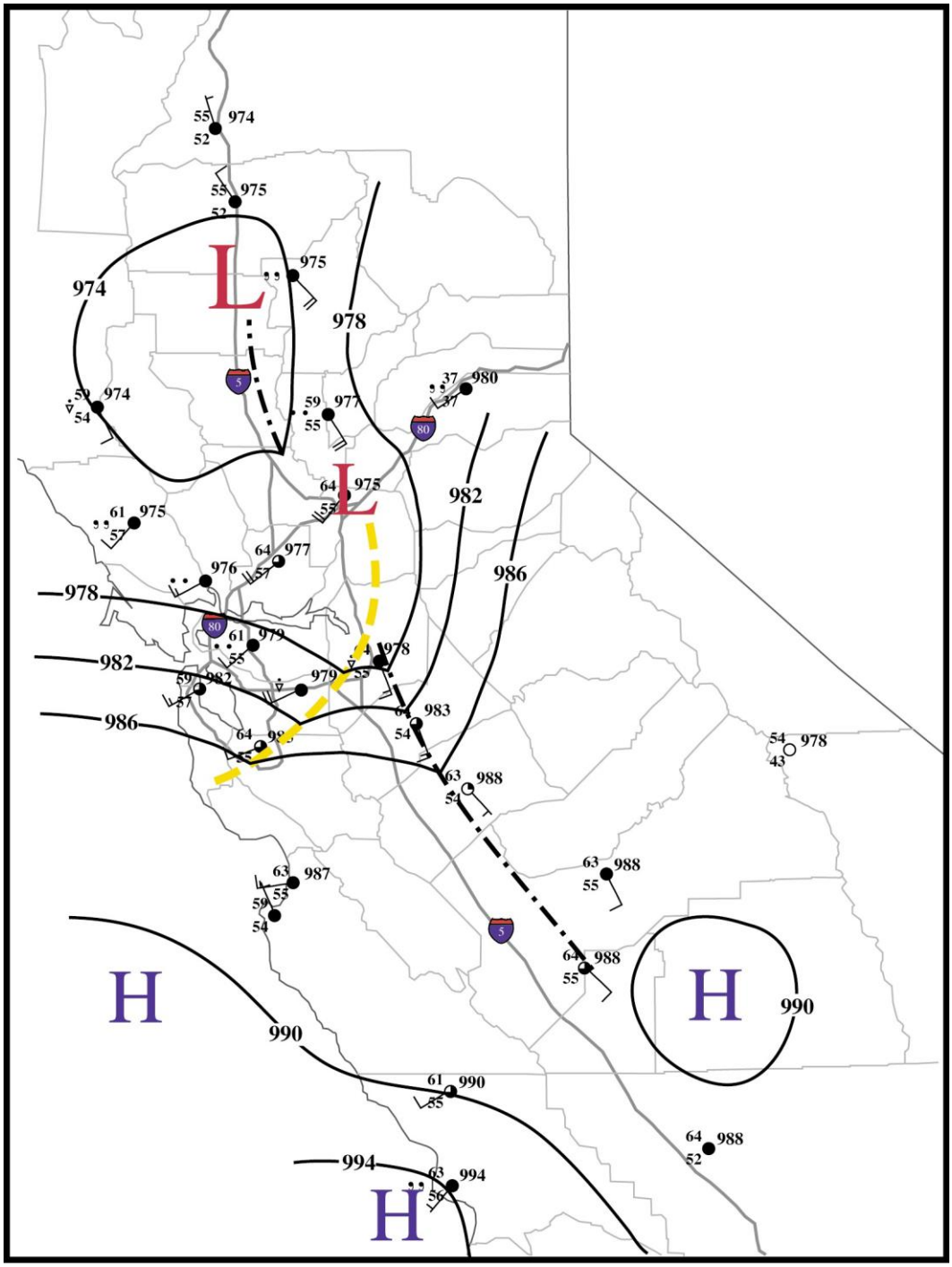

Fig. 4–1. Surface hourly observations for Northern and Central California valid at 2000 UTC (1200 PST) 22 November 1996. The positions of the lee-side trough/meso-low (hashed) and the post-frontal trough (dashed) are also shown.

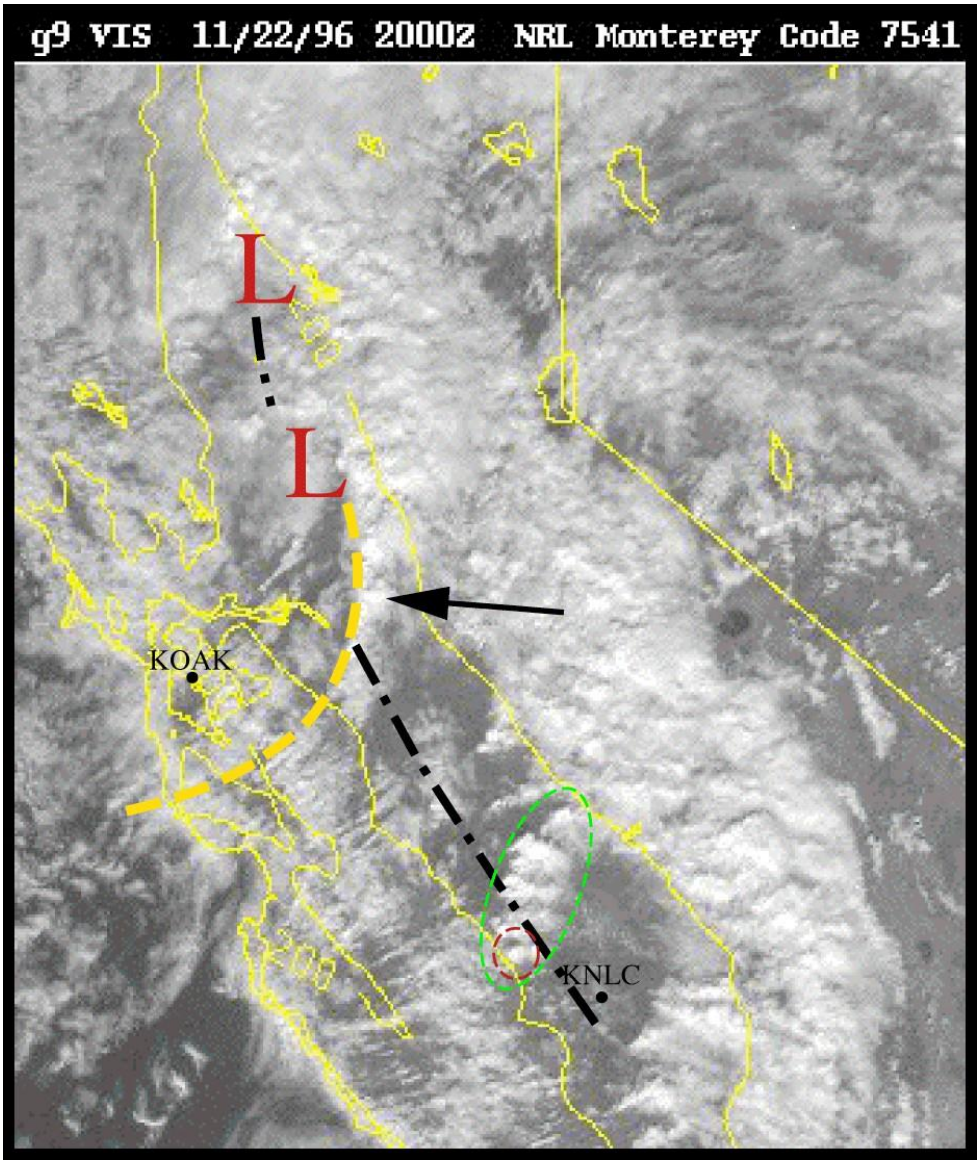

Fig. 4–2. GOES-9 visible satellite image for 2000 UTC 22 November 1996. The position of the lee-side trough/meso-low (black hashed) and the post-frontal trough (yellow dashed) and surface low is also shown. Arrows and circled regions are discussed in the text.

pressure gradient in the northern San Joaquin Valley that supported sustained southerly winds of 15 knots. The southerly winds advected moist air northward

during the time of maximum diurnal heating that probably caused low-level air parcel destabilization in the same region.

Three lines of surface-based convection developed in that hour at or near the lee-side trough axis (Fig. 4–2). The most developed line of storms at 2000 UTC was associated with the progressive surface trough and most intense convection at the intersection of that mobile trough and the quasi-stationary lee-side trough (Fig. 4–2, black arrow). Farther south, steering flow off the Diablo and Hamilton Range likely provided the lift to free parcel motions within the upward motion field centered over southern Sacramento and northern San Joaquin Valleys and a line of storms developed (Fig. 4–2, green dashed circle) that included what was to be the Lemoore storm (Fig. 4–2, red dashed circle). A third disorganized line of storms was forming between the two others.

During the next half an hour, rapid development of the thunderstorms continued as the convective lines generally moved eastward (Fig 4–2; Fig 4–3). Although an analysis of BRNs (Fig 4–5) shows that the entire Central Valley was in range for the occurrence of supercells, satellite imagery suggested that the line of storms associated with the mobile trough resembled a multicellular squall line (Fig 4–3, black arrow). The line of storms slowly developing just to the south still appeared unorganized on satellite imagery. Deep-layer (0–6-km) shear values (Fig 4–6) for this region were below 3.0 X $10^{-3}s^{-1}$ **,** except near Modesto (3.5 X $10^{-3}s^{-1}$**).** Modeling studies have shown that storms that develop in an

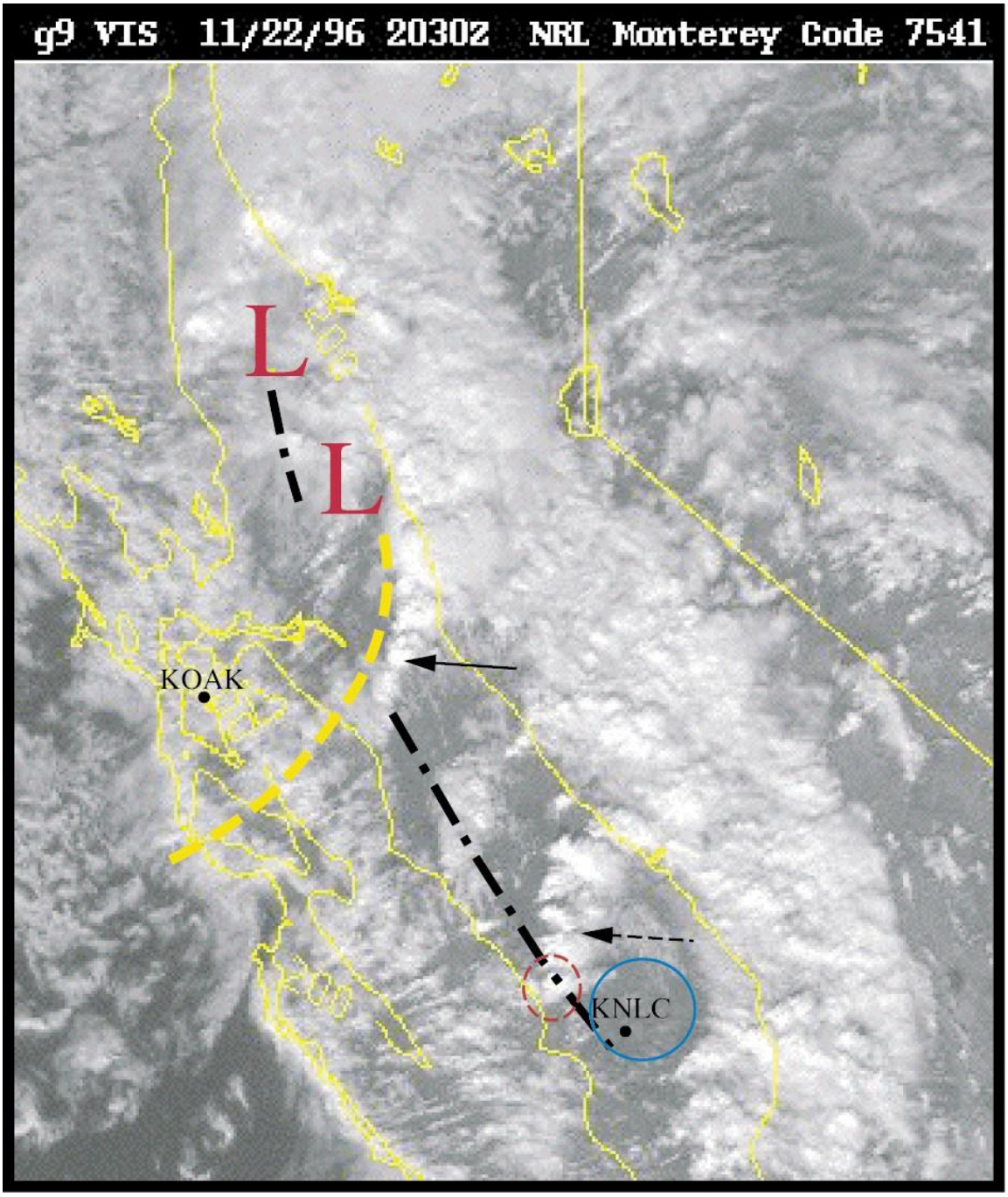

Fig. 4–3. Same as Fig. 4–2 except valid for 2030 (1230 PST) UTC 22 November 1996. Arrows and circled regions are discussed in the text.

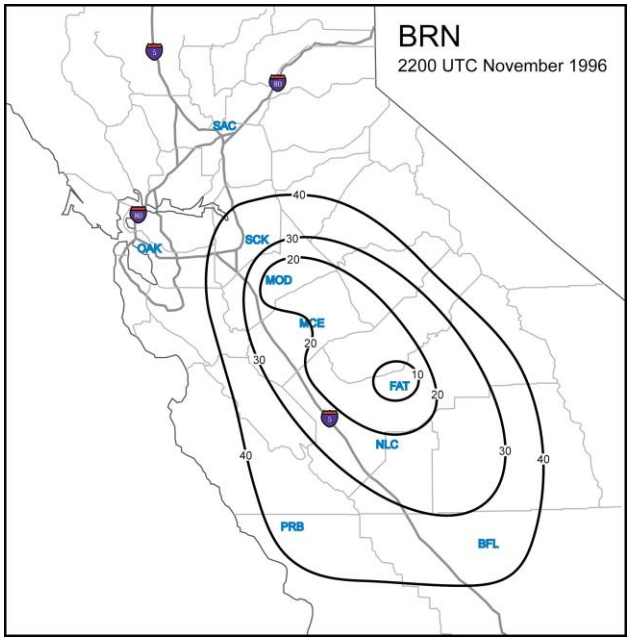

Fig. 4–4. Analysis of BRN at 2200 UTC 22 November 1996.

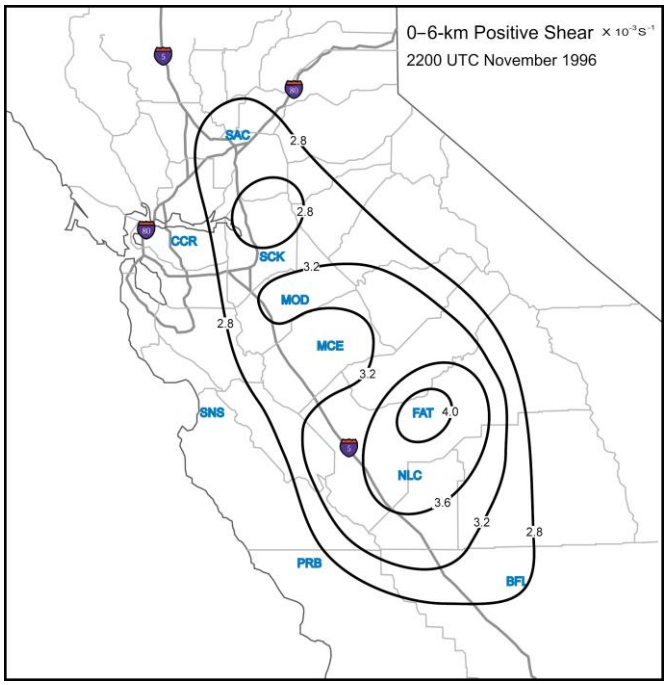

Fig. 4–5. Analysis of 0–6-km Positive Shear for 2200 UTC 22 November 1996.

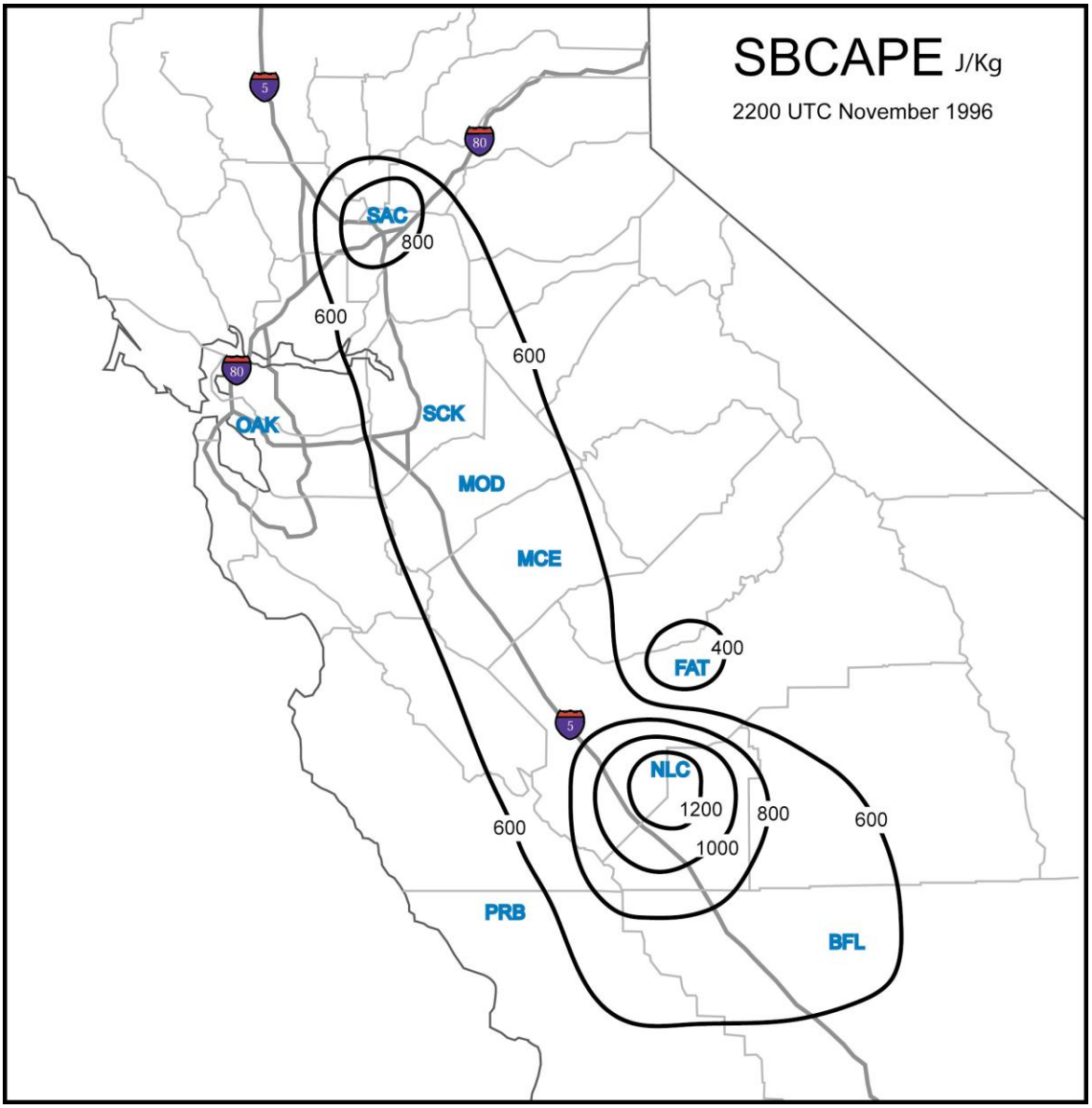

Fig. 4–6. Analysis of SBCAPE for 2200 UTC 22 November 1996.

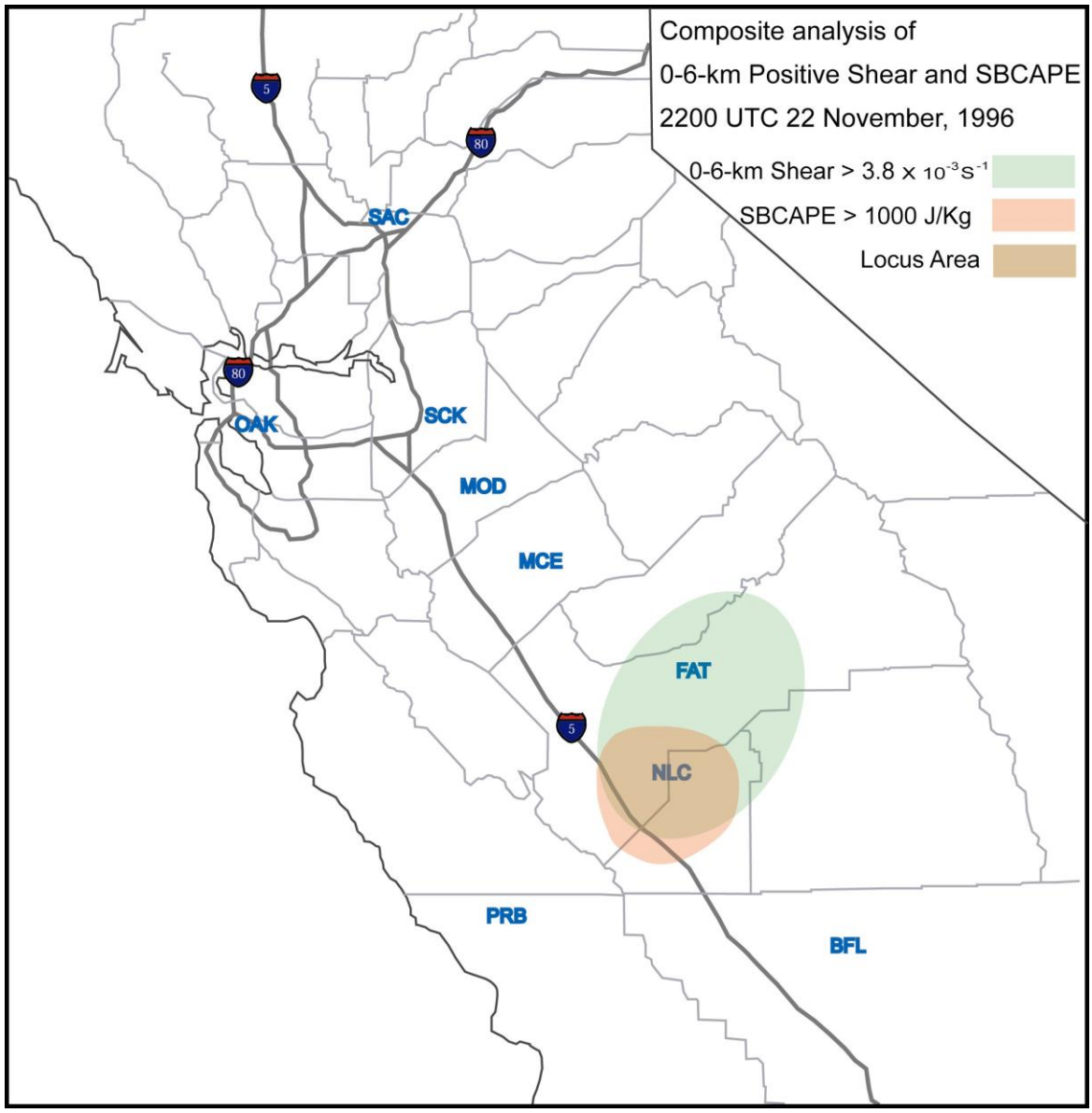

Fig. 4–7. Overlay of 0–6-km Positive Shear (> 3.8 X $10^{-3}s^{-1}$**)** and SBCAPE (> 1000 J/Kg) for 2200 UTC 22 November 1996.

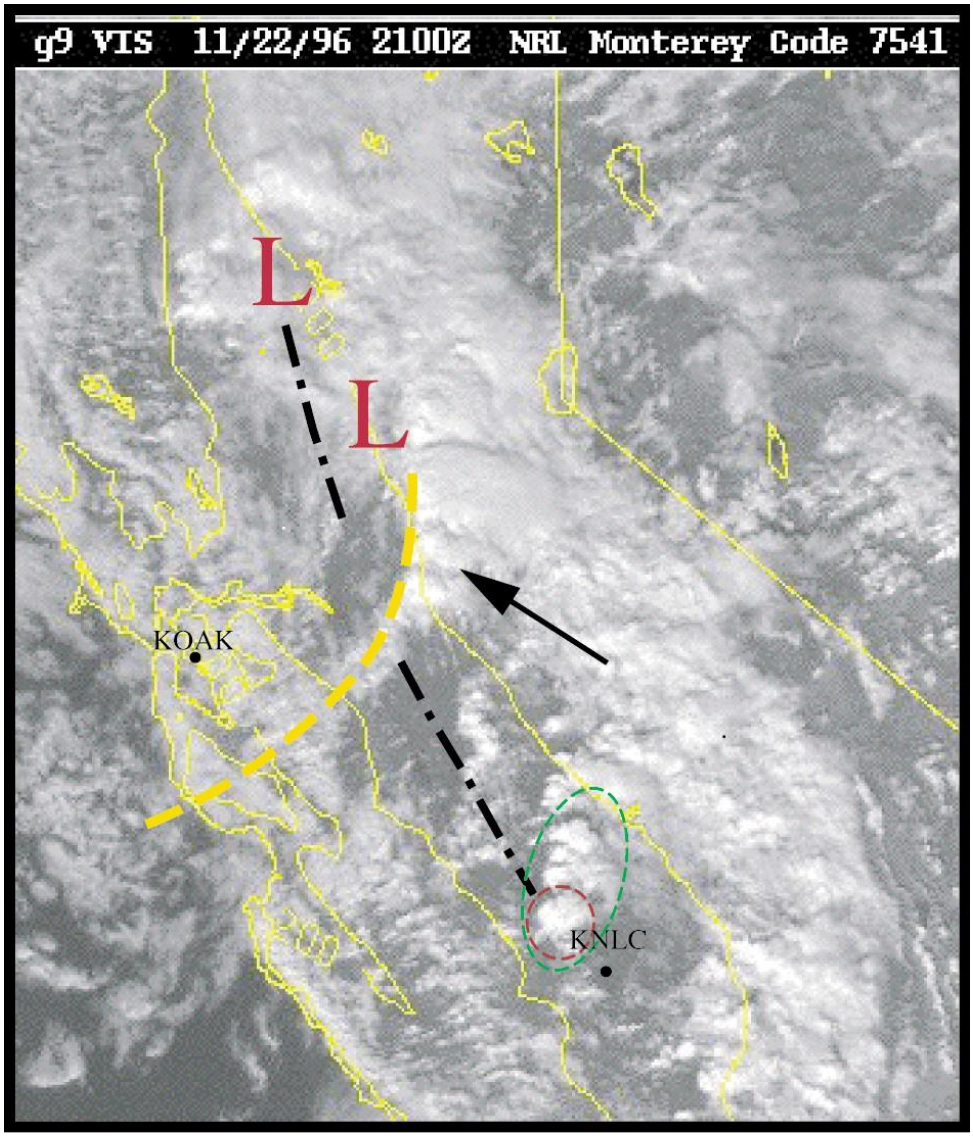

Fig. 4–8. Same as Fig. 4–2 except valid for 2100 (1300 PST) UTC 22 November 1996. Arrows and circled regions are discussed in the text.

environment of weak deep-layer shear (< 3.0 X $10^{-3}s^{-1}$ **)** show minimal tendencies for organization and usually no supercell characteristics (Weisman and Klemp, 1982).

The Lemoore storm (Fig. 4–3, red dashed circle) continued to rapidly develop along with the other storms within that convective band (Fig. 4–3, black-dashed arrow). South of this convection, a clear slot evident on satellite imagery (Fig. 4–3, blue dashed circle) acted to help maximize buoyancy through strong radiational heating in the potential inflow air for the Lemoore storm. This is also reflected in the SBCAPE analysis for 2200 UTC (Fig. 4–6) that shows that the highest buoyancies were located in that same region in the central San Joaquin Valley with a CAPE "bulls-eye" near Lemoore. Furthermore, deep-layer (0–6-km) shear values (Fig 4–6) for this region were above 3.6 X $10^{-3}s^{-1}$ and modeling studies have shown that storms developing in such an environment are more likely to have supercell characteristics (Weisman and Klemp, 1982). Furthermore, an overlay of SBCAPE and deep-layer shear (Fig 4–7; brown shading) shows that the Lemoore area had the best combination of buoyancy to shear for the development of organized convection and/or supercells. Under these conditions, these storms, and especially the Lemoore Storm farthest to the south, were moving into an area favorable for continued development, including the possibility of supercells.

4.3 Maturation period of the Lemoore Storm

The visible satellite image for half an hour later at 2100 UTC (1300 PST) (Fig. 4–8) shows continued development and southeast movement of all three

lines of storms, especially the convection associated with the subsynoptic trough (Fig. 4–8, black arrow) and Lemoore storm (Fig. 4–8, green-dashed circle). The subsynoptic analysis (Fig. 4–9) showed the meso-low associated with the subsynoptic trough had moved eastward into the Sierra Foothills with the low pressure trough extended southeastward across the northern San Joaquin Valley, and the lee-side trough remained quasi-stationary. New convection continued to develop at the intersection of the mobile trough and lee-side trough (Fig. 4–10, solid black arrow). This position of the surface low and trough (Fig. 4–9) resulted in surface pressure falls and backing winds south of the trough (i.e. KMCE, Merced) and surface pressure rises and veering winds north of the trough axis (i.e. KSCK, Stockton) resulting in continued surface convergence along the trough axis. The other effect was an increase in the low-level (i.e. 0–1-km) shear in the central and southern San Joaquin Valley and a decrease in that shear in the northern San Joaquin and southern Sacramento Valleys.

The Lemoore storm was rapidly maturing into a supercell within that region of stronger wind shear. The (KHNX) WSR-88D vertical wind profile from the Hanford radar shows considerable wind shear including strong veering in the layer just above the surface (Fig. 4–11). Satellite imagery indicated the storm was associated with flanking line of cumulus (Fig. 4–10, green arrow), and a large cirrus cloud shield east of the storm (Fig. 4–10, red-dashed circles). At 2130 UTC, a cell just north of the Lemoore Storm also appeared to be associated

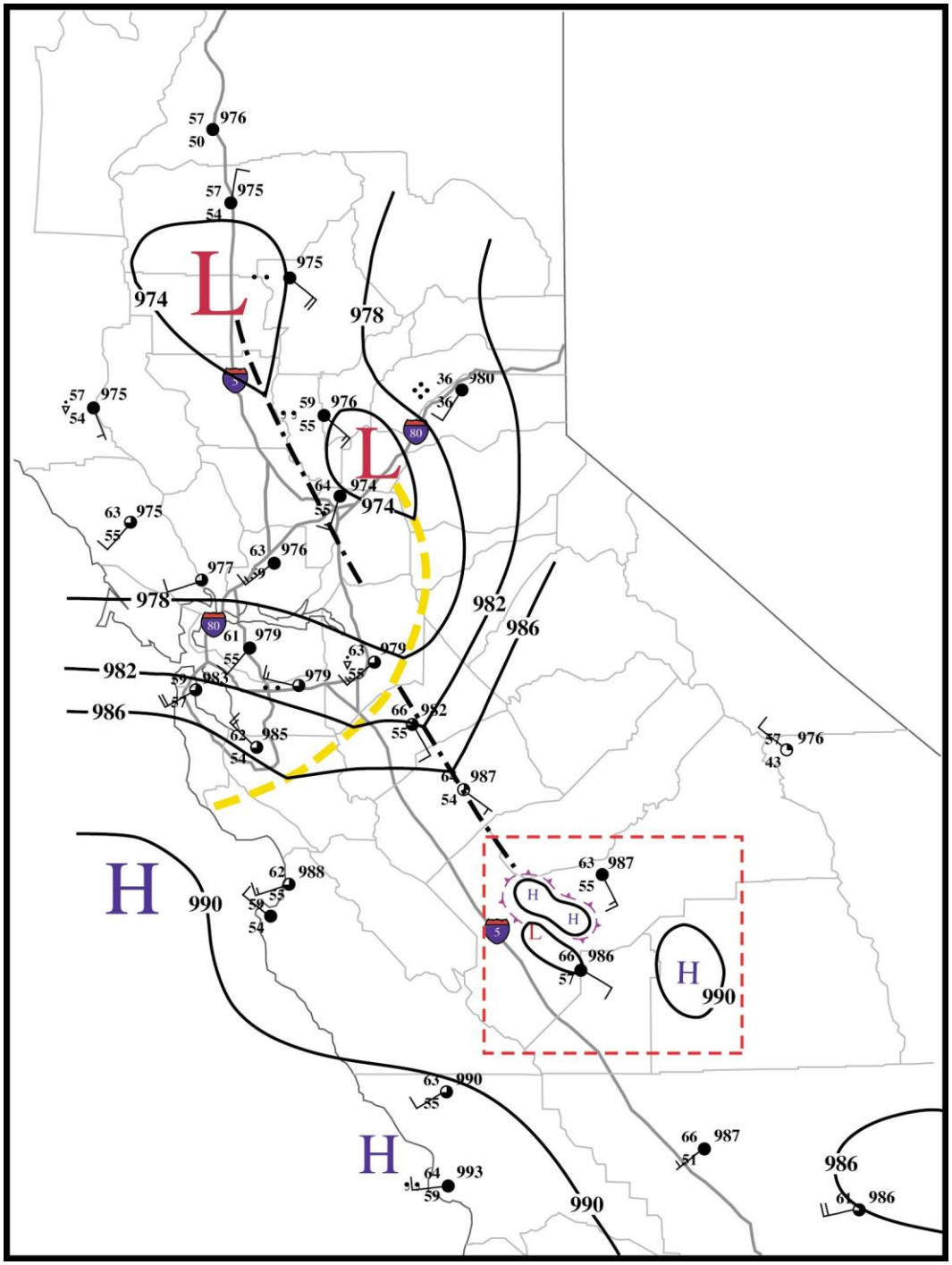

Fig. 4–9. Same as Fig. 4–1 except valid for 2100 (1300 PST) UTC 22 November 1996. Dashed red box outlines the border for Fig. 4–12.

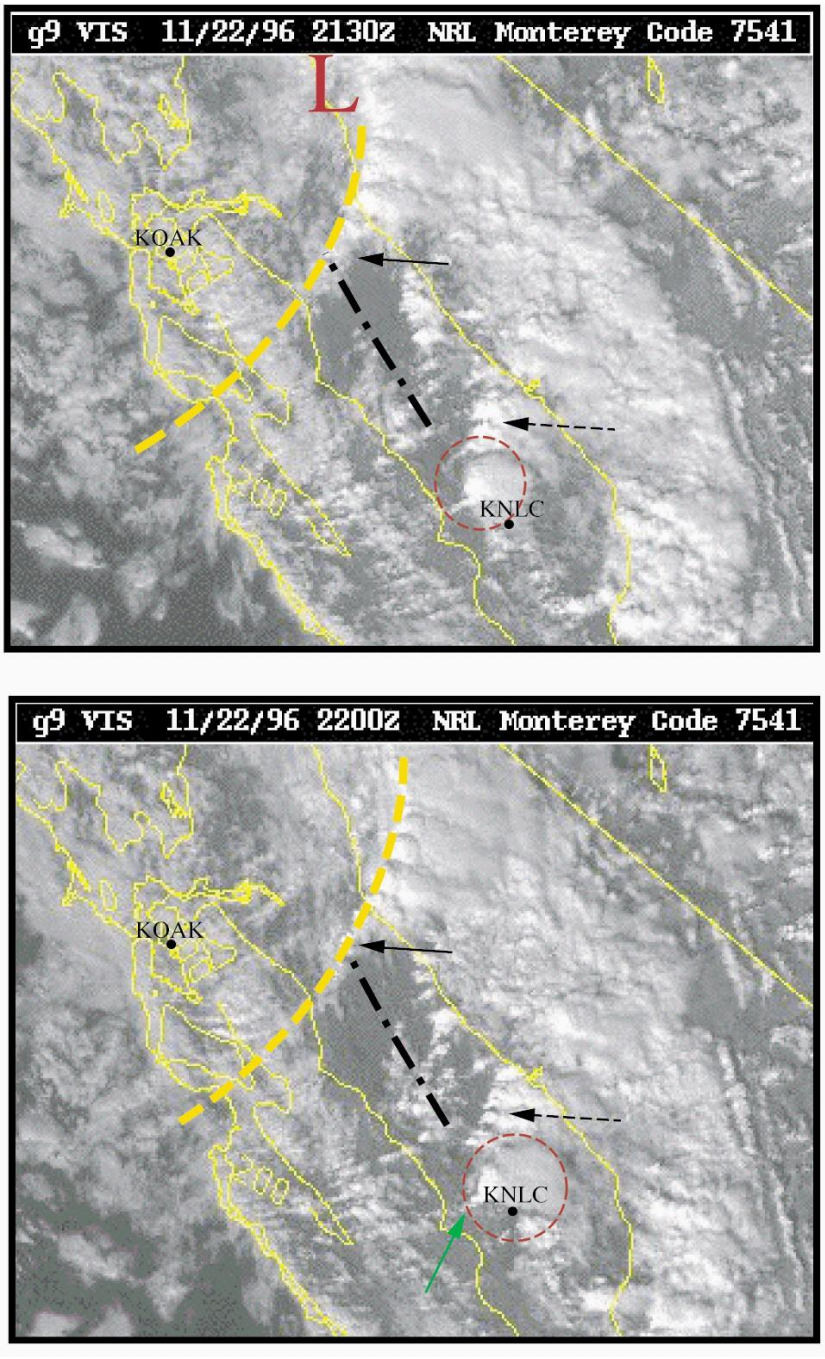

Fig. 4–10. Same as Fig. 4–2 except valid for 2130 (1330 PST) and 2200 (1400 PST) UTC 22 November 1996. Arrows and circled regions are discussed in the text.

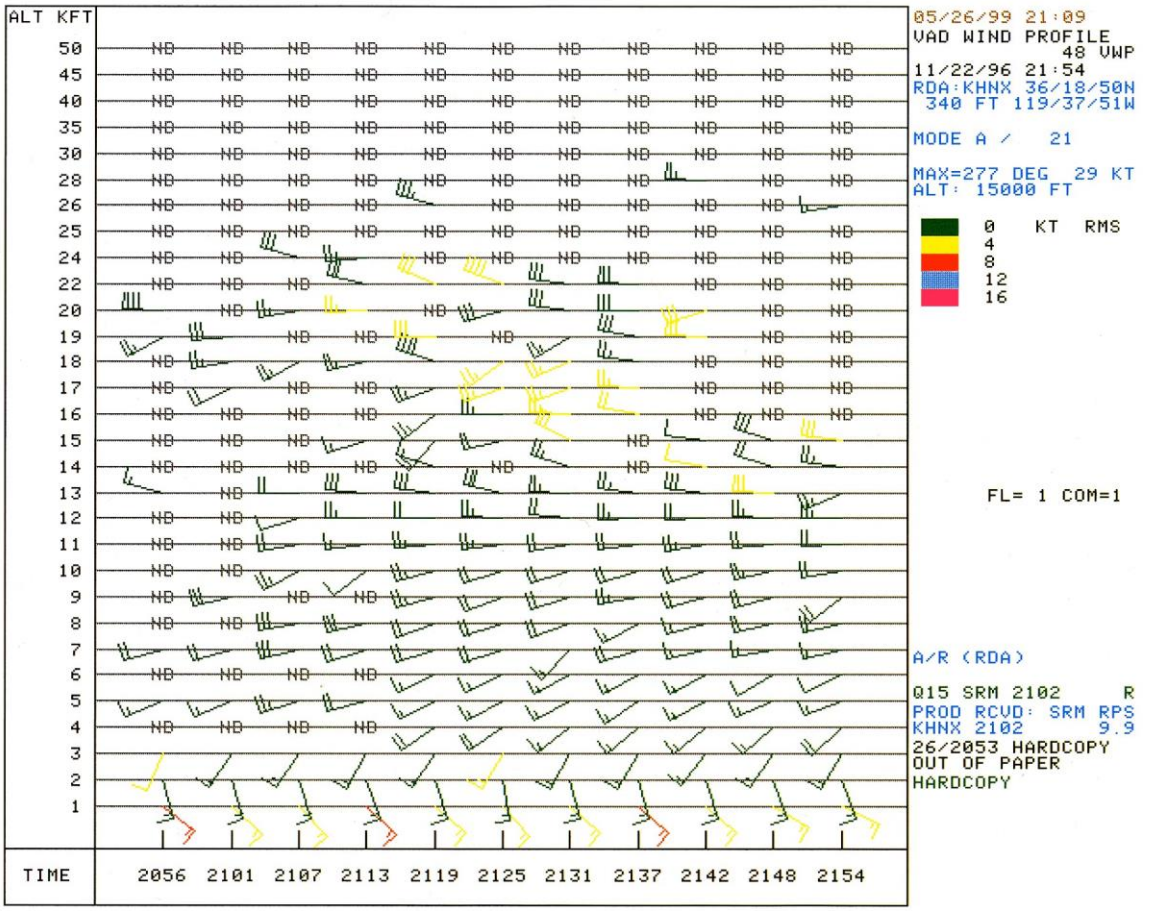

Fig. 4–11. WSR-88D Vertical Azimuth Display (VAD) wind profile from KHNX at 21:54 UTC 22 November 1996. Green wind plots indicated high, yellow medium, and red low confidence in accuracy of Doppler wind observations.

with a flanking line cumulus and may have been the cyclonic cell that resulted from supercell storm split (Fig. 4–10, dashed-black arrow). A brief F1 tornado was reported at 2150 UTC in the vicinity of this storm cell that damaged a roof of a farmhouse (USDC, 1996). The storm dissipated at 2200 UTC due to the likely

ingestion of negatively buoyant air from cool, dry outflow from the Lemoore storm (Fig. 4–12).

A localized subsynoptic analysis (Fig. 4–12) of the southern San Joaquin Valley revealed the development of a pool of warm moist air associated with

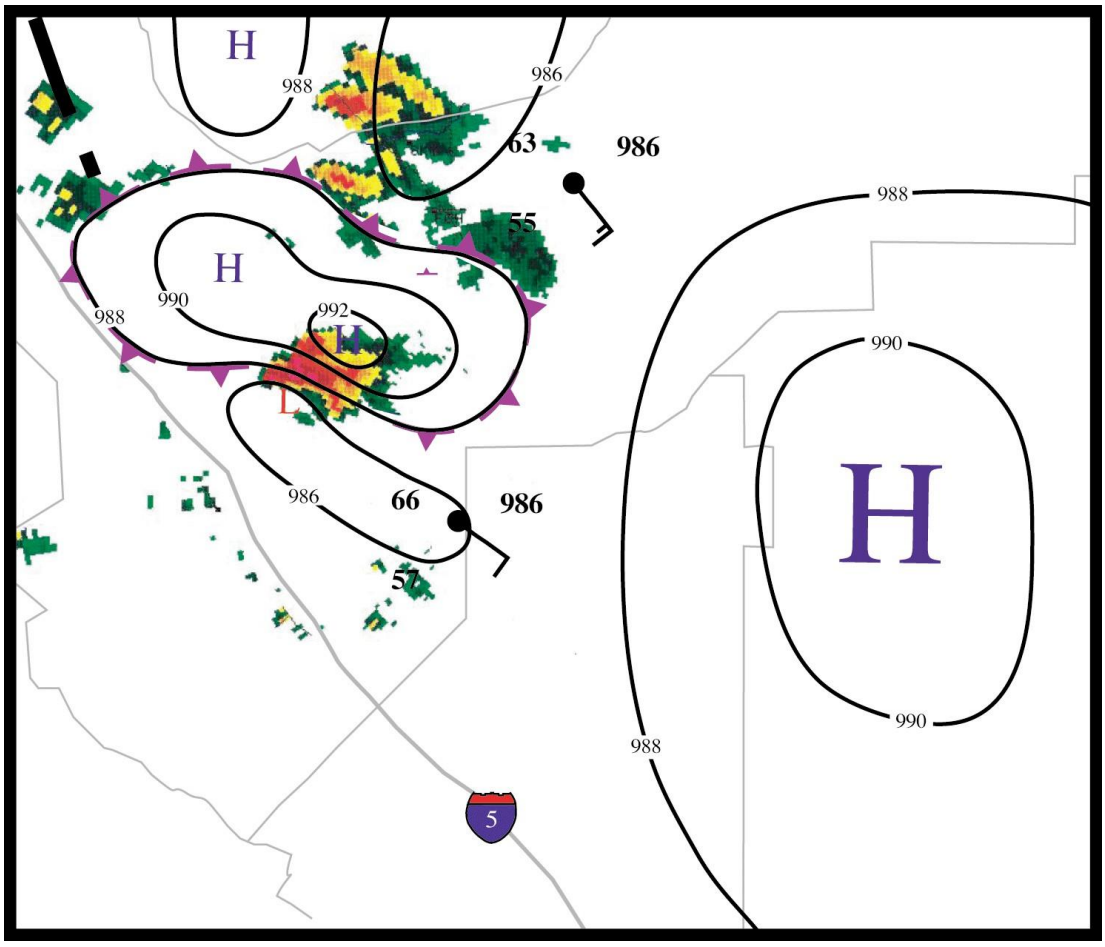

Fig. 4–12. Surface hourly observations for the Central San Joaquin Valley valid at 2100 UTC (1300 PST) 22 November 1996 overlaid with 0.5 degree base-reflectivity from the KHNX WSR-88D radar at 2137 UTC. The positions of the lee-side trough (hashed) and outflow boundary (purple-dashed cold front symbols) are also shown.

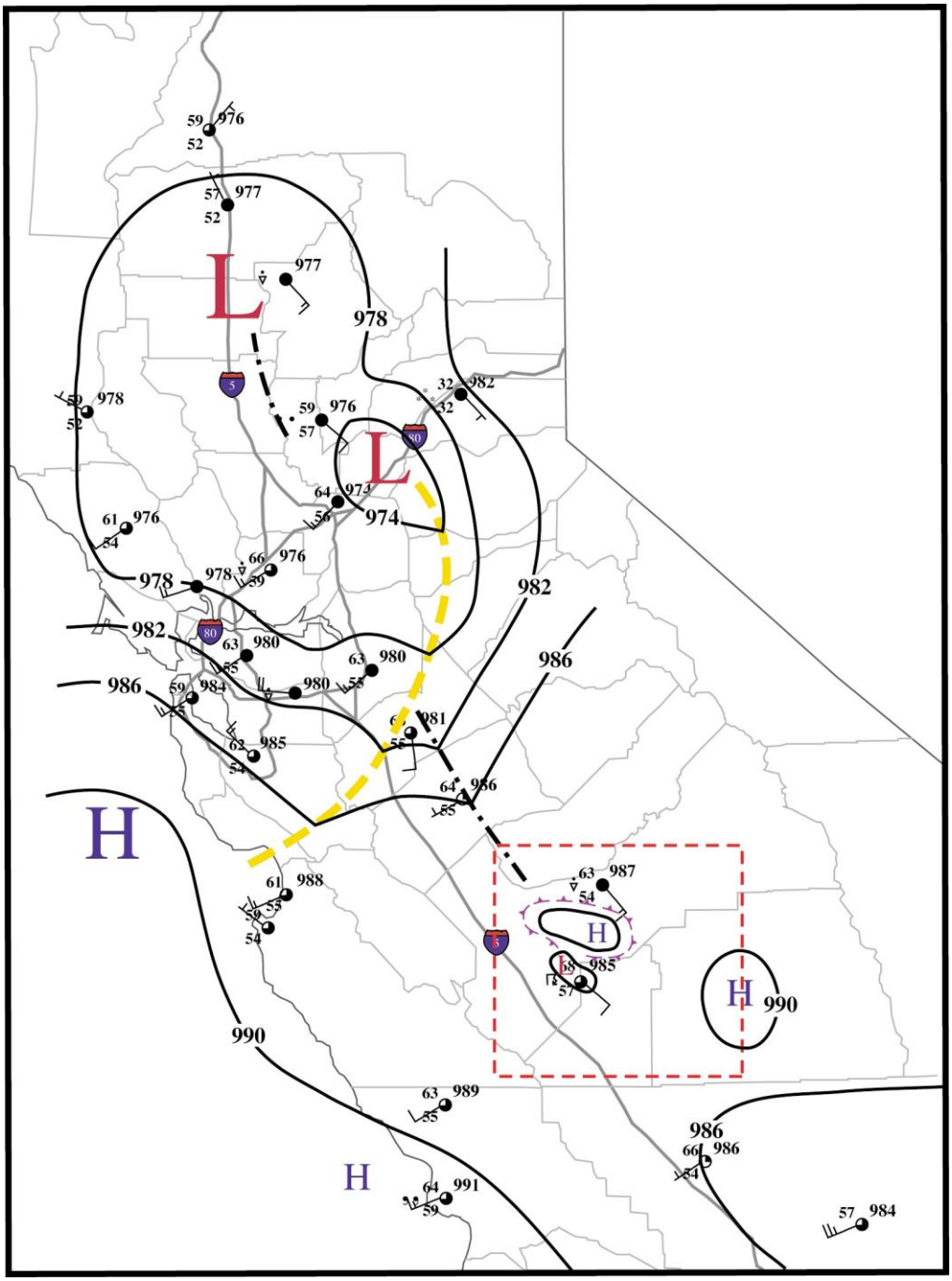

Fig. 4–13. Same as Fig. 4–1 except valid for 2200 (1400 PST) UTC 22 November 1996. Dashed red box outlines the border for Fig. 4–15 and Fig. 4–17.

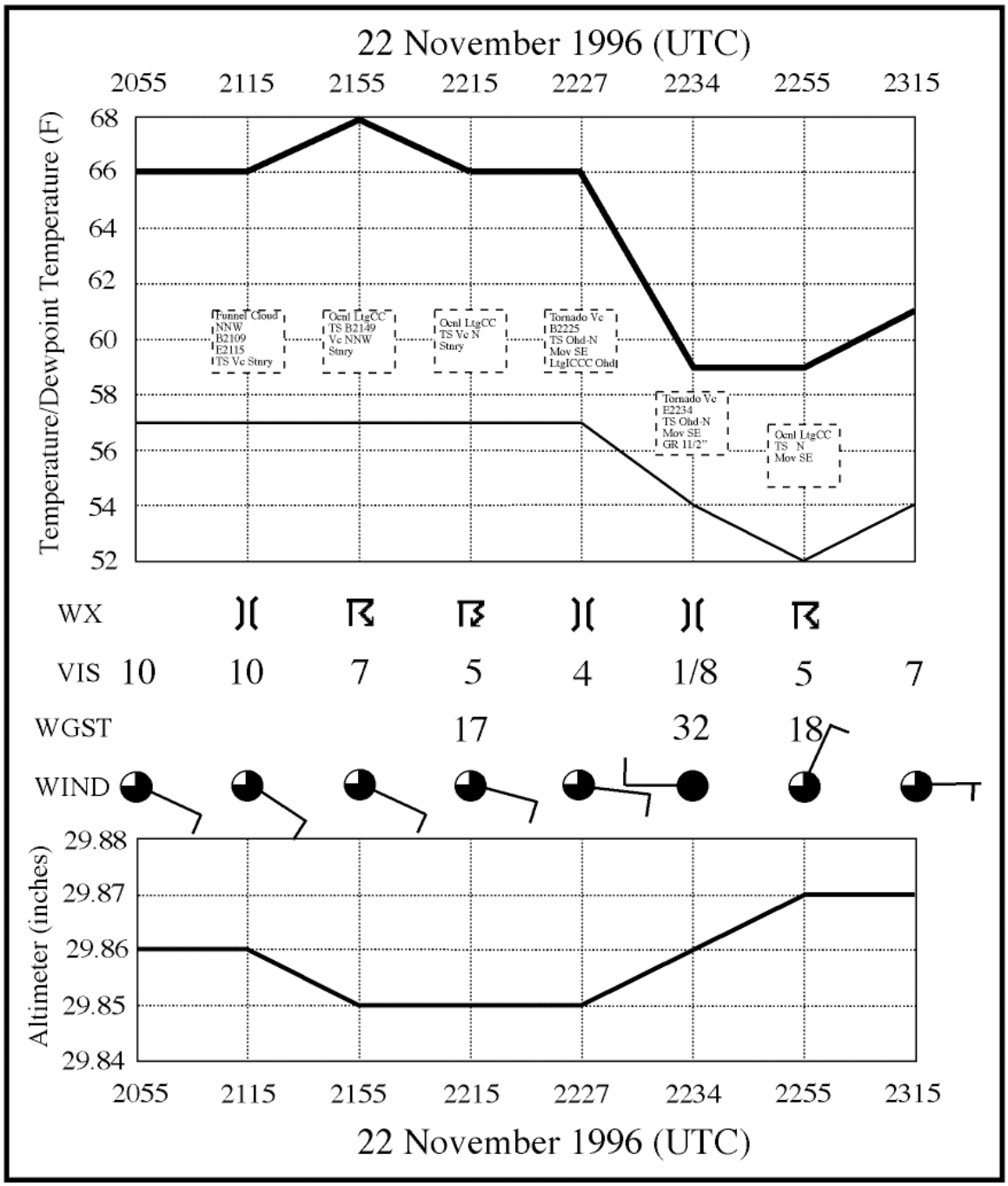

Fig. 4–14. Meteogram for KNLC valid from 2055 UTC through 2315 UTC 22 November 1996.

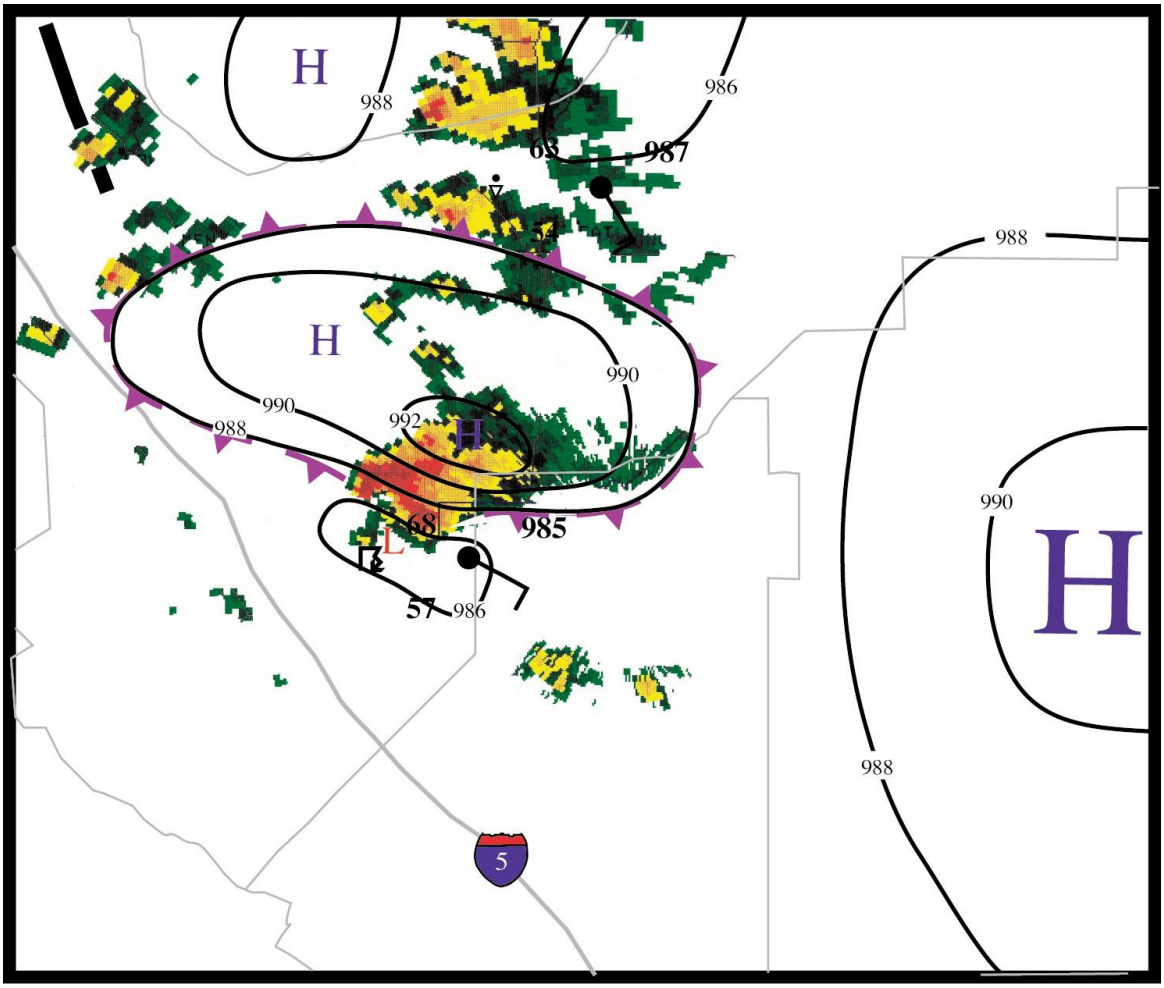

Fig. 4–15. Surface hourly observations for the Central San Joaquin Valley valid at 2200 UTC (1400 PST) 22 November 1996 overlaid with 0.5 degree base-reflectivity from the KHNX WSR-88D radar at 2200 UTC. The positions of the lee-side trough (hashed) and outflow boundary (purple-dashed cold front symbols) are also shown.

localized convergence near Lemoore (KNLC). Temperatures at Lemoore (KNLC) rose several degrees between 2000 (Fig. 4–1) and 2200 UTC (Fig. 4–13) due to partly sunny skies (Fig. 4–10) that increased insolation. For several hours, temperatures at Lemoore (KNLC) were several degrees warmer than the surrounding METAR sites (Fig. 4–1; Fig. 4–9; Fig. 4–13). Surface pressure falls

(5 mb of sea level pressure between 2115 and 2215 UTC) combined with steady southeast at Lemoore (Fig. 4–14) increased moisture convergence and caused a similar rise in dewpoint temperatures (Fig. 4–1; Fig. 4–9) that remained unchanged until the passage of the tornado (Fig. 4–14). The result probably was a localized solenoid field that likely contributed to enhance the low-level streamwise vorticity over the central San Joaquin Valley.

As shown by the WSR-88D base-reflectivity at a 0.5 degree tilt from the Hanford (KHNX) radar at 2137 UTC (Fig. 4–12) and at 2200 UTC (Fig. 4–15), the Lemoore storm had now developed classic supercell-like characteristics that included a hook-echo, a persistent highly-reflective core (>65 DbZ), and significant precipitation downstream in the forward flank of the storm. The strong outflow on the forward flank continued to expand as well (Fig. 4–12, Fig. 4–15) and was affecting surrounding cells with the closest cell to the north starting to dissipate. The analyses also show that the convergence zone near Lemoore remained fixed and winds remained backed at KNLC (Fig. 4–12, Fig. 4–15).

Over that same time frame (23 minutes), the Lemoore storm developed a new updraft core on the right flank of the original updraft with a new hook echo forming just south of the initial reflectivity hook, signifying a new region of mid-level storm rotation or mesocyclone (Fig. 4–12, Fig. 4–15). The initiation of a rear-flank downdraft (RFD) often coincides with the formation of the hook echo. Rear-flank downdrafts (RFDs) are regions of descending warm or cold air that

develop on the rear side of the main updraft and have a well-established association with hook echoes (Markowski, 2002). The formation of the rear-flank downdraft and the hook echo are often linked with observations of increases of vorticity near the ground (Davies-Jones and Brooks, 1993). With the formation of a new hook echo around the rejuvenated updraft core, an acceleration of the RFD occurred that likely increased low-level storm rotation.

The strength of the mid-level winds is also important in determining the amount of forcing for near ground rotation (Brooks et al., 1994; Davies-Jones, 2000). When the mid-level flow is too weak, the RFD outflow undercuts the updraft and the source of inflow for the mesocyclone, thus there is little or no generation of low-level vorticity. If the flow is too strong, the descending air pool linked with the RFD often is not oriented suitably for vorticity generation in the baroclinic zone adjacent to the updraft. Classic supercells often have the right balance between mid-level storm speeds and storm downdrafts to maximize low-level vorticity generation, although a recent observational study concluded that surface baroclinicity within this region is not a necessary condition for tornadogenesis (Markowski et al., 2002).

The RFD is either dynamically (linear forcing) and/or thermodynamically (evaporative cooling and/or precipitation drag) driven and is likely responsible for increasing low-level storm rotation through the transfer of air with high angular momentum to the surface that is twisted, tilted and then stretched to produce

amplified cyclonic rotation when re-ingested into the updraft core (Davies-Jones and Brooks, 1993). First observed in the 1960s (Garrett and Rockney.,1962), many observational case studies (Bluestein, 1983; Johnson et al., 1987, Markowski et al., 2002) since have shown that warm, not cold RFDs have been associated with tornadoes. Most recently, Markowski et al. 2002 used direct observations of RFDs in both tornadic and non-tornadic storms to conclude that tornado likelihood, intensity, and longevity increases as the equivalent potential temperature in the RFD rises and convective inhibition (CIN) associated with the RFD parcels at the surface decreases. In addition, the temperature of the air in the RFD is likely associated with the boundary-layer relative humidity profile. Low relative humidity at low-levels is associated cold RFDs and high-cloud bases, likely due to evaporative cooling within the hook echo. High boundary-layer relative humidity results in low-cloud bases that are more conducive to warm RFDs containing SBCAPE. SBCAPE within the RFD is likely a necessary condition for tornadogenesis (Markowski et al., 2002).

In addition to the potential increase in low-level vertical vorticity induced by the RFD, the Lemoore storm was also moving in the proper direction to interact with the solenoidal circulation/convergence zone near Lemoore (KNLC) within thirty minutes of the 2206 UTC position. Individual cells within the line of storms associated with the Lemoore Storm in the central San Joaquin Valley were

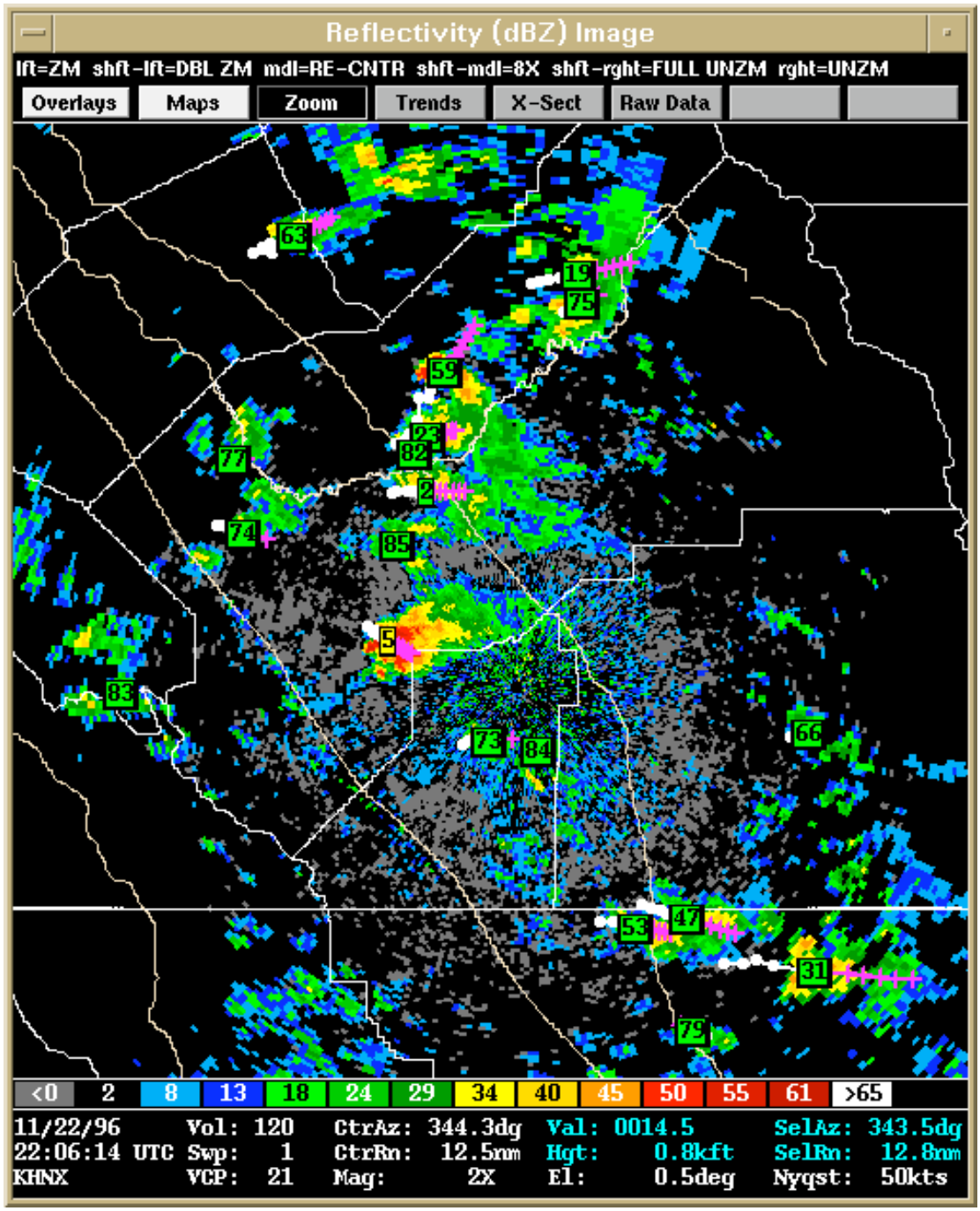

Fig. 4–16. KHNX WSR-88D composite reflectivity image for 2206 UTC 22 November. White dots represent actual storm tracks and magenta crosses are the forecast storm track.

moving mostly east/northeast at 2200 UTC (Fig. 4–16, white dots) and parallel to the 500-mb mean wind (Fig. 3–17). However, the Lemoore storm was moving to the right of the mean wind (Fig. 4–16, storm #5, white dots) and that movement (Fig. 4–16 magenta crosses) would lead to interaction with the solenoid near Lemoore. Potential updraft ingestion of inflow air latent with solenoidally-generated vorticity would further strengthen the low-level circulation already likely associated the Lemoore Storm. About 20 minutes later (2229 UTC), a mesocyclone was depicted by the KHNX WSR-88D volume scan and the first F0 tornado was observed moving slowly over barren ground near the Lemoore Naval Air Station (USDC, 1996).

4.4 Tornado Phase of the Lemoore Storm

The first tornado began at 2227 UTC, ended nine minutes later at 2234 UTC, moved slowly southeastward over a barren field (~2 km) near a runway complex at the Lemoore Naval Air Station, reduced visibility to 1/8 of a mile, and caused no damage (USDC, 1996). During and just after the first tornado event, winds shifted to westerly then northerly, temperature decreased 7 °F, dewpoints decreased 5 °F, and pressure started to rise, due to the passage of the gust front and subsequent arrival of cool, dry outflow air (Fig. 4–14). Often the hook echo slightly trails the surface wind shift (Haglund, 1969) and at 2234 UTC (Fig. 4–17) the back end of the hook appendage associated with the Lemoore Storm was

moving across the Lemoore Naval Air Station. Large hail (3.75 cm/1 _”) was also observed simultaneously with the first tornado event at 2234 UTC (Fig. 4–14) when the hook echo was basically overhead Lemoore.

The subsynoptic analyses (Fig. 4–15; Fig. 4–17) during the initial tornado event show a continued northward expansion of the convective outflow from the Lemoore Storm. Radar reflectivity returns show cell dissipation occurred with the storms along the northern boundary likely due to updraft ingestion of negatively buoyant cool, dry, outflow from the forward flank of the Lemoore Storm (Fig. 4–15; Fig. 4–17). However, active convection was still being observed north of this periphery and just east of the lee-side trough with mature and developing storms showing strong radar reflectivities (Fig. 4–17), but no severe weather was reported with these cells. The analyses (Fig. 4–15; Fig. 4–17) also show a contraction of the convergence zone near Lemoore associated with the advection of warm moist southerly surface winds that characterized the inflow air for the Lemoore Storm. The decrease in size of this convergence zone (Fig. 4–17) was the result of the southeast movement of the Lemoore storm that narrowed the gap between that storm and the meso-high in the southern San Joaquin left in the wake from the passage of the cold front and the remnants of nocturnal thunderstorms. The contraction of the convergence zone suggests that the highest amount of surface-based CAPE (due to insolation and moisture

convergence) had been reached in the Lemoore area and that the updraft associated with tornadic cell has reached maximum strength.

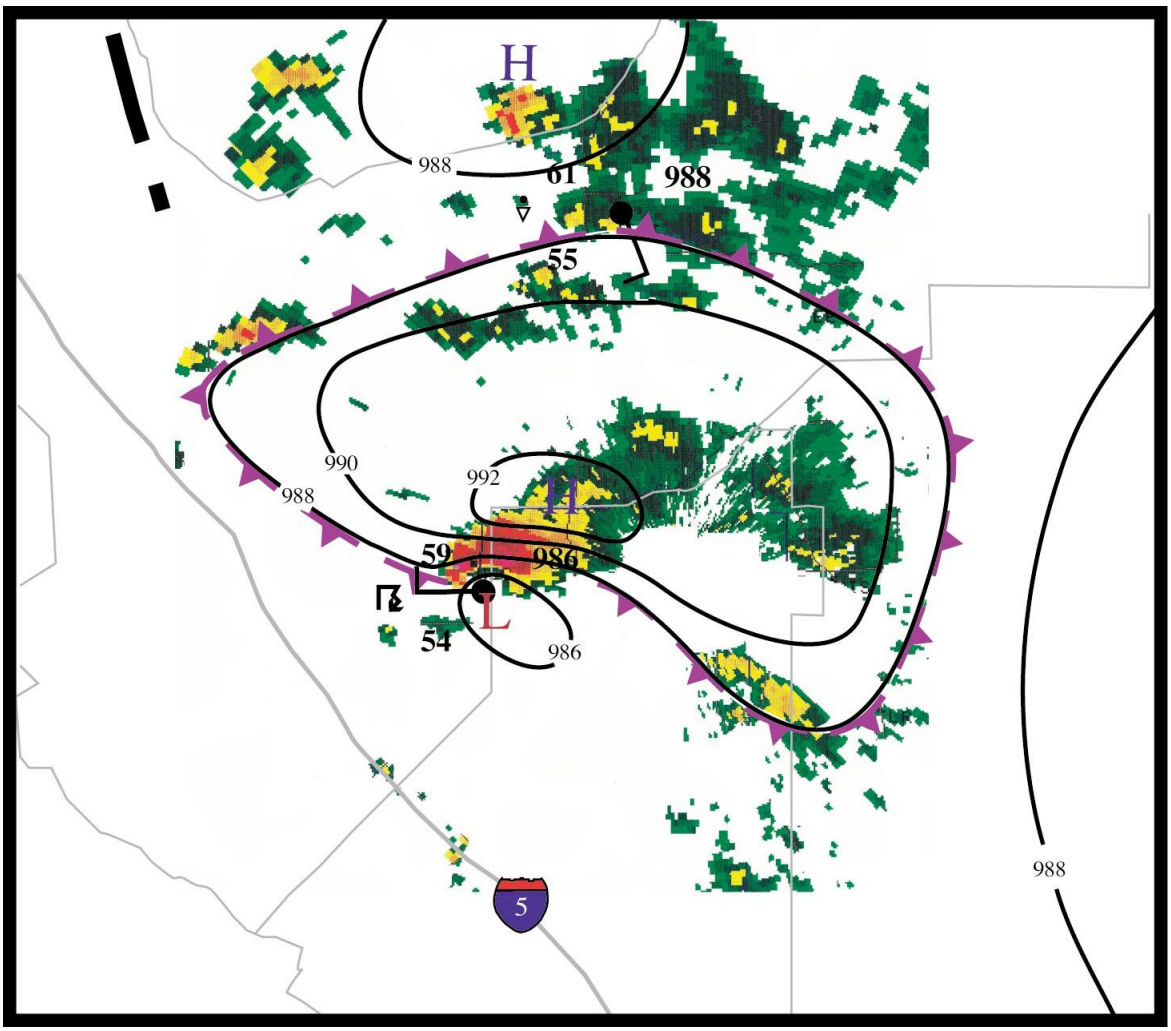

Fig. 4–17. Surface hourly observations for the Central San Joaquin Valley valid at 2230 UTC (1430 PST) 22 November 1996 overlaid with 0.5 degree base-reflectivity from the KHNX WSR-88D radar at 2234 UTC. The positions of the lee-side trough (hashed) and outflow boundary (purple-dashed cold front symbols) are also shown.

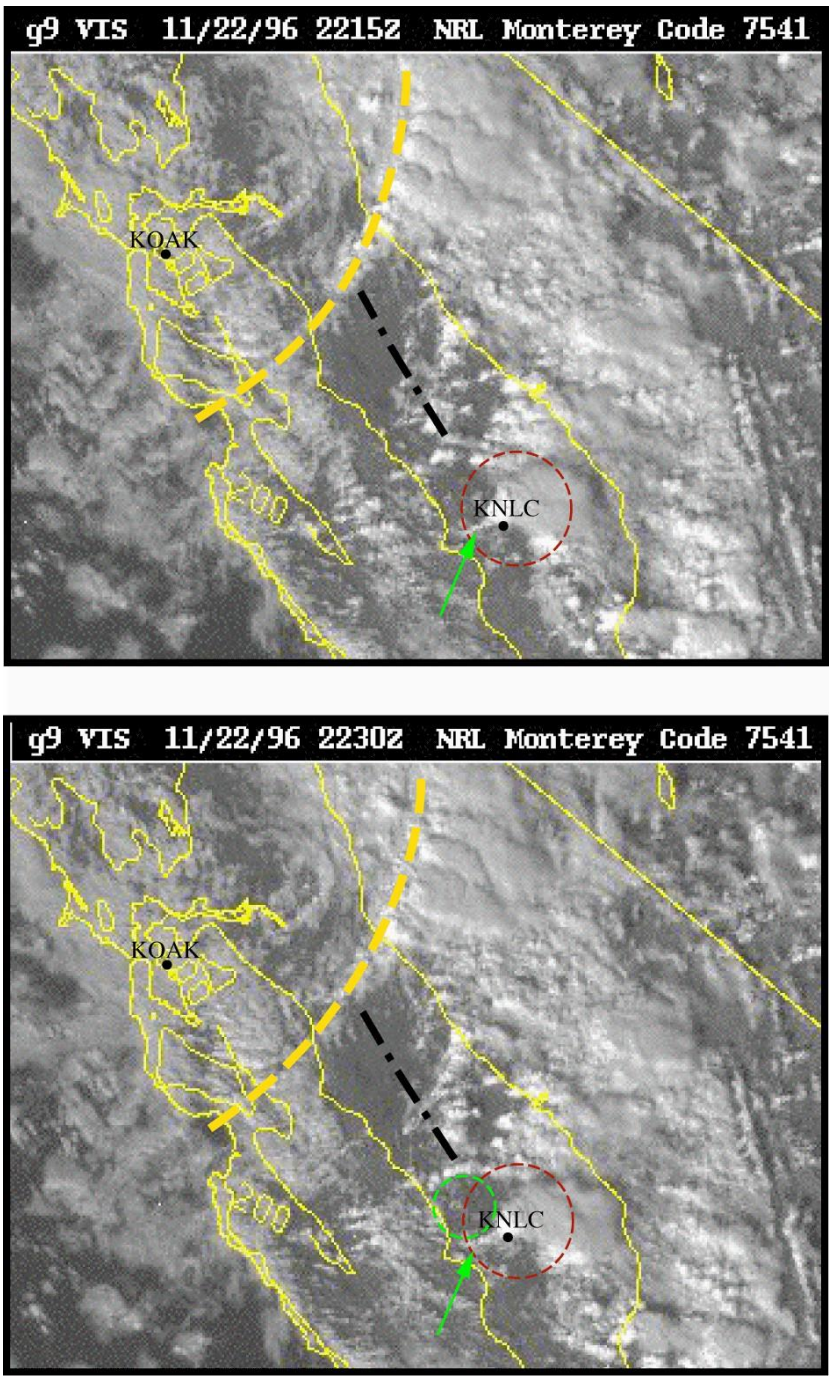

Fig. 4–18. Same as Fig. 4–2 except valid for 2215 (1415 PST) and 2230 (1430 PST) UTC 22 November 1996. Arrows and circled regions are discussed in the text.

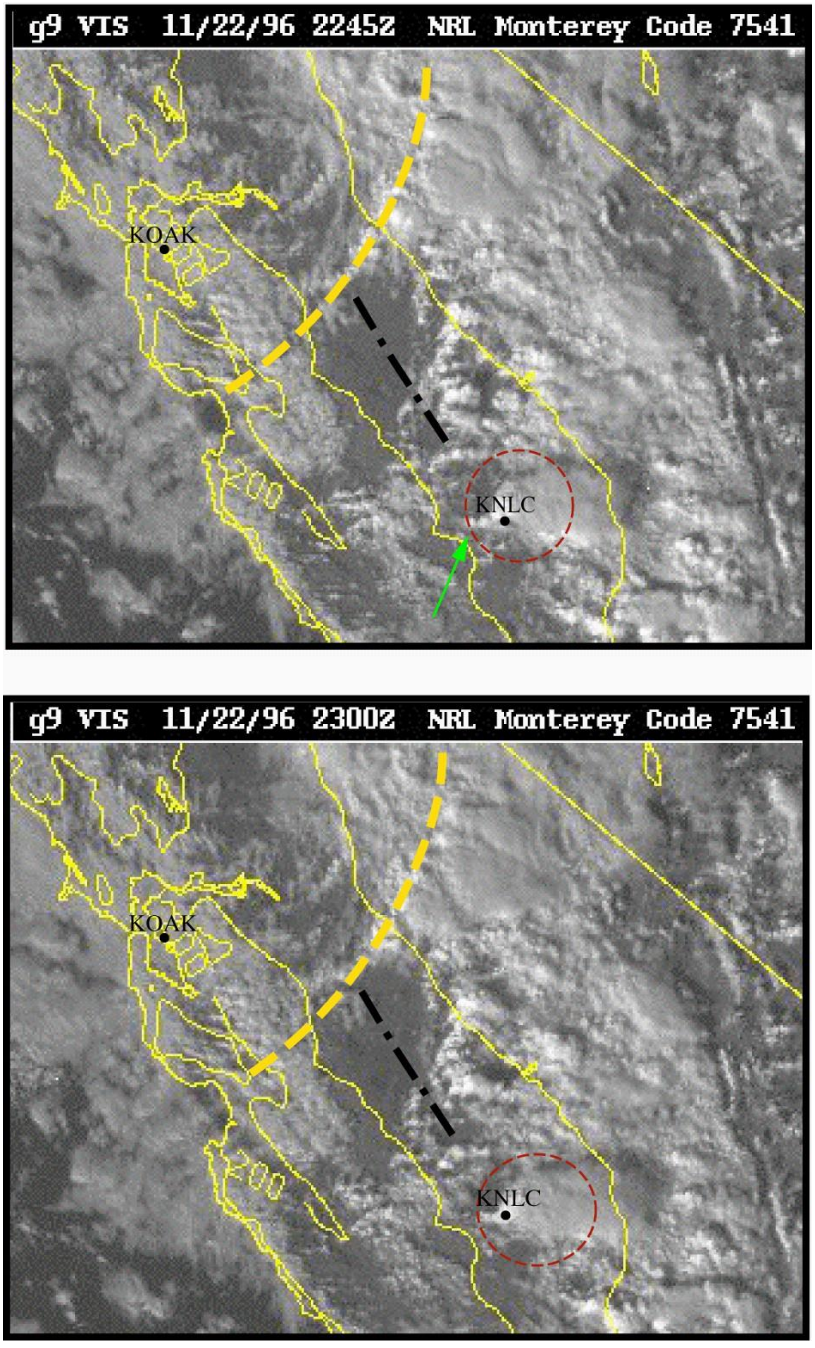

Fig. 4–19. Same as Fig. 4–2 except valid for 2245 (1445 PST) and 2300 (1500 PST) UTC 22 November 1996. Arrows and circled regions are discussed in the text.

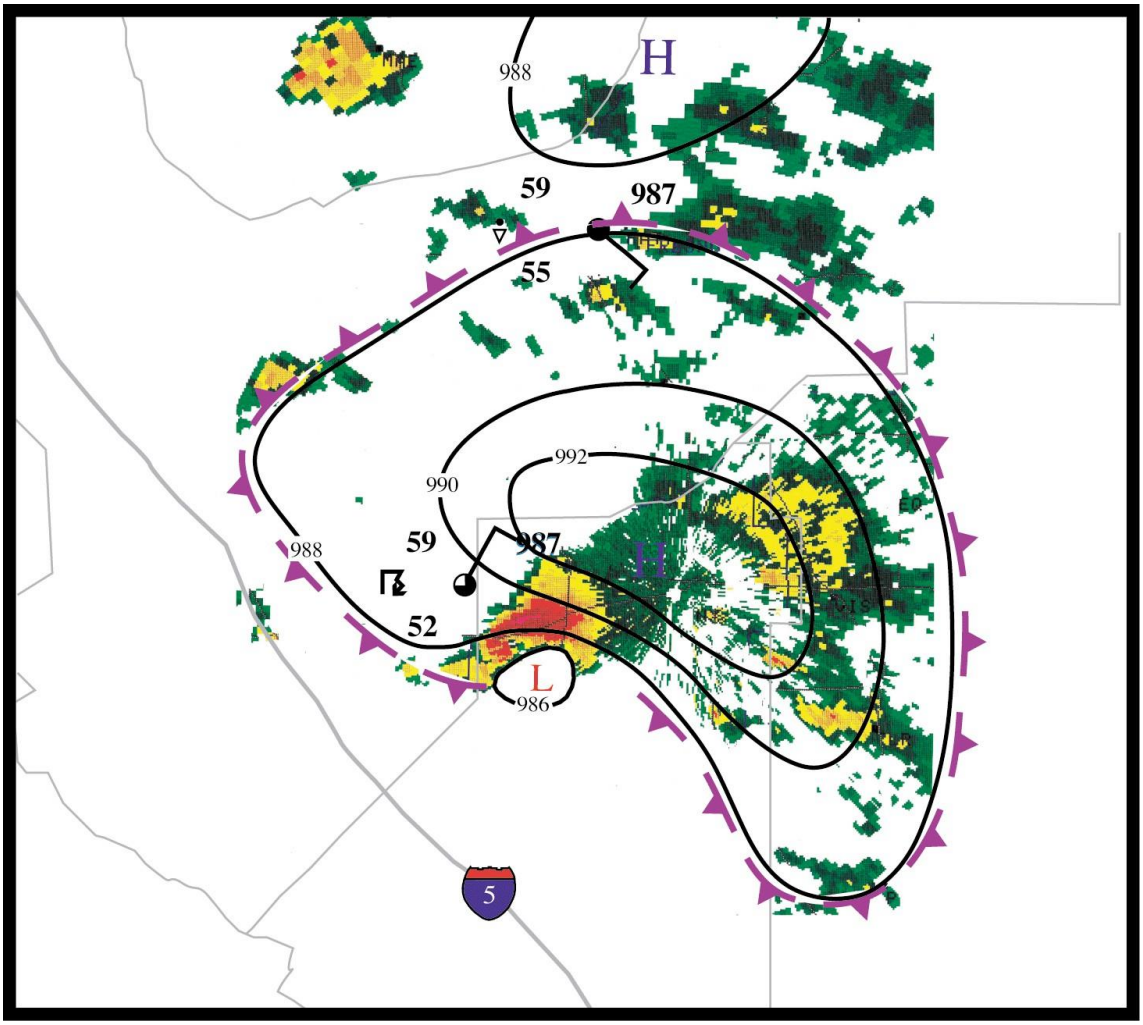

Fig. 4–20. Surface hourly observations for the Central San Joaquin Valley valid at 2300 UTC (1500 PST) 22 November 1996 overlaid with 0.5 degree base-reflectivity from the KHNX WSR-88D radar at 2258 UTC. The position of the outflow boundary (purple-dashed cold front symbols) is also shown.

The evolution of the Lemoore Storm during the first tornado episode was evident on satellite imagery. An expansion of cirrus debris anvil (Fig. 4–18 and Fig. 4–19-top image, red-dashed circle), flanking towering cumulus (Fig. 4–18 and Fig. 4–19-top image, green arrow), and an overshooting

top were associated with this storm in this period. Also evident was a stable evaporatively-cooled clear air dome (Fig. 4–18-lower image, green-dashed circle) immediately adjacent to the supercell. This clear air dome was caused by a cool air mass generated beneath the supercell echo due to evaporation of rain in the forward flank downdraft (FFD) and its subsequent movement away from its origin (Purdom, 1993). The arc cloud line along the northern perimeter of the clear air dome also marks the boundary of the convective outflow from the Lemoore storm. Mesoscale lift was likely occurring in that region and new cumulonimbus were growing along that intersection (Fig. 4–18-lower image, green-dashed circle) with strong radar reflectivities observed with one particular cell along the extreme northern and western portions of the outflow boundary (Fig. 4–17; Fig. 4–20).

The Lemoore storm was the most intense between 2245 UTC and 2300 UTC during the second tornado episode. This F1 tornado caused substantial damage as it tracked through the administration portion of the base (USDC, 1996). The storm was also associated with hail up to 6.25 cm (2 _”) in diameter in the same area (USDC, 1996). Although the time of occurrence of the second F1 tornado event was between 1305 UTC and 1315 UTC from Storm Data (USDC, 1996), based on radar and surface observations, the author believes that this tornado may have actually occurred about 15 minutes earlier. Base reflectivity images from the WSR-88D at Hanford show the southeasterly

moving Lemoore storm crossing Hwy 198 at around 2258 UTC (shown later), seven minutes before the official start of the second tornado episode. The Lemoore Naval Air Station is located on the north side of Hwy 198.

Visible satellite images between 2245 and 2300 UTC (Fig. 4–20) show that the Lemoore storm may have begun to weaken during this time period, although the storm was still intense. Cumulus towers no longer are developing on the flanks of the updraft, the overshooting top appears to be collapsing, and the consolidated structure of the storm was indicative of a mature thunderstorm containing a weakening core updraft. Updrafts have been shown to weaken during the stage when low-level rotation rapidly increases due to the formation of a downward-directed dynamic pressure gradient induced by that rotation (Brooks et al., 1993). Radar imagery also shows that the storm now has a classic/high-precipitation (HP) hybrid supercell structure with significantly more precipitation wrapped around the circulation center (Fig. 4–20). The downward-directed dynamic vertical pressure gradient that resulted from the increase in low-level rotation and precipitation loading, appear to be potential factors in the start and strengthening, respectively, of possibly a storm-scale occlusion downdraft. Klemp and Rotunno (1983) noted that non-tornadic supercells persist for long periods of time with a well-defined gust front and that if the storm progresses to the tornadic phase, the gust front often becomes occluded and a strong downdraft forms directly behind the gust front at low- and mid- storm levels. The

downdraft, a small-scale localized intensification of the RFD that occurs in response to a rapid increase in near ground vertical vorticity (Rotunno, 1986), would have occurred nearly simultaneously as the occurrence of the F1 tornado. This is a possible mechanism for the amplification of the low-level vorticity field associated with the tornadogenesis process near Lemoore that resulted in the F1 tornado event.

4.5 Dissipation stage of the Lemoore Storm

The Lemoore Storm slowly dissipated after the second tornado event. The subsynoptic analysis for 2300 UTC (Fig. 4–21) shows that the meso-low associated with the mobile surface trough that initiated the convection across the Central Valley earlier in the day had moved into the Sierra. Synoptic-scale ridging (Fig. 3–34) caused high pressure to build at the surface along the coastal sections of California that resulted in a westerly wind shift in most locations across California. The lee-side trough had also eroded when mid-tropospheric flow became more parallel to the Coast Range due to ridging that shifted the flow to northwesterly in the mid-troposphere (Fig. 3–34). Furthermore, low-level destabilization from insolation could no longer be expected during the late afternoon hours in November due to the low sun angle. The end result was a sharp decrease in the amount and intensity of convection across the valley and

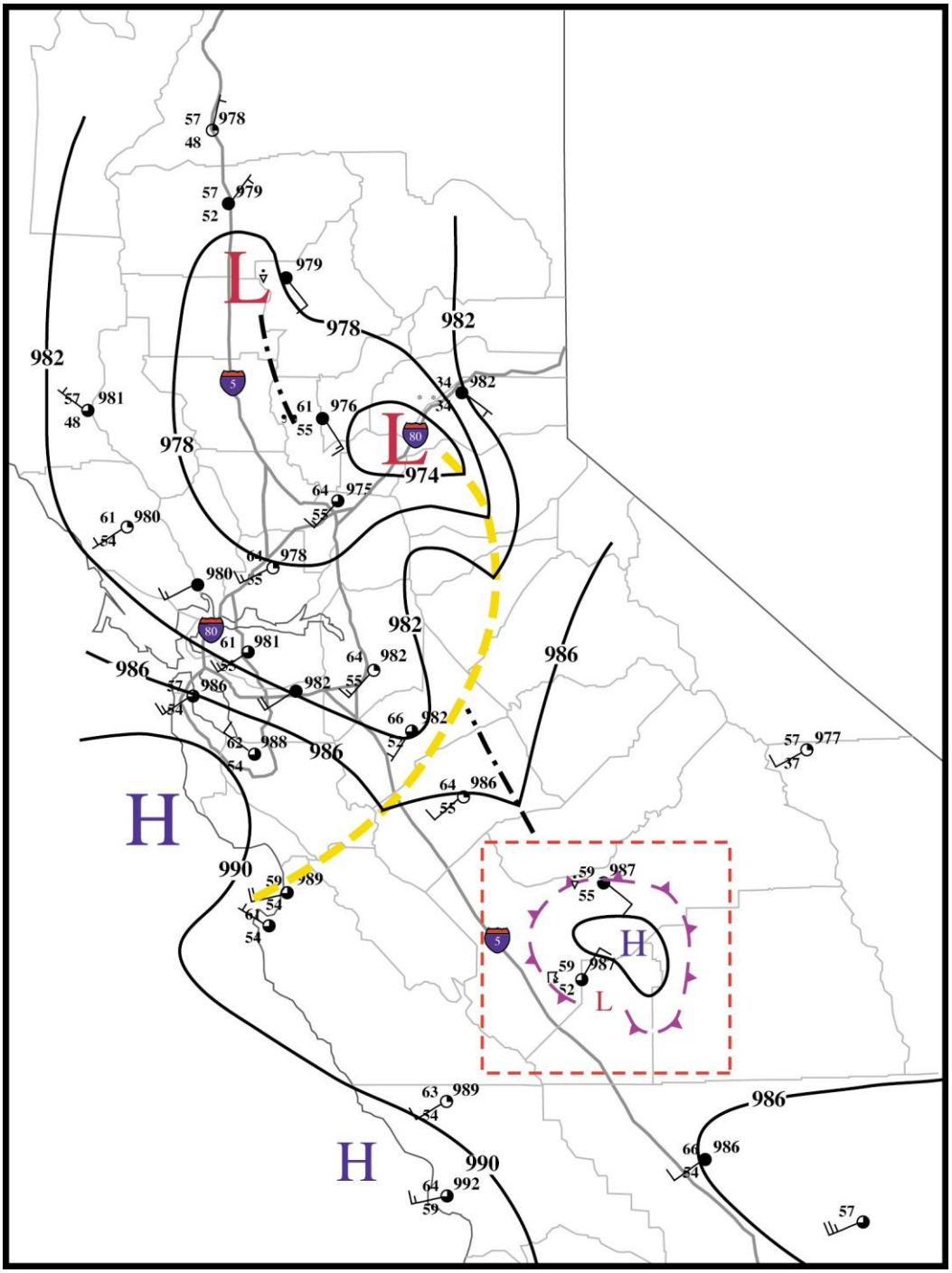

Fig. 4–21. Same as Fig. 4–1 except valid for 2300 (1500 PST) UTC 22 November 1996. Dashed red box outlines the border for Fig. 4–20.

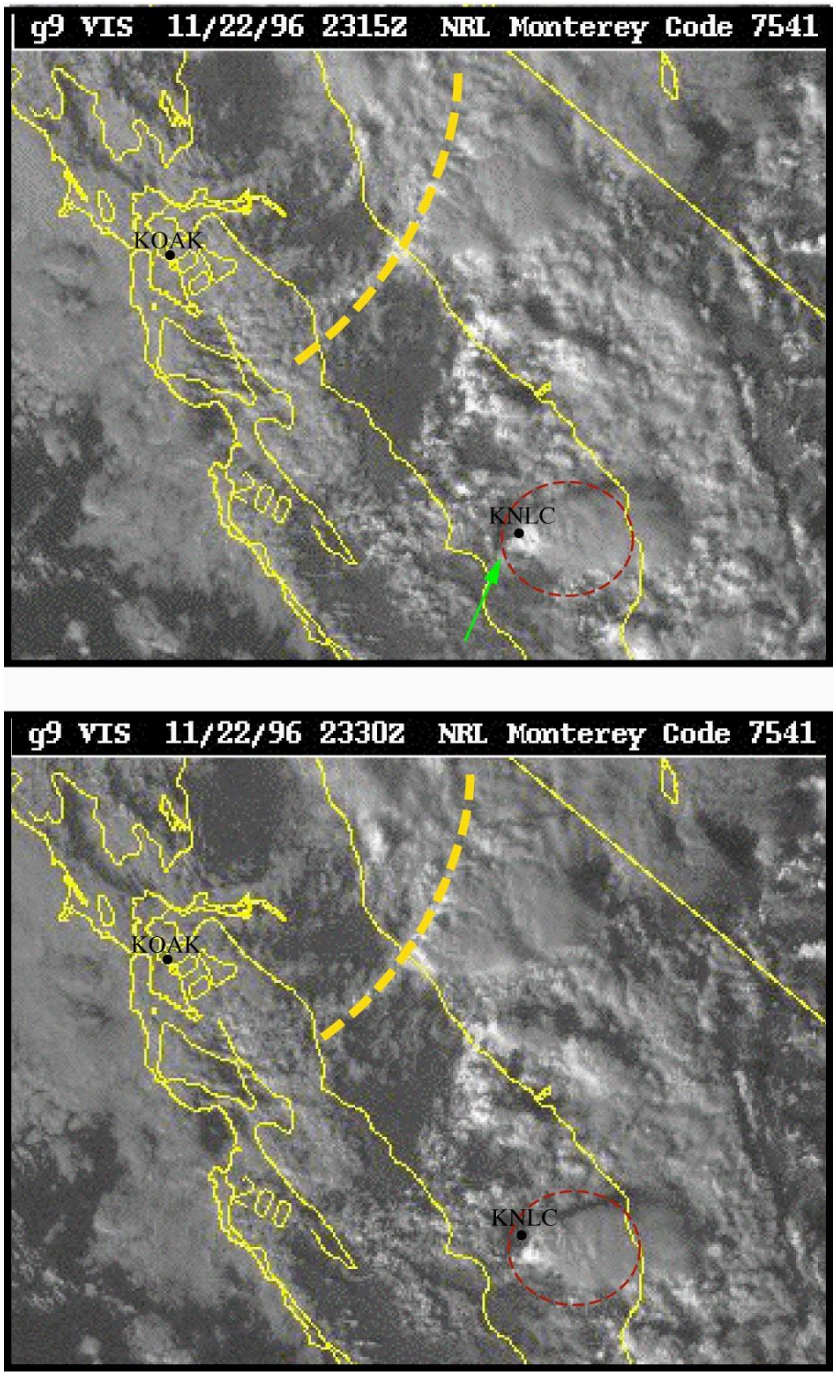

Fig. 4–22. Same as Fig. 4–2 except valid for 2315 (1515 PST) and 2330 (1530 PST) UTC 22 November 1996. Arrows and circled regions are discussed in the text.

an end to the initiation of new storms.

The Lemoore Storm evolved on radar imagery into an apparent high-precipitation supercell after the second tornado event. Radar reflectivities show significantly more precipitation had advected into the hook appendage between 2234 UTC (Fig. 4–17) and 2258 UTC (Fig. 4–20). Often classic supercells appear like HP storms during the dissipation stage when abundant precipitation is wrapped around the mesocyclone as the mid-level storm flow weakens (instead of the precipitation moving downstream into the FF downdraft) (personal comm. Doswell, 2000). In addition, precipitation loading likely caused an acceleration of the gust front (laden with cool, dry air) that undercut the storm inflow of warm moist air and weakened the core updraft. High-resolution visible satellite imagery shows the slow dissipation of the Lemoore storm between 2300 and 2345 UTC that included continued expansion of a large cirrus debris field downstream (Fig. 4–22, red-dashed circle), the collapse of the overshooting top (Fig. 4–22, green arrow), and no developing cumulonimbus. By 0000 UTC 23 November (just before sunset), almost all convection in California had ended.

5. Radar evolution and structure of the Lemoore Storm

Accurate and operationally useful detection and analysis of severe thunderstorms using Doppler radar dates back to the 1950s and early 1960s (Donaldson, 1990). On the other hand, historically, detection of tornadoes by radar has been difficult. Even though Doppler radar can be used to obtain wind velocity information, the small size of the tornado often makes clear identification of the vortex almost impossible. Burgess et al. (1993) summarized the usefulness and limitations of using Doppler radar in detecting tornadoes or, more importantly, the evidence of tornado potential from the larger parent circulation(s) surrounding the tornado. During the early and mid-1990s, WSR-88D radar systems were installed across the United States. This and the Next-Generation Doppler Radar (NEXRAD) are currently used by the National Weather Service (NWS) to issue severe thunderstorm and tornado warnings based on radar signatures (for summary, see Crum and Alberty, 1993).

Radar documentation of tornadic thunderstorms in California was generally scarce before the implementation of the WSR-88D radar network (see Carbone, 1982, 83; Monteverdi and Johnson, 1996). Notable case studies since the inception of the Doppler radar systems include Staudenmaier and Cunningham (1995), Krudzlo (1998), and the first radar documentation of an anticyclonic supercell and tornado by Monteverdi et al. (2001). The Lemoore

storm of November 1996 was a unique California event due to the close proximity of the storm to the WSR-88D radar at Hanford. Furthermore, because of the flat expanse of the San Joaquin Valley, the Doppler radar had an unobstructed view of the tornadic storm. These factors lead to an unprecedented quality of the low (0.5°) elevation radar scans for this storm. Due to such detail in the Doppler reflectivity and velocity data, the radar evolution and structure of the Lemoore Storm that produced a pair of tornadoes can readily be explored.

5.1 Sources of information and methods

Doppler radar base reflectivity and storm-relative radial wind velocity data analyzed in this section were obtained from 0.5° volume scans from the Hanford (KHNX) WSR-88D radar. Reflectivity and radial velocity cross-sections were created using the Advanced Weather Interactive Processing System (AWIPS) at the NWS field office in Hanford. Other miscellaneous radar analyses were also acquired from KHNX WSR-88D radar data.

Rotational shear associated with mesocyclones is often classified on the basis of a mesocyclone recognition nomogram that relates rotational velocity and range from the WSR-88D data to mesocyclone strength. However, due to the relatively small size of mini-supercells observed in California, the nomogram (Andra, 1997) was modified to account for this type of thunderstorm. For this

case study of the Lemoore Storm, the author uses a technique developed by Falk and Parker (1998) that utilizes mesocyclone diameter in addition to rotational velocity/range detected from low- level scans of wind velocity to assess at various times the strength of the low-level mesocyclone and likelihood of a tornado. Rotational velocity is calculated from averaging the sum of the estimate of the maximum observed inbound and outbound wind speeds from the radial velocity data or (Vin + Vout/ 2).

5.2 Formation Stage of the Lemoore Storm

Radar signatures showed that well-defined supercell structure were present and had been in existence 0.5 hour before the first report of severe weather (large hail) associated with the Lemoore storm at 2204 UTC (NCDC, 1996). At 2137 UTC 22 November 1996, the Lemoore supercell had a 'kidney bean' type appearance, a bird-shaped hook echo (Fig. 5–1, top image–brown arrow) (Fujita, 1973), and a highly reflective updraft core containing two areas of 68-dBZ returns (Fig. 5–1, top image—inset—blue arrow 2137). Strong radar reflectivities (>65 dBZ) were still detected as the updraft core propagated into the region adjacent to the hook echo at 2142 UTC (Fig. 5–2, top image—inset—blue arrow 2137).

The storm relative velocity (SRV) images for the same time show that a

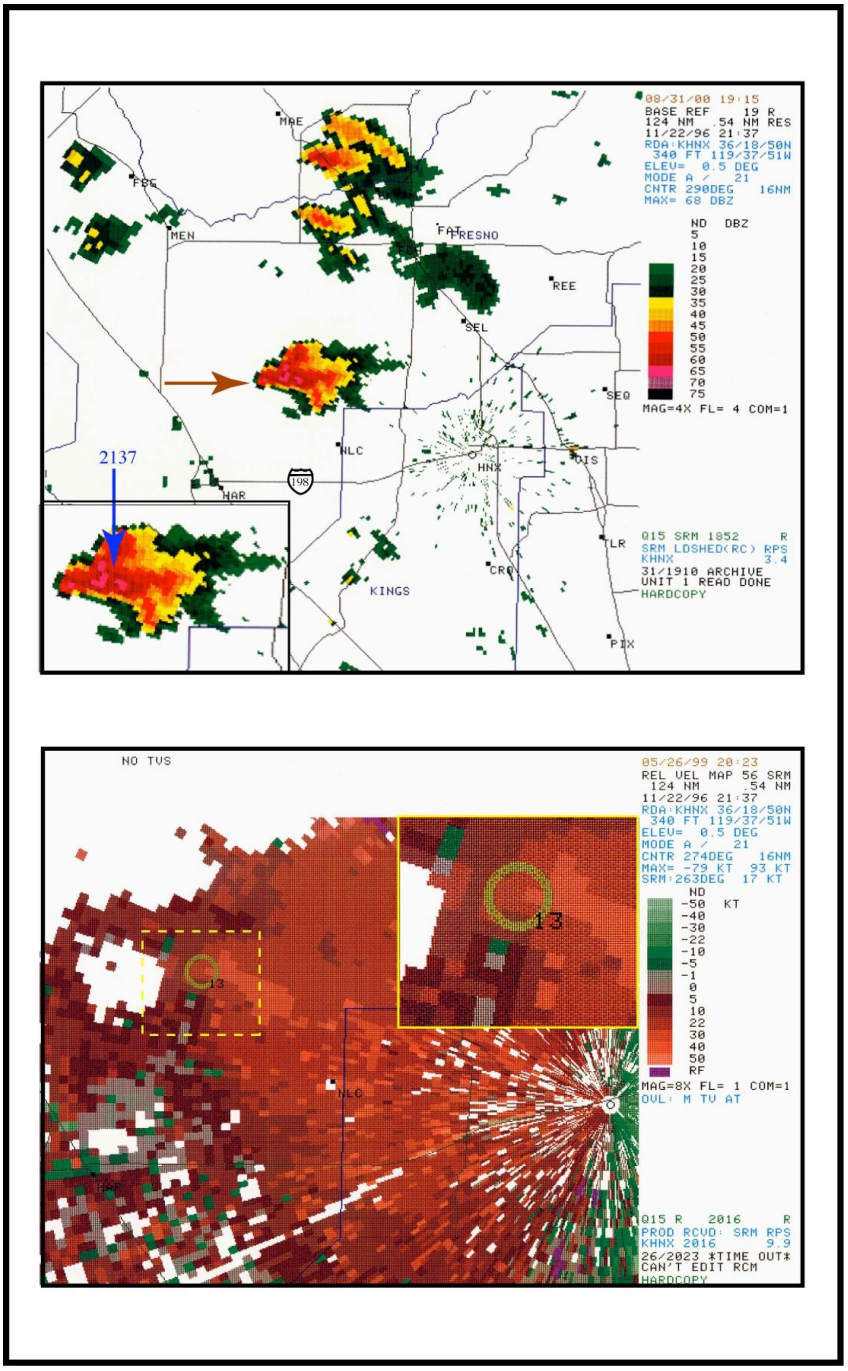

Fig. 5–1. 0.5° KHNX WSR-88D base reflectivity (top) with storm magnified in bottom left corner and storm-relative velocity (bottom) with dashed yellow box indicating magnified area in top right at 21:37 UTC 22 November 1996. Arrows are discussed in text. Note: Top and bottom images not to scale.

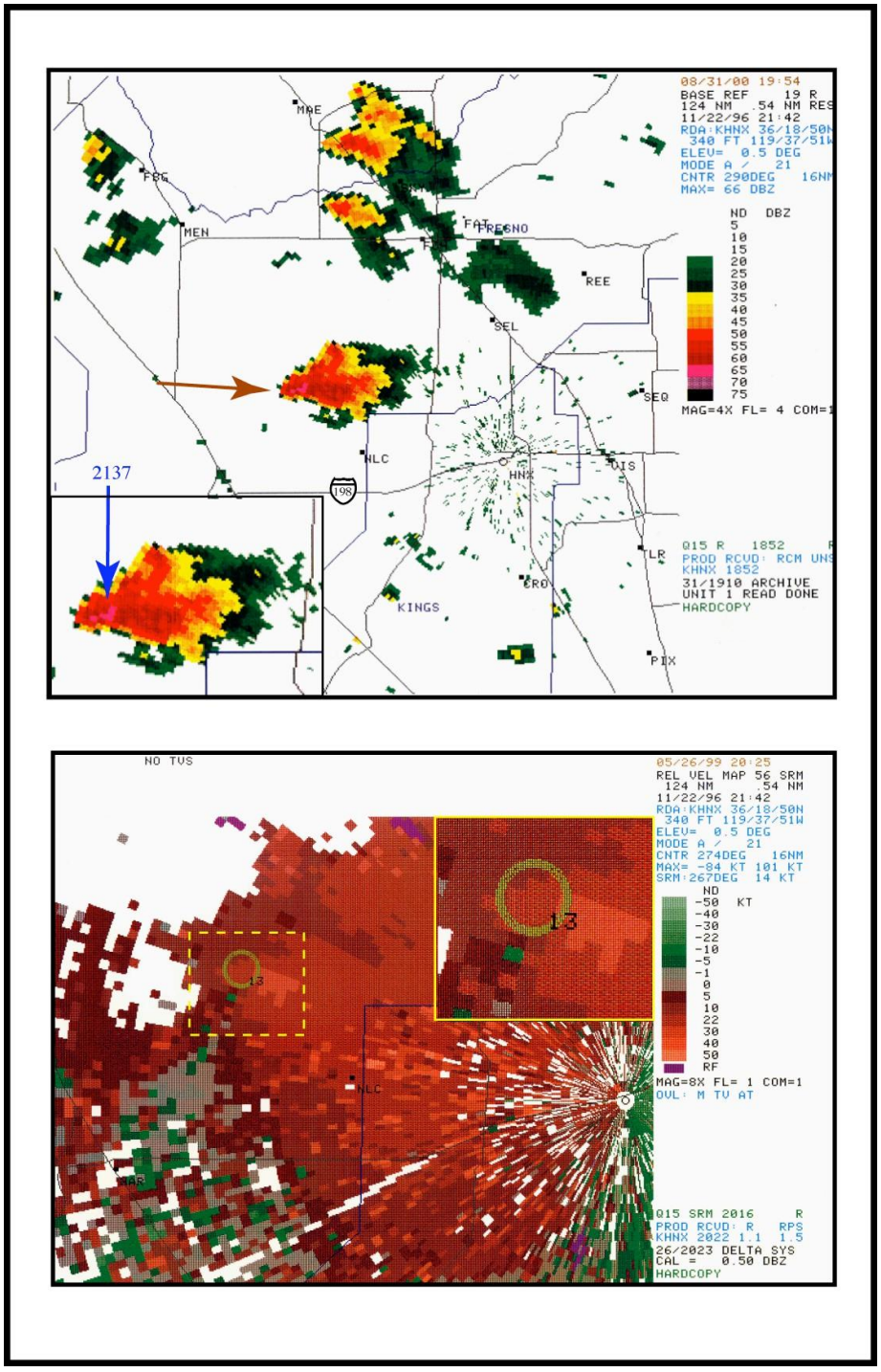

Fig. 5–2. Same as Fig. 5–1 except valid at 21:42 UTC 22 November 1996.

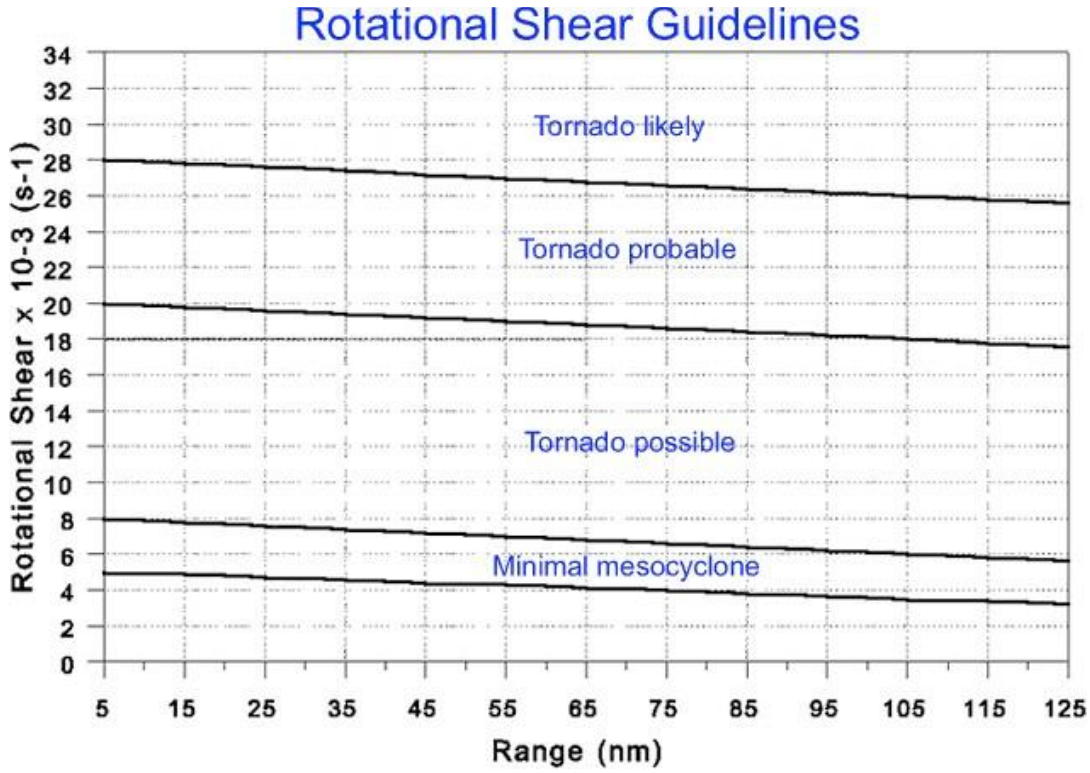

Fig. 5–3. A rotational shear nomogram divided into categories of minimal mesocyclone, tornado possible, tornado probable, and tornado likely based on 50 mesocyclone events of south central and southeaster United States (from Falk and Parker, 1998).

mesocyclone was detected by the mesocyclone algorithm (Fig. 5–1, bottom image inset–pale yellow circle) from the KHNX Doppler radar volume scans in the same vicinity as the hook echo and a very weak low-level velocity couplet (Fig. 5–1, bottom image—inset). Doppler estimated 0.5° elevation rotational velocity at 2137 UTC was approximately 22.5 knots (11.5 ms^{-1}) (40 kts outbound and 5 kts inbound) across 2 nm (4 km). The mesocyclone weakened slightly by 2142 UTC (Fig. 5–2, bottom image-top right inset) as shear decreased to 17.5

knots (9.0 ms^{-1})(30 kts outbound and 5 kts inbound). Such rotational shear values can be associated with mesocyclone strengths of 5.8 X $10^{-3}\ s^{-1}$ and 4.5 X $10^{-3}\ s^{-1}$ respectively, and are on the lower end of threshold ranges (Fig. 5–3) for a minimal strength mesocyclone (Falk and Parker, 1998). The detection of a circulation by the WSR-88D mesocyclone algorithm on both images (Fig. 5–1; Fig. 5–2, bottom image–pale yellow circle) indicates vertical continuity of the couplet was present above the 0.5° elevation. With a 0.5° sampling height in excess of 3000 feet (914 m) at this distance (~25 nm/46.3 km) and only very weak rotation observed on the low-elevation scans, the SRV images suggest storm rotation was mostly confined to the mid-levels of the storm. The RFD (and low-level mesocyclone) had yet to develop since inbound winds were not detected in the vicinity of the hook appendage, an indicator of the downdraft descending to lower levels.

5.3 Maturation Stage of the Lemoore Storm

The Lemoore Storm underwent a cycle of numerous updraft redevelopments during the maturation stage before becoming tornadic. Base reflectivity images for 2148 and 2154 UTC show that a new updraft core was developing on the right flank of the storm (Fig. 5–4; top and bottom image inset–blue arrow 2148) and that the original updraft on the left flank of the storm

began

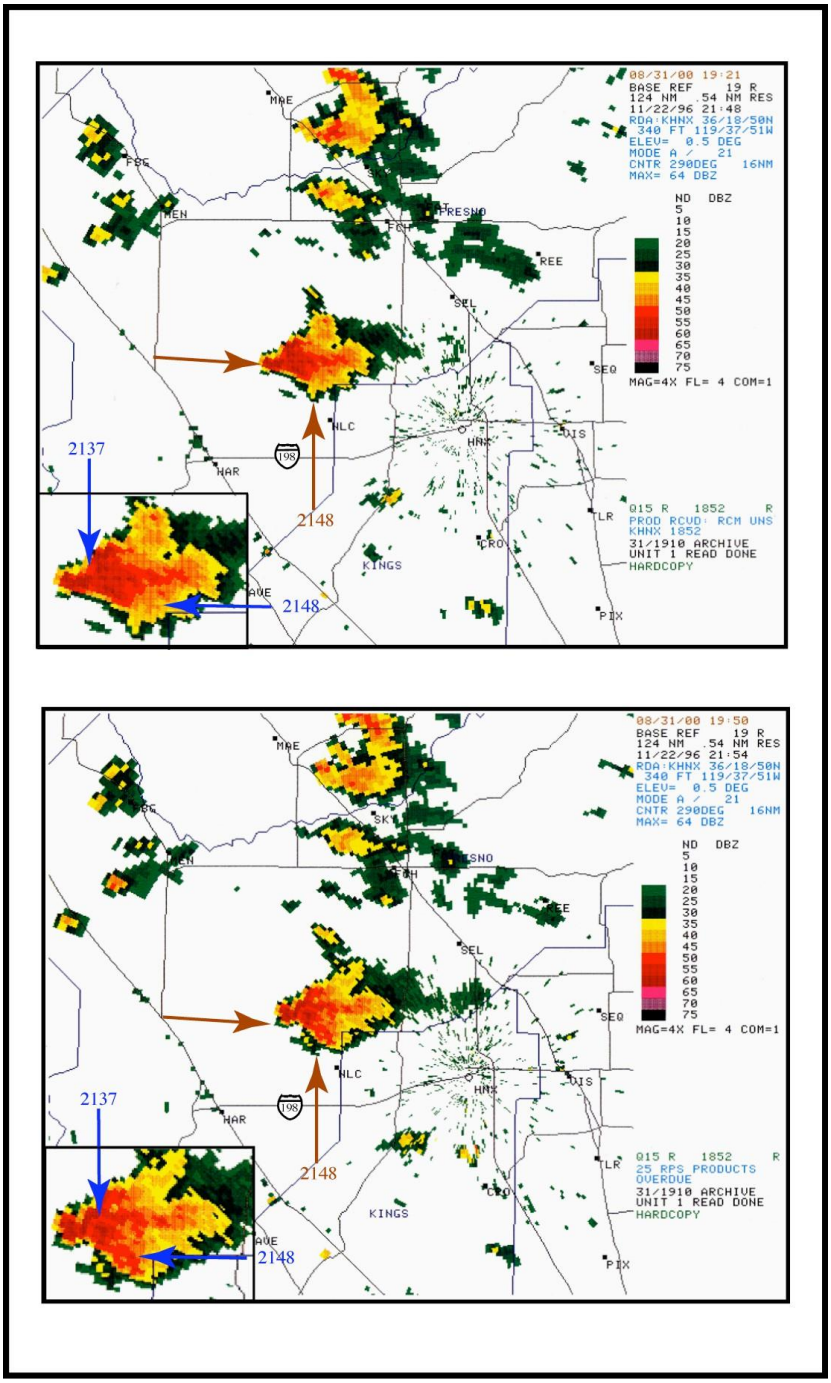
08/31/00 19:21
BASE REF 19 R
124 NM .54 NM RES
11/22/96 21:48
RDA:KHNX 36/18/50N
340 FT 119/37/51W
ELEV= 0.5 DEG
MODE A / 21
CNTR 290DEG 16NM
MAX= 64 DBZ
ND DBZ
5
10
15
20
25
30
35
40
45
50
55
60
65
70
75
MAG=4X FL= 4 COM=1
015 R 1852 R
PROD RCVD: RCM UNS
KHNX 1852
31/1910 ARCHIVE
UNIT 1 READ DONE
HARDCOPY
MAE
FSE
MEN
FCH
FRESNO
REE
SEL
SEQ
NLC
HNX
DIS
HAR
198
LR
CRO
KINGS
AVE
PIX
2137
2148
2148
08/31/00 19:50
BASE REF 19 R
124 NM .54 NM RES
11/22/96 21:54
RDA:KHNX 36/18/50N
340 FT 119/37/51W
ELEV= 0.5 DEG
MODE A / 21
CNTR 290DEG 16NM
MAX= 64 DBZ
ND DBZ
5
10
15
20
25
30
35
40
45
50
55
60
65
70
75
MAG=4X FL= 4 COM=1
015 R 1852 R
25 RPS PRODUCTS
OVERDUE
31/1910 ARCHIVE
UNIT 1 READ DONE
HARDCOPY
MAE
SKY
SEL
SEQ
NLC
HNX
DIS
HAR
198
LR
KINGS
AVE
PIX
2137
2148
2148

Fig. 5–4. The 0.5° KHNX WSR-88D base reflectivity images at 21:48 (top) and 21:54 (bottom) UTC 22 November 1996. Arrows are discussed in text.

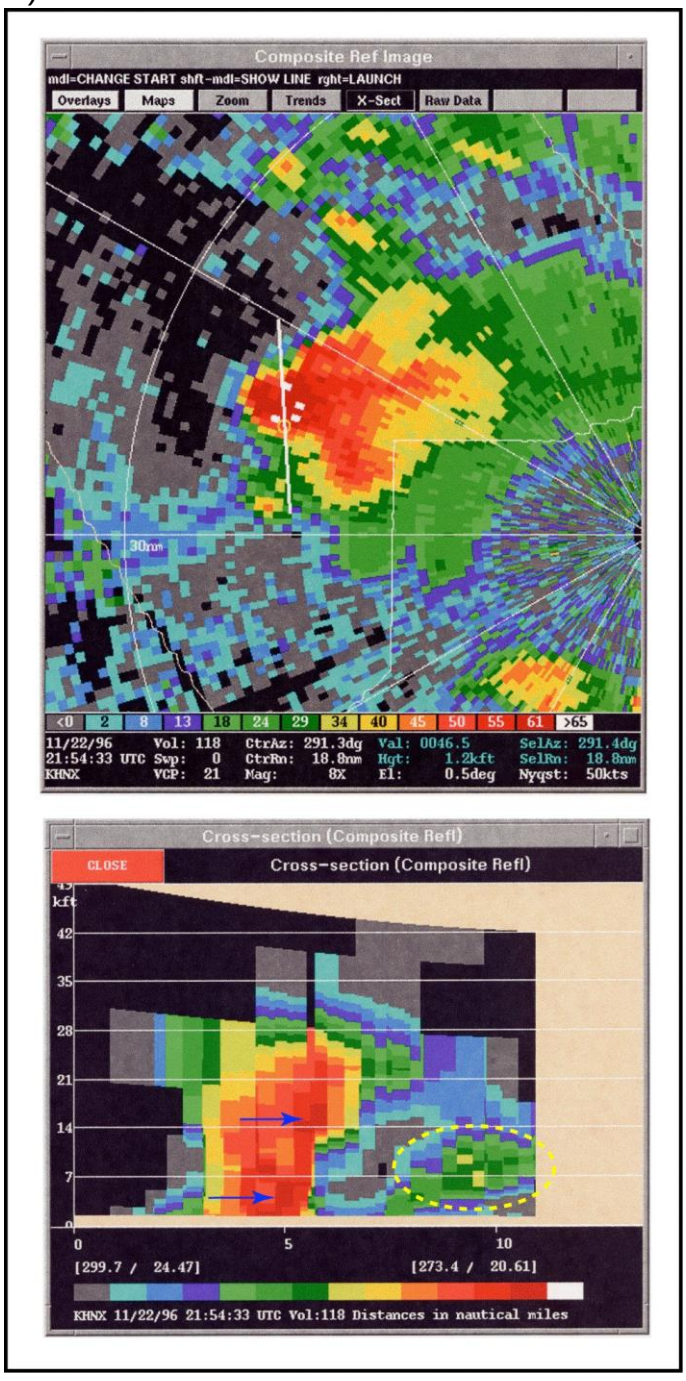

Fig. 5–5. KHNX WSR-88D composite base reflectivity image (top) and cross-section (bottom) at 21:54 UTC 22 November 1996. The white line shows the slice path for the cross-section. Arrows and circle are discussed in text.

to weaken slightly (65 dBZ to 60 dBZ). A new hook echo also appears to be forming in the same region as the new updraft (Fig. 5–4, top image--brown arrow 2148) with the main hook echo remaining distinct on the back edge of the storm.

The cross-section reflectivity scan through the updraft vault and new hook appendage in the composite reflectivity image (Fig. 5–5, top image – white line) shows two distinct areas of strong echo returns (Fig. 5–5, bottom image, blue arrows) associated with the tilted updraft core on the north flank and moderate reflectivity returns with the new hook echo (Fig. 5–5, bottom image, dashed yellow circle). The area in the middle of the updraft (~16,000 ft) with reflectivity greater than 60 dDZ was likely developing large hail observed to fall from the storm in 14 minutes. The other region near the base of the updraft was the redeveloping updraft core. The elevated (~7000 ft) and horizontal aspect of the reflectivity returns associated with the hook echo indicates that the origin of the precipitation was not linked with a surface-based updraft, but the result of precipitation being wrapped around the new mesoscale mid-level circulation on the southern flank (Fig. 5–5, top image). Additionally, a Weak Echo Region (WER) was developing adjacent to the main updraft (Fig. 5–5, bottom image) with the echoes above the WER forming a mid-level echo overhang.

The main core updraft (Fig 5–6, top image – blue arrow 2137) and the

new updraft (Fig 5–6, top image – blue arrow 2148) continued to display strong returns from the KHNX 0.5° base reflectivity scan at 2200 UTC. Both hook

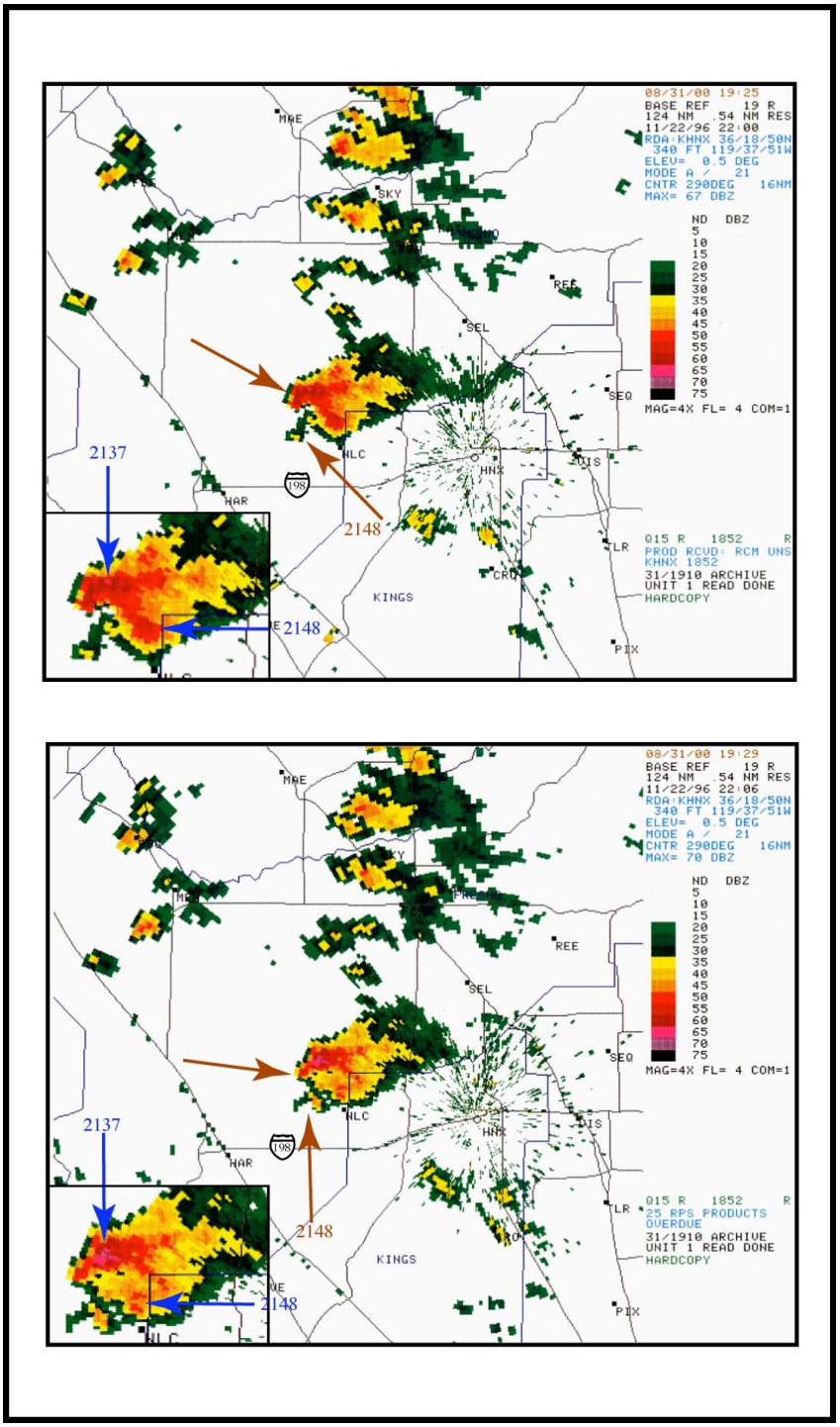

Fig. 5–6. Same as Fig. 5–3 except valid at 22:00 (top) and 22:06 (bottom) UTC 22 November 1996.

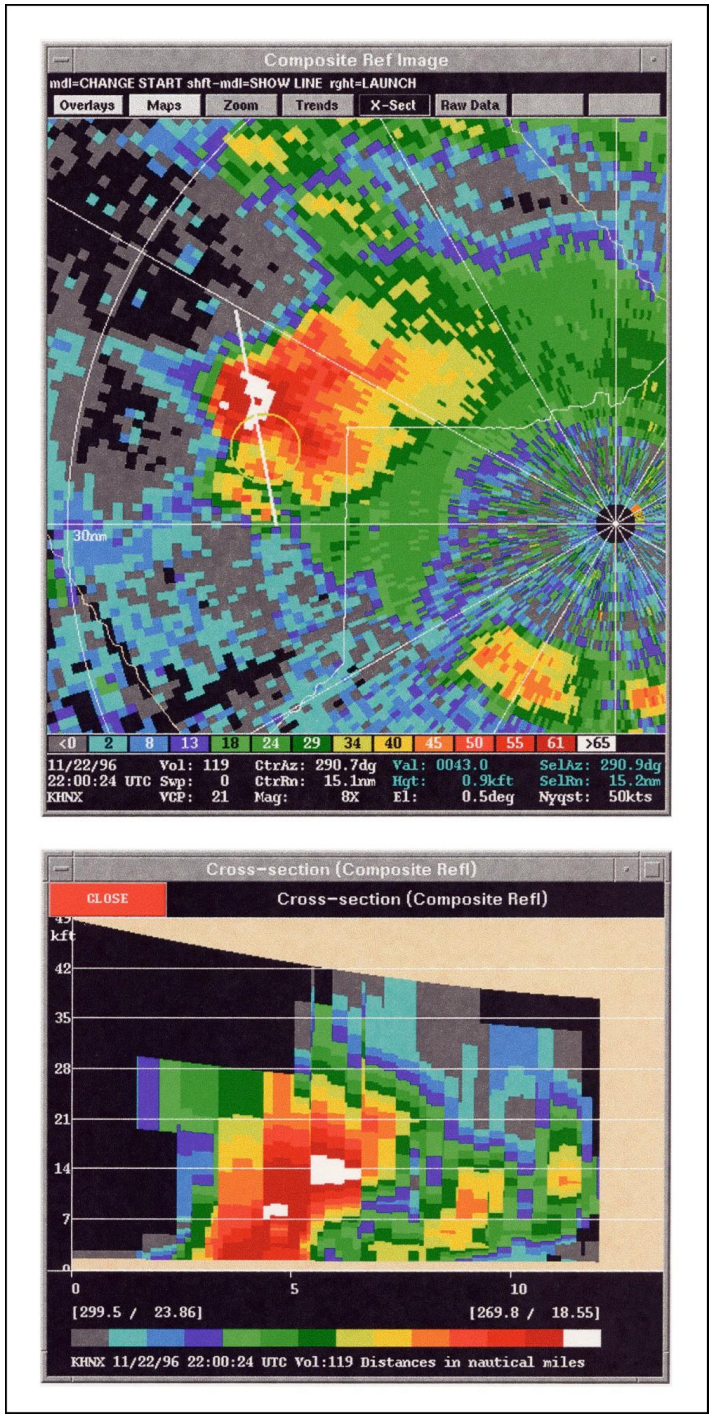

Fig. 5–7. Same as Fig. 5–4 except valid at 22:00 UTC 22 November 1996.

echoes also remained distinct (Fig 5–6, top image – brown arrow and brown arrow 2148). The cross-section (Fig. 5–7, bottom image) and plan-view composite reflectivity (Fig. 5–7, top image) images for the same time indicate mesocyclonic rotation (Fig. 5–7, top image – yellow circle) in the same vicinity of the WER. The WER continued to develop adjacent to and underneath the updraft vault that was significantly more tilted since 2154 UTC, contained reflectivities greater than 65 dBZ, and was associated with strong mid-level echo overhang.

The area of strong reflectivities in the middle region of the storm was now greater than 65 dBZ (Fig. 5–7, bottom image), but was located slightly lower in the storm (~14,000 ft). This is large hail suspended in the updraft that was observed 4 minutes later at 2204 UTC as 2.5 cm (1”) hail at the surface (NCDC, 1996). At 2206 UTC, the area of very strong reflectivities (> 65 dBZ) in the middle region of the storm was now located at the base and low-levels of the storm (Fig. 5–8, bottom image) as the large hail was likely falling from the storm at this time. This was also reflected by an increase in echo returns in the core updraft to 70 dBZ in the 0.5^{o} elevation base reflectivity scan (Fig. 5–6, bottom image inset– blue arrow 2137).

The updraft vault was even more tilted and the storm now contained a distinct BWER adjacent to the core updraft (Fig. 5–8, bottom image) at 2206 UTC. Together with the continued detection of a circulation by the WSR-88D

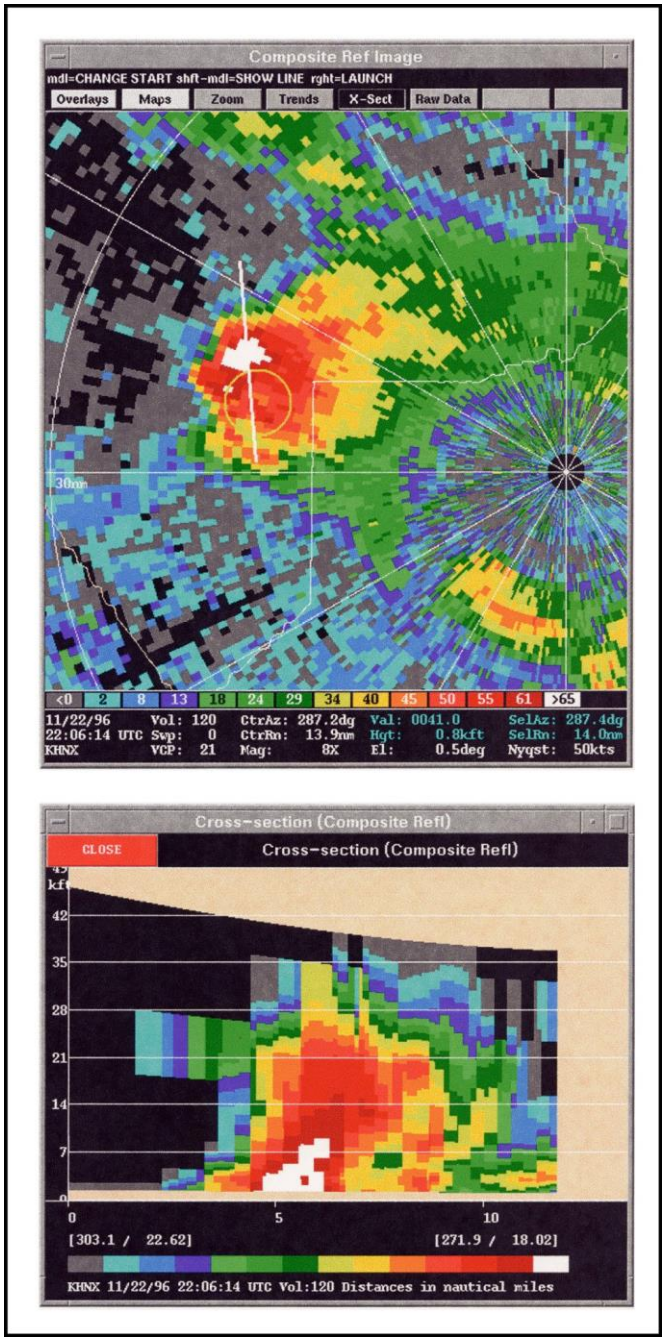

Fig. 5–8. Same as Fig. 5–4 except valid at 22:06 UTC 22 November 1996.

mesocyclone algorithm (Fig. 5–8, top image – pale yellow circle), the Lemoore supercell appears to be associated with a distinct and long-lived mid-level mesocyclone. However, there were likely two circulations associated with the storm, a strong one with the original updraft (Fig. 5–6, bottom image inset– blue arrow 2137) and a weaker one with the new core updraft (Fig. 5–6, bottom image inset– blue arrow 2148). No detection by the WSR-88D mesocyclone algorithm after 2206 UTC (not shown) indicates that the mid-level mesocyclone weakened when the new updraft core and hook echo (Fig. 5–6, top image – brown arrow 2148) merged with the original updraft and hook echo (Fig. 5–6, top image – brown arrow). This likely briefly interrupted the supercell cascade process.

The "supercell cascade" leading to tornadogenesis is a conceptual model that starts with the development of the midlevel mesocyclone, advection of precipitation by the mesocyclone around the updraft area, development of a rear flank downdraft (RFD) simultaneous with the development of the mesocyclone at lower levels, and interaction of the RFD with the low-level shear to produce the low-level tornado cyclone and, eventually, the tornado.

Over the next seventeen minutes (2206–2223 UTC) the Lemoore storm redeveloped. The original core updraft moved into the hook echo region causing a prominent “knob” shape to the radar appendage (Fig. 5–9, top image – brown arrow 2137) as the new updraft core (Fig. 5–9, top image inset– blue arrow 2148) became the dominant updraft in the center of the storm. A RFD then developed

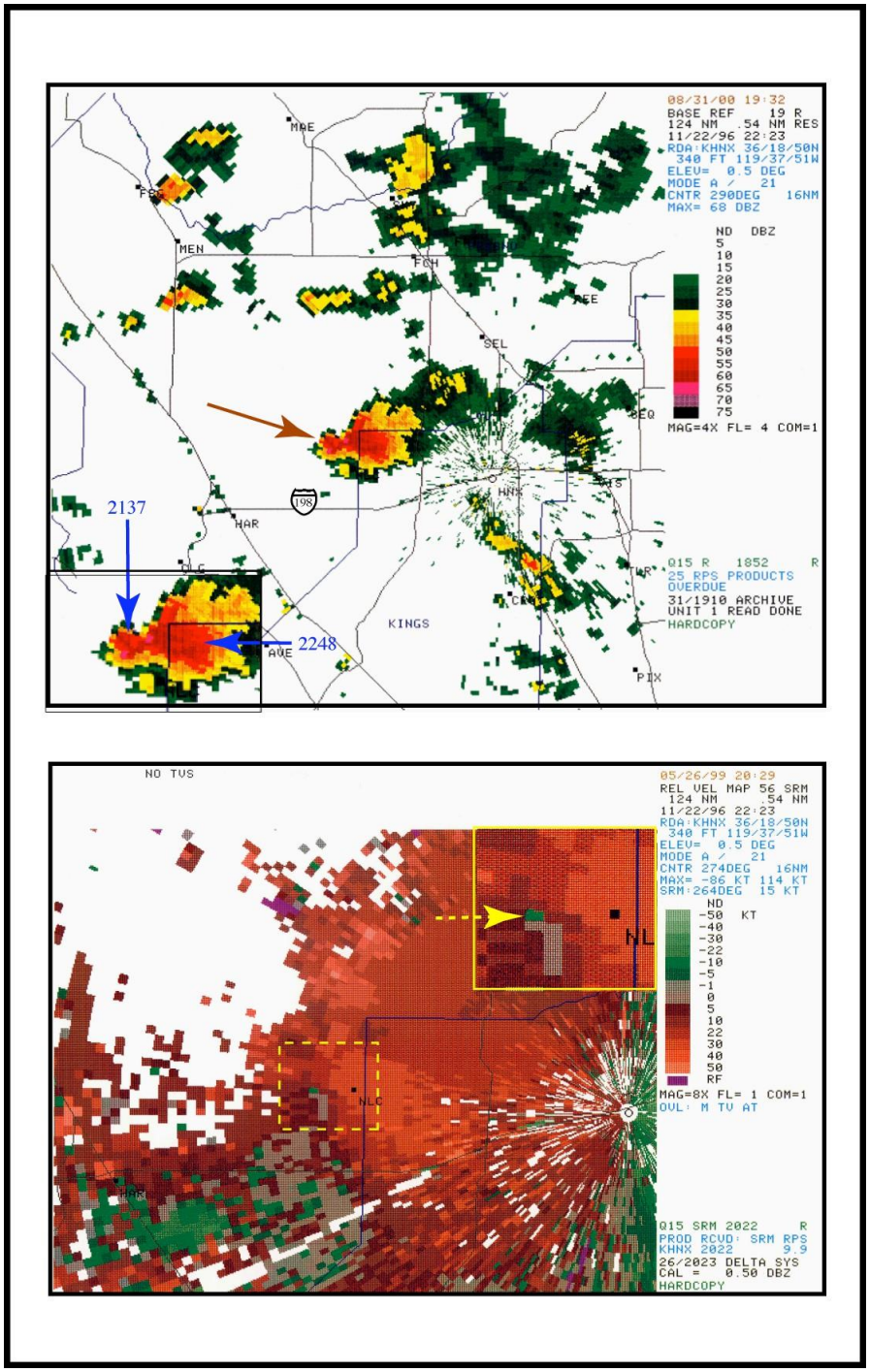

Fig. 5–9. Same as Fig. 5–1 except valid at 22:23 UTC 22 November 1996.

on the up-shear flank of the storm indicated on the 0.5° elevation WSR-88D SRV scan of inbound radial velocities (Fig. 5–9, bottom image inset–dashed yellow arrow) that associate well with the location of the knob-shaped hook echo. A 2 nm (4 km) wide region of weak low-level rotation on the 0.5° WSR-88D SRV image was also forming simultaneously (Fig. 5–9, bottom image inset–yellow arrow) with the RFD. Calculated mesocyclone strength was 5.2 X $10^{-3}\ s^{-1}$ from 20 knots (10.3 ms^{-1}) of gate-to-gate shear (30 outbound and 10 inbound). At a range of 15 nm from the Doppler site, this value of mesocyclone rotational shear translates to a minimal strength mesocyclone (Fig. 5–3). This re-strengthening of the Lemoore mid-level mesocyclone between 2206 and 2223 UTC instigated the supercell cascade that led to the first tornado between 2227 and 2237 UTC.

5.4 Tornado Phase of the Lemoore Storm.

The first observed tornado occurred between 2227 and 2237 UTC causing no damage traversing across a barren field near a runway complex in the Lemoore Naval Air Station. It was rated an F0 on the Fujita scale (Appendix 1). The base-reflectivity radar image at 0.5° tilt from the KHNX WSR-88D for 2229 UTC shows that the new updraft core had become well-established at the rear flank of the storm with maximum reflectivities of 69 dBZ (Fig. 5–10, top image inset– blue arrow 2148) at the time of this first tornado event. The hook echo

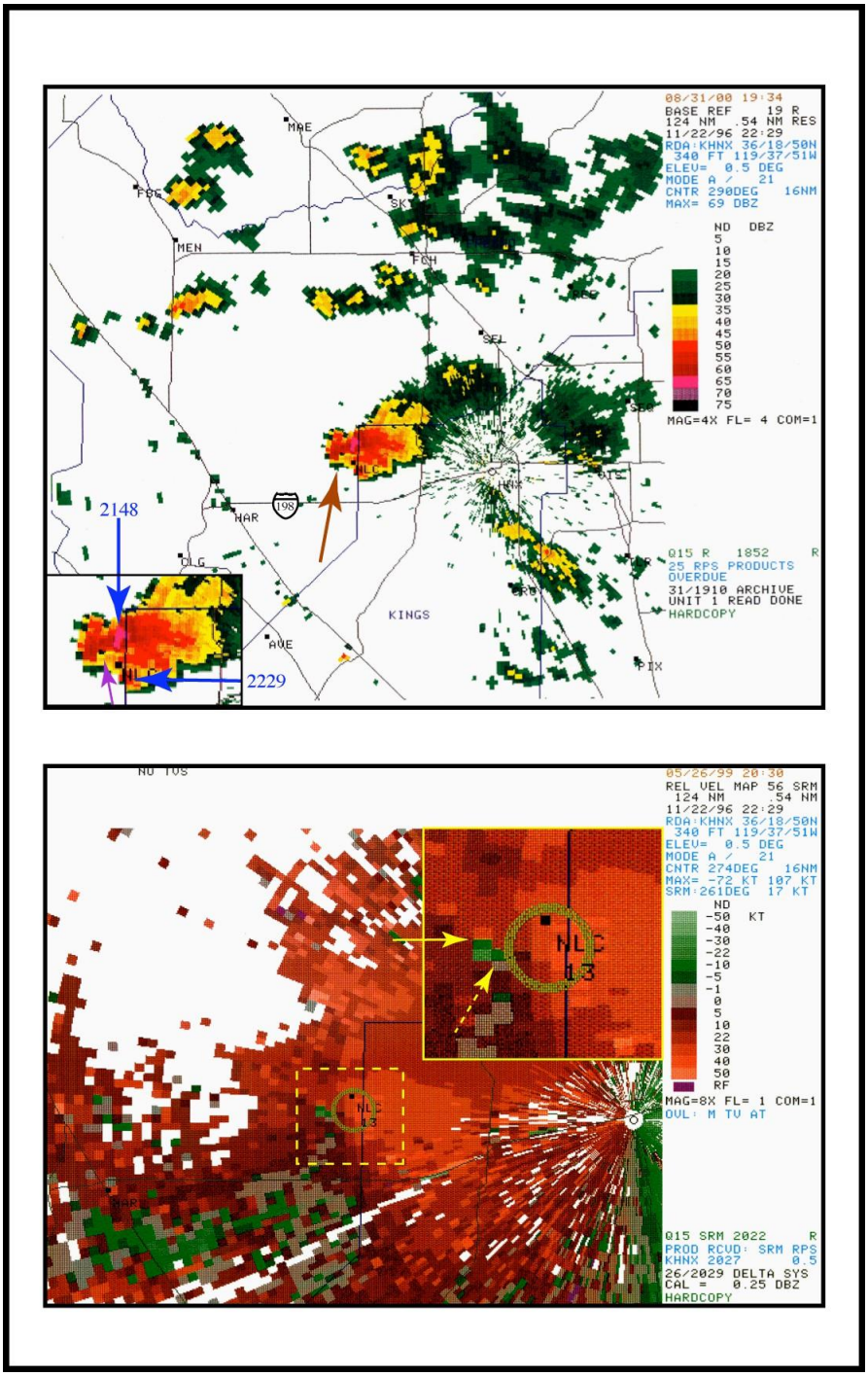

Fig. 5–10. Same as Fig. 5–1 except valid at 22:29 UTC 22 November 1996.

region (Fig. 5–10, top image – brown arrow) also appears to have developed a V-notch signature (Fig. 5–10, top image inset – purple arrow). V-notch radar reflectivity signatures form when the mean flow is blocked by the updraft and heavier precipitation is carried around the updraft forming the V-notch. This feature is usually a signal of increased mesocyclonic rotation and is often associated with a WER or Bounded Weak Echo Region (BWER) on cross-sectional reflectivity scans. Nonetheless, although the storm was tornadic at this time, the storm was also in the last cycle of an updraft re-development with new cell growth evident in the inflow region on the down-shear flank of the storm (Fig. 5–10, top image inset– blue arrow 2229). This core would eventually become the dominant updraft during the F1 tornado event.

The low and mid-level mesocyclone intensified in unison with the new updraft core during the first tornado episode with the 0.5° elevation KHNX WSR-88D SRV image showing a low-level velocity couplet and the WSR-88D mesocyclone algorithm detecting a mid-level circulation (Fig. 5–10, bottom image inset–pale yellow circle). The shear magnitude between gate-to-gate velocities of this approximately 2 nm (4 km) wide circulation was 45 knots (23 ms^{-1}) and rotational shear was 11.5 X 10^{-3} s^{-1}. This suggests that the low-level mesocyclone associated with the Lemoore Storm is now strong enough for a tornado to be possible (Fig. 5–3). Furthermore, an intense [45 knots (23.2 ms^{-1}) of shear] small-scale [~1 nm nm (2 km) in diameter] circulation on the rear-flank

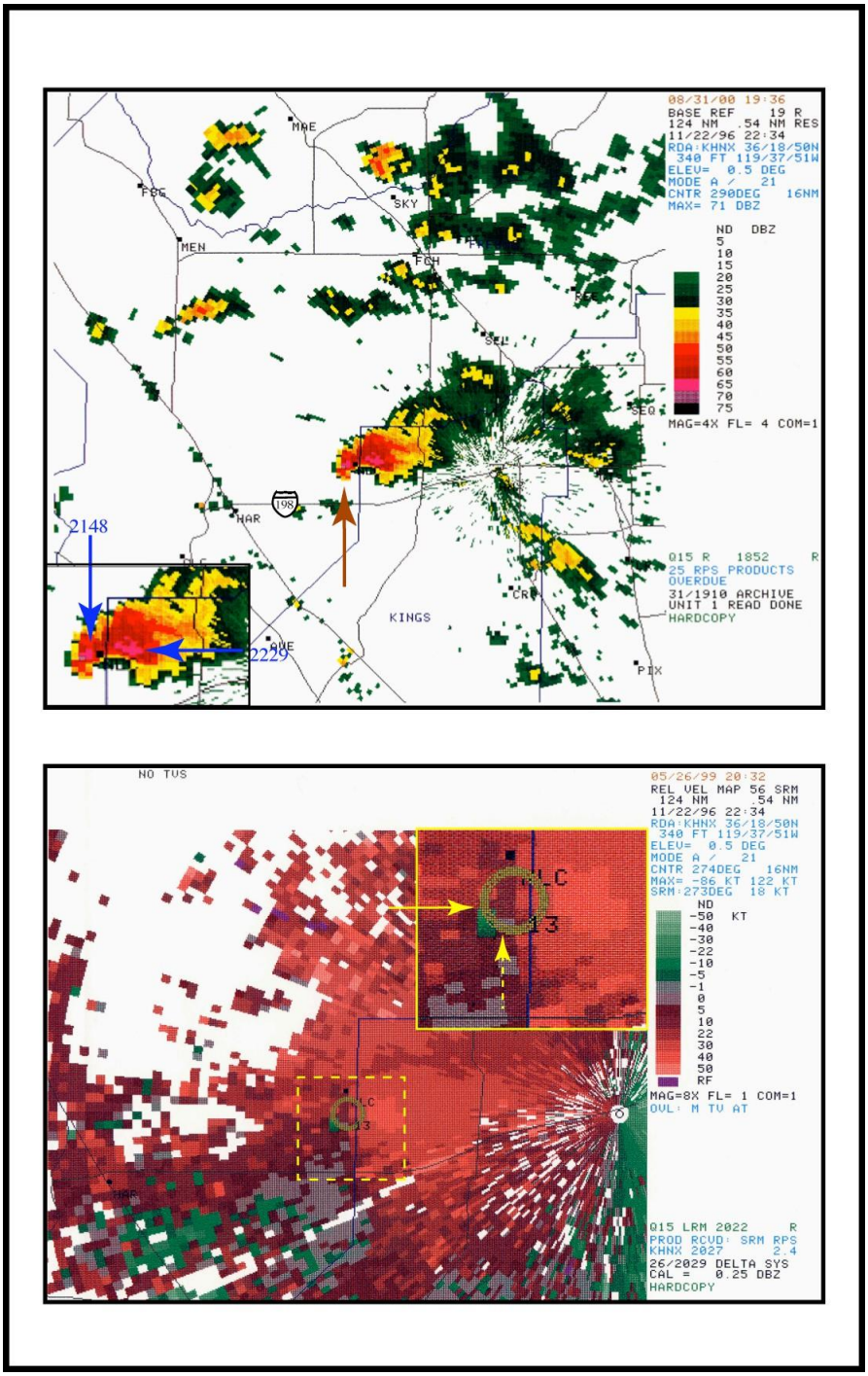

Fig. 5–11. Same as Fig. 5–1 except valid at 22:34 UTC 22 November 1996.

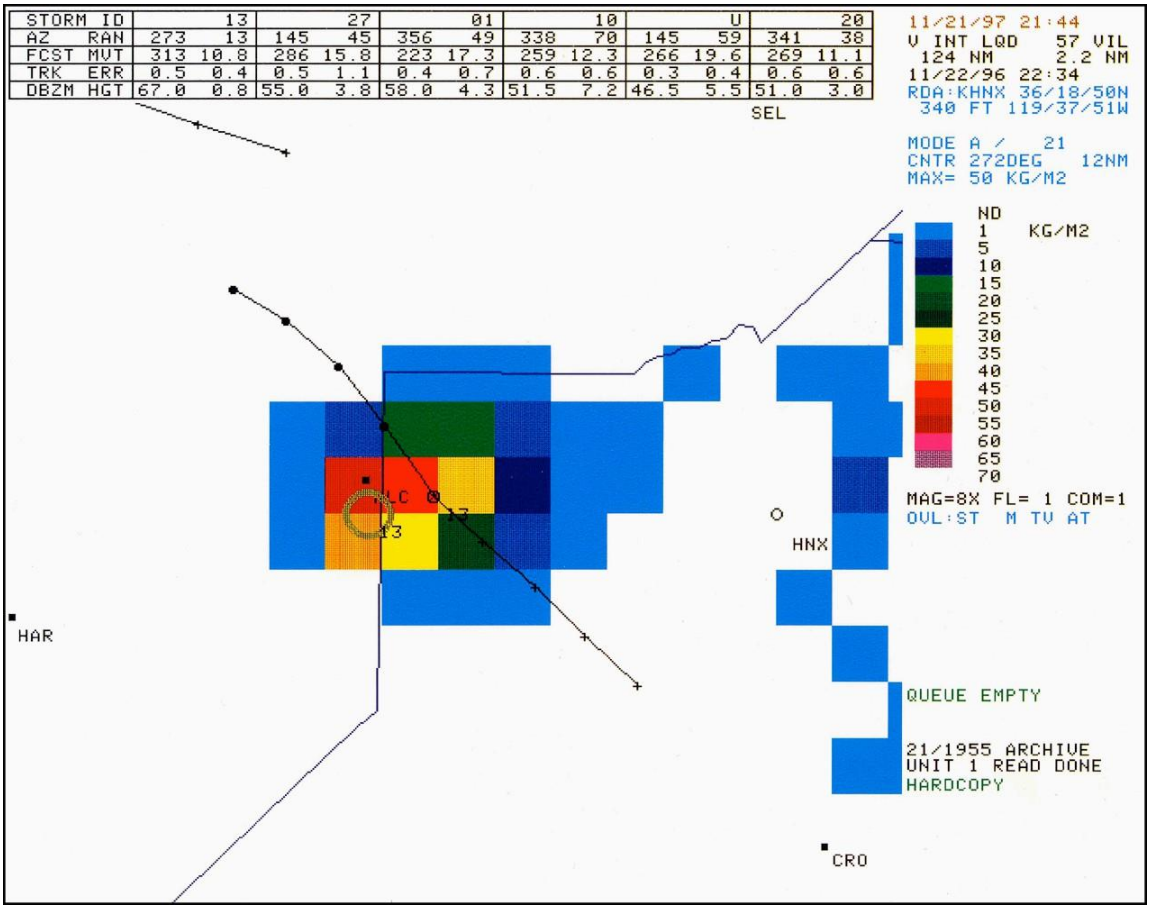

Fig. 5–12. KHNX WSR-88D Vertically Integrated Liquid (VIL) image at 22:34 UTC 22 November 1996.

of the mesocyclone within the reflectivity hook appears to have developed over the last six minutes and shortly before the formation of the first tornado (Fig. 5–10, bottom image inset–yellow arrow). The rotational shear associated with this couplet was 23.2 X $10^{-3}\,s^{-1}$ and indicates a tornado was probable with this vortex (Fig. 5–3). Furthermore, the RFD continued to expand downstream in the cyclonic circulation of the mesocyclone indicated by storm relative inbound winds

located at tip of the hook echo (Fig. 5–10, bottom image inset–dashed yellow arrow).

Recent evidence has led severe storm researchers to believe that the tornado may only be sampled in rare cases and that it is the tornado cyclone signature (TCS), an intermediate sized circulation between the tornado and the mesocyclone, which is actually detected by WSR-88D SRV scans (Mitchell and Stumpf, 1996, Rasmussen and Straka, 1996, Straka et al., 1996). The case study by Mitchell and Stumpf (1996) observed a small-scale circulation (presumably the tornado cyclone) embedded within the larger region of the mid-level mesocyclone and other observations of near-range tornadoes appear to support such structure. Mitchell and Stumpf (1996) theorized that the vortex is perhaps the circulation whose outer limit is basically the encircling RFD at the lowest altitudes. Rasmussen and Straka (1996) have shown that this vortex tends to be less than 2 km wide and often is present and associated with the storm scale occlusion process prior to tornado formation.

Gate to gate shear with the mesoscale vortex weakened to 40 knots (20.6 ms^{-1}) and 20.6 X $10^{-3}\ s^{-1}$ of rotational shear, but still remained distinct on the next WSR-88D 0.5° elevation scan at 2234 UTC (Fig. 5–11, bottom image inset–yellow arrow). This is likely a TCS linked with the first F0 tornado between 2227 and 2237 UTC. Furthermore, the 2234 UTC scan continued to detect two distinct highly reflective (>65 dBZ, maximum 71 dBZ) updraft cores embedded in

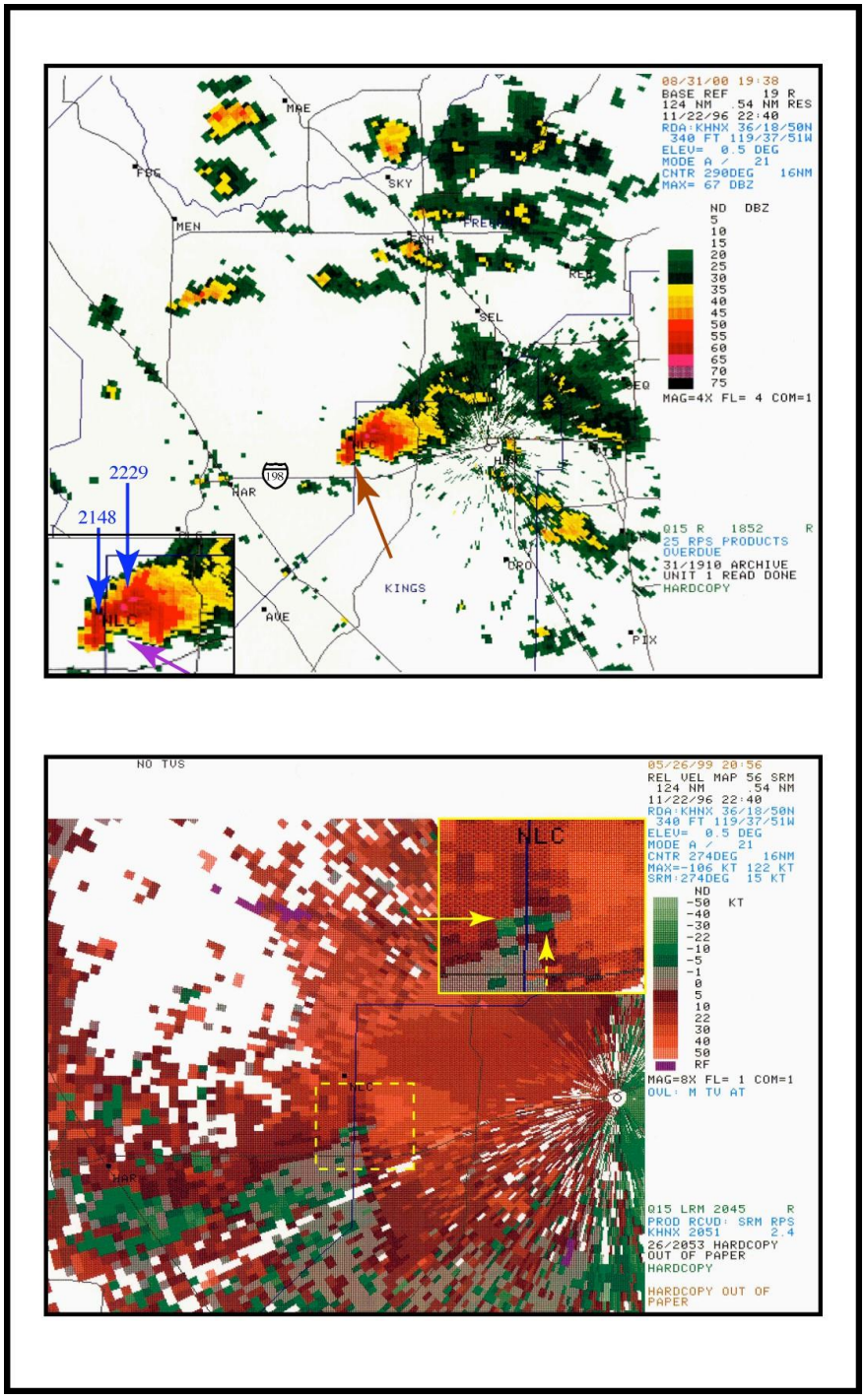

Fig. 5–13. Same as Fig. 5–1 except valid at 22:40 UTC 22 November 1996.

the storm structure (Fig. 5–11, top image inset– blue arrow 2148 and 2229). The vertically integrated liquid (VIL) (Fig. 5–12) product shows that large hail (maximum 50 kgm^2) was likely associated with these intense updrafts and especially with the updraft in the hook echo region (Fig. 5–11, top image – brown arrow) that contained the 71 dBZ reflectivity echo (Fig. 5–11, top image inset– blue arrow 2148). This coincides with the report of large hail (2 _"/6.25 cm) in the Lemoore Naval Air Station at 2250 UTC that smashed the sides and fronts of vehicles (NCDC, 1996).

The large hail was also likely a factor in the initiation of a storm-scale occlusion downdraft within the RFD that occurred just prior to the formation of the second tornado. Precipitation loading was a likely partial cause of that downdraft since maximum radar echo reflectivities within the hook echo region decreased from 71 dBZ to 60 dBZ between 2234 UTC (Fig. 5–11, top image inset– blue arrow 2148) and 2240 UTC (Fig. 5–13, top image inset– blue arrow 2148). SRV signatures confirm this RFD acceleration reached the lower-levels since radial inbound winds increase from 1 (0.51 ms^{-1}) (Fig. 5–11, bottom image inset–dashed yellow arrow) to 10 knots (5.1 ms^{-1}) (Fig. 5–13, bottom image inset–dashed yellow arrow) in the area near the tip of the hook appendage during that same time frame.

The other updraft core continued to be associated with strong radar reflectivities (>65 dBZ) while showing progressive movement into the rear flank of

the storm (Fig. 5–13, top image inset– blue arrow 2229). However, the WSR-88D mesocyclone algorithm at 2240 UTC did not detect a vertically stacked circulation (Fig. 5–11, bottom image inset) and that suggests the mid-level mesocyclone had weakened. Rotational shear at the 0.5^{o} elevation scan decreased to 10.3 X 10^{-3} s^{-1} as well, although a tornado is still possible with this strength low-level circulation (Fig 5–3). The small-scale intense vortex had also weakened from 40 knots to 30 knots of shear (Fig. 5–13, bottom image inset–yellow arrow) and, consequently, the first tornado had dissipated by this time. Nevertheless, the precipitation in the hook echo (Fig. 5–13, top image – brown arrow) continued to wrap around the mid-level circulation and a distinct V-notch (Fig. 5–13, top image inset – purple arrow) is evident on the base-reflectivity image indicating the observed weakening of the mesocyclone was likely only temporary.

Over the next twelve minutes to 2252 PST, the Lemoore storm rapidly intensified with the tornado forming and producing F1 damage around 2250 PST. The storm had moved through the Naval Air Station and was poised just north of Hwy 198 where the administration offices on the base are located (Fig. 5–14). The continued southeast movement of the storm meant a direct strike on that portion of the naval base was imminent.

The SRV 0.5^{o} elevation (2500 ft/760 m AGL at 14 nm) image for 2246 UTC indicates the intensification of the low-level mesocyclone had not occurred yet. The shear magnitude between gate-to-gate velocities of this approximately

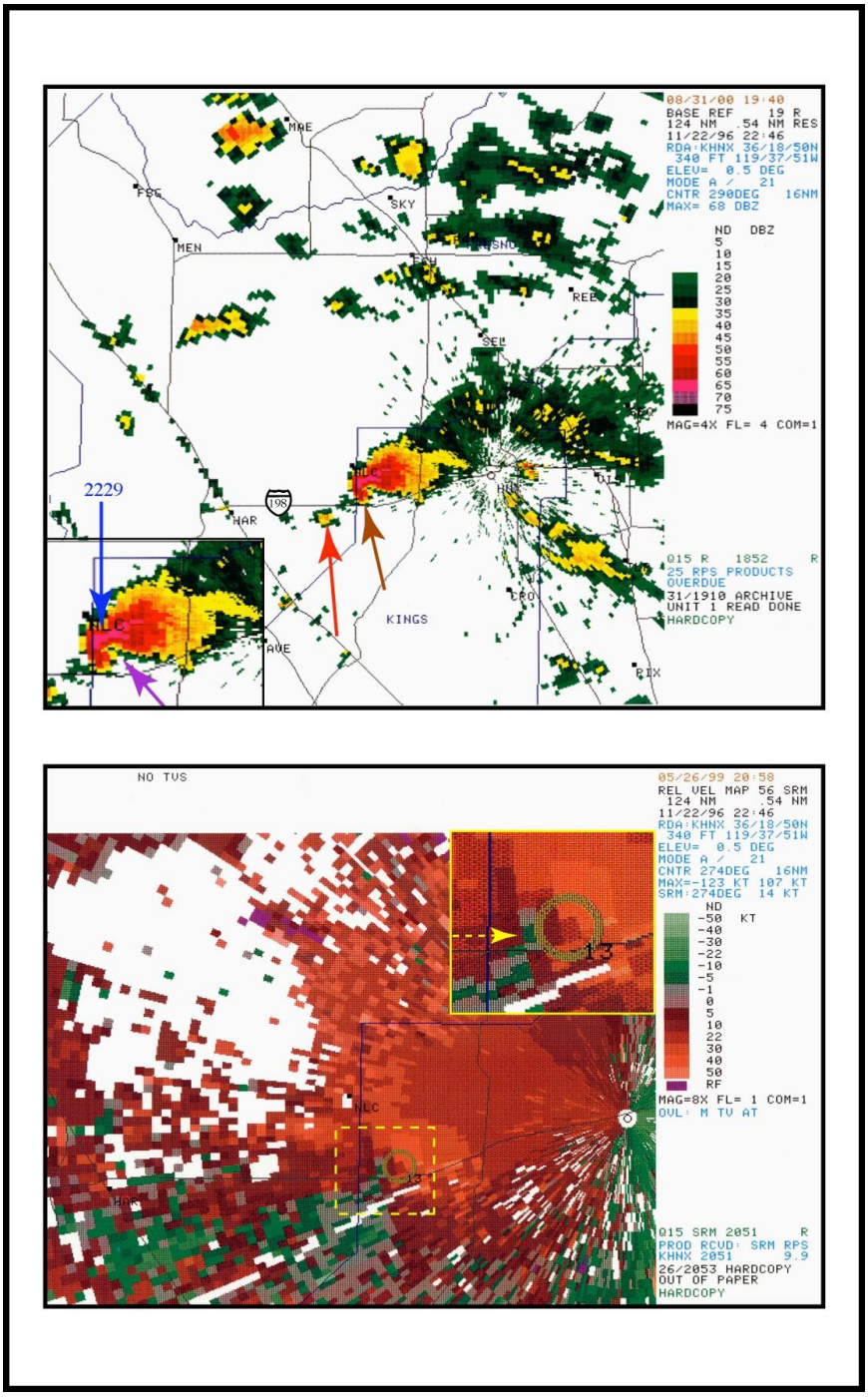

Fig. 5–14. Same as Fig. 5–1 except valid at 22:46 UTC 22 November 1996.

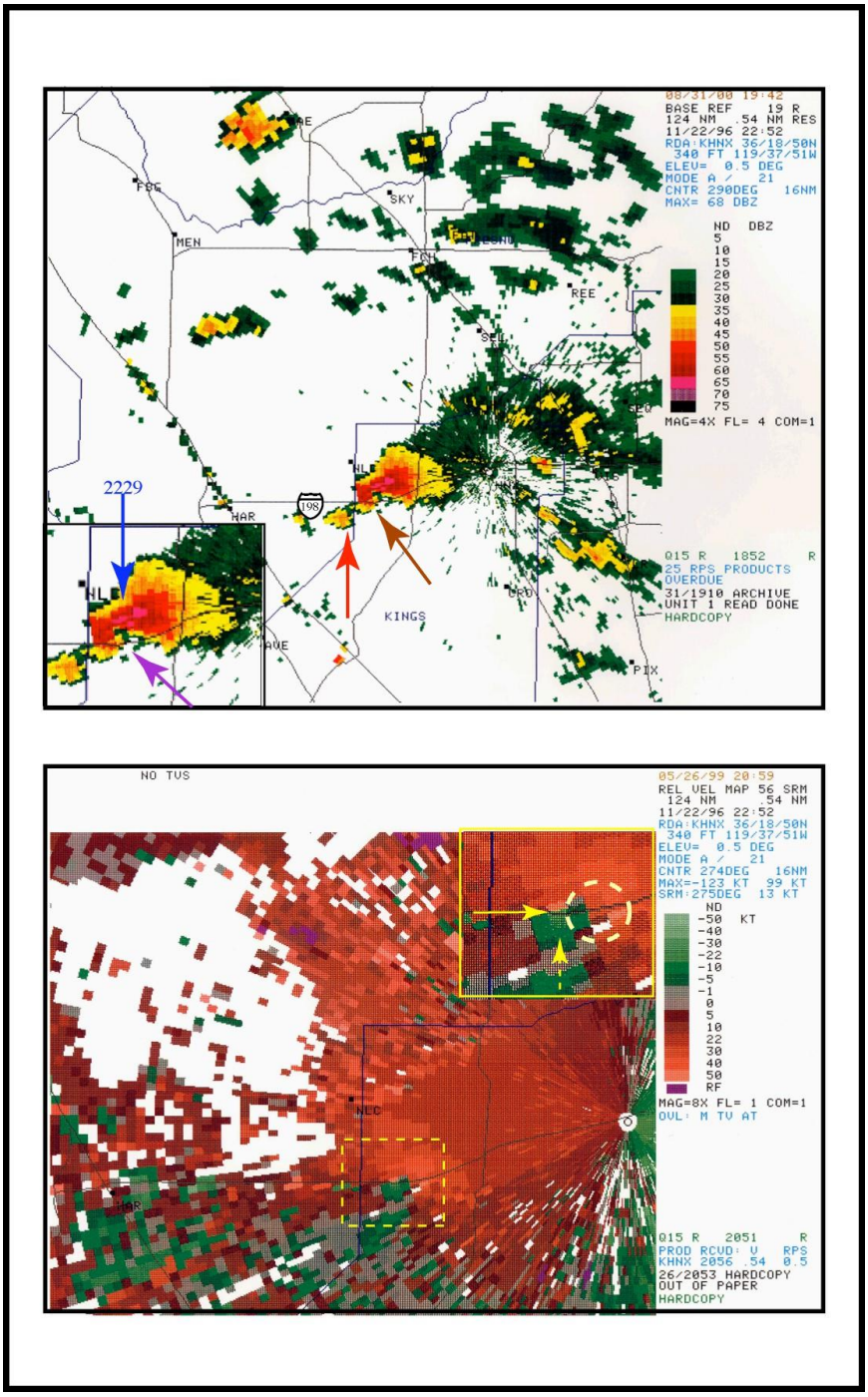

Fig. 5–15. Same as Fig. 5–1 except valid at 22:52 UTC 22 November 1996.

1.75 nm (3.5 km) wide circulation, although a little smaller in diameter, was only 30 knots (15.4 ms^{-1}) and rotational shear was 8.8 X 10^{-3} s^{-1} or minimal mesocyclone strength (Fig. 5–3). The mesoscale couplet had completely dissipated as well. However, a detection of a circulation by the WSR-88D mesocyclone algorithm (Fig. 5–14, bottom image inset–pale yellow circle) in the same region as the V-notch signature/hook echo region indicates that the mid-level mesocyclone had strengthened. A more pronounced WER developed in the V-notch signature within the hook echo region between 2246 (Fig. 5–14, top image inset – purple arrow) and 2252 UTC (Fig. 5–15, top image inset – purple arrow) that also suggests mid-level mesocyclone intensification.

The 0.5° elevation base reflectivity image for 2246 UTC shows that the core updraft (Fig. 5–14, top image inset– blue arrow 2229) was now very strong (68 dBZ) and positioned in the rear flank of the storm. Hydrometeors continued to circulate in the mid-level circulation of the hook echo (Fig. 5–14, top image – brown arrow) from the updraft core, and although the updraft remained distinct and strong (68 dBZ) on the right flank of the storm, aerial coverage of the very strong reflectivity echoes (> 65 dBZ) decreased in the updraft region between 2246 (Fig. 5–14, top image inset– blue arrow 2229) and 2252 UTC (Fig. 5–15, top image inset– blue arrow 2229) and increased within the hook (Fig. 5–14 and Fig. 5–15, top image –brown arrow) likely re-enforcing surges of embedded small-scale downdrafts within the RFD. This is indicated on the 0.5° elevation

SRV images by a strong increase in maximum inbound velocities from 10 knots at 2246 UTC (Fig. 5–14, bottom image inset–dashed yellow arrow) to 40 knots at 2252 UTC (Fig. 5–15, bottom image inset–dashed yellow arrow) that continue to associate well with the notch of high reflectivities at the tip of the hook. With the downdraft accelerations within the RFD, the low-level mesocyclone strengthened through the baroclinic generation of low-level vorticity as the supercell cascade had commenced again. At approximately 2250 UTC, the F1 tornado occurred.

Two distinct circulations were embedded within the storm on the 2252 UTC 0.5^{o} elevation SRV image. The larger (~1.75 nm/3.5 km) parent circulation (Fig. 5–15, bottom image inset–dashed pale yellow circle) was the low-level mesocyclone that had indeed re-strengthened with rotational velocities of 50 knots (25.7 ms^{-1}) and rotational shear of 14.6 X 10^{-3} s^{-1}. This value of mesocyclone shear is now in the middle to upper range for the occurrence of a tornado to be possible (Fig 5–3). However, the smaller circulation (Fig. 5–15, bottom image inset–yellow arrow) had gate-to-gate velocities of 50 knots (25.7 ms^{-1}) across only approximately 0.5 nm (1 km). That yields a rotational shear of 51.4 X 10^{-3} s^{-1} that is similar in strength (although only one eighth the size) to strong and violent mesocyclones observed outside of California (Andra, 1997). This vortex is likely a TCS and the strength and size of this circulation is very similar to other TCSs observed elsewhere (Wurman et al., 1996; Straka et al., 1996, Rasmussen and Straka, 1996). The TCS evolved from small-scale

downdrafts in the RFD that descended to near the surface and developed into an area of intense and increasingly rotational convergence. In this region of strong vertical shear is where the tornado occurred. The author believes this feature and the small-scale circulation that was detected on the SRV data with the F0 tornado is the first documentation of a TCS in California.

The F1 tornado lasted approximately 10 minutes before starting to dissipate at around 2300 UTC. The next WSR-88D radar volume scan at 2258 UTC shows that the TCS (Fig. 5–16, bottom image inset–yellow arrow) weakened slightly but remained distinct on the up-shear flank of the larger mesocyclonic circulation (Fig. 5–15, bottom image inset–dashed pale yellow circle). Rotational velocity at 2258 UTC was 45 knots (23.2 ms^{-1}) and rotational shear 46.4 X $10^{-3}\ s^{-1}$ indicating a tornado was still likely with that vortex. The low-level mesocyclone had begun to weaken slightly too. Rotational shear decreased to 11.6 X $10^{-3}\ s^{-1}$ as rotational velocities decreased to 45 knots (23.2 ms^{-1}) indicating that low-level support for near ground circulations was already weakening. The updraft core (Fig. 5–16, top image inset– blue arrow2229) also began to weaken with maximum echoes decreasing further in coverage and intensity (68 dBZ to 66 dBZ), possibly due to the rapid rise in low-level rotation that often is related to the formation of a downward-directed dynamic pressure gradient induced by that rotation (Brooks et al., 1993). The storm now resembled a high-precipitation (HP) supercell on reflectivity imagery

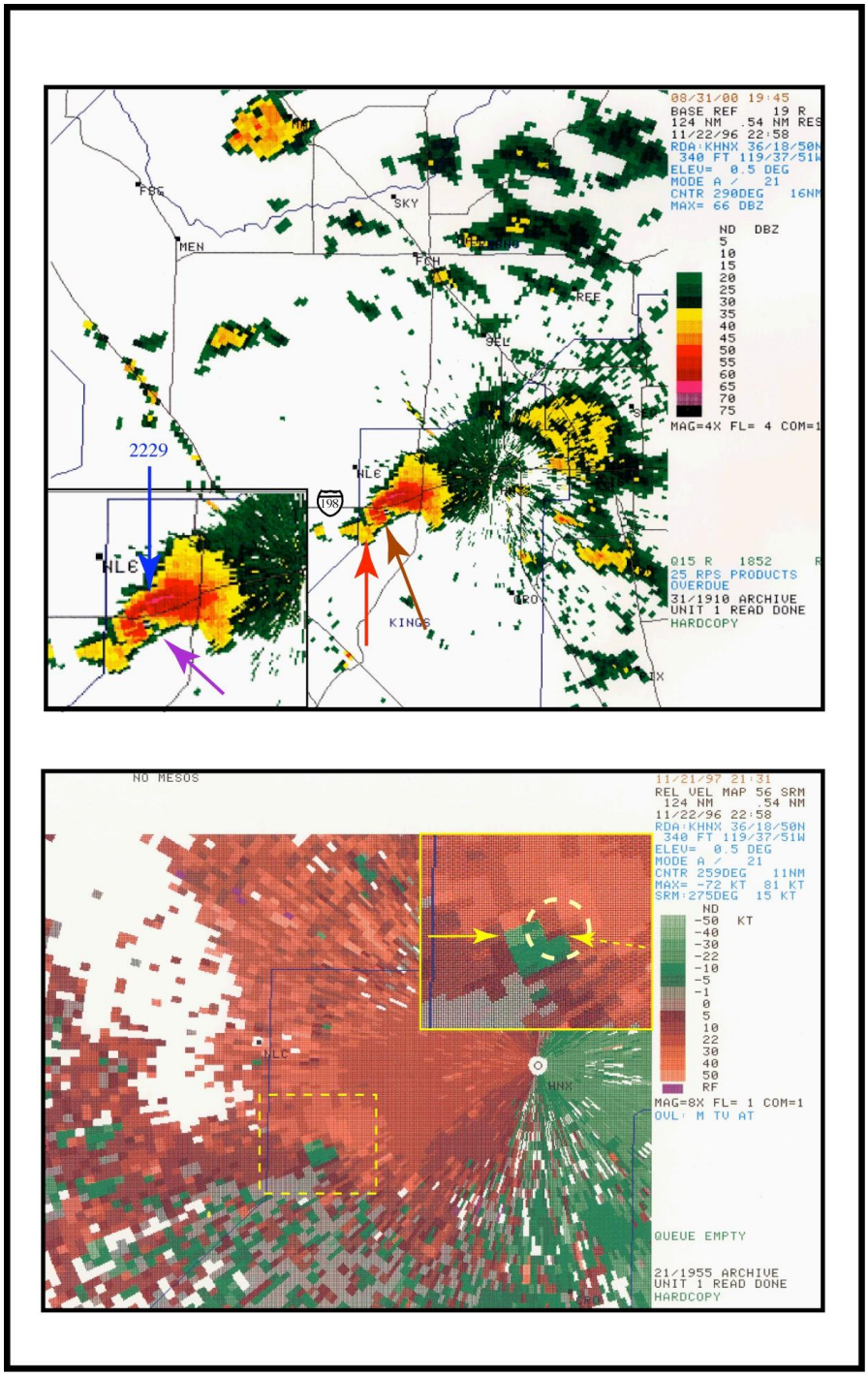

Fig. 5–16. Same as Fig. 5–1 except valid at 22:58 UTC 22 November 1996.

with strong returns across a wide swath of the hook echo (Fig. 5–16, top – brown arrow) adjacent to the intersection with another cell that approached the Lemoore storm from the right flank (Fig. 5–14, Fig. 5–15 and Fig. 5–16; top image – red arrow). The base reflectivity image and the 0.5° elevation SRV scan also indicated respectively, that the V-notch was associated with a BWER (Fig. 5–14, top image inset– purple arrow) and that the gust front had undercut the low-level inflow jet (Fig. 5–16, bottom image inset–dashed yellow arrow). This would cause the Lemoore supercell to weaken further suggesting the storm had reached maximum strength and was now about to dissipate.

5.5 Dissipation stage of the Lemoore Storm

The dissipation stage of the Lemoore storm began when the storm and associated tornado interacted with a neighboring cell. This cell developed quickly within the flanking line of cumulus adjacent to the storm at 2246 UTC (Fig. 5–14, top image, red arrow) showing strong reflectivities (45–50 dBZ) across a wide area by 2252 UTC (Fig. 5–15, top image, red arrow). The track of the cell was northeasterly in the mean tropospheric flow toward the hook echo region of the Lemoore Storm at 2258 UTC (Fig. 5–16, top image, red arrow). The tornado then ingested stable air from outflow of this cell and dissipated at 2300 UTC just after the storm crossed Hwy 198 (Fig. 5–16).

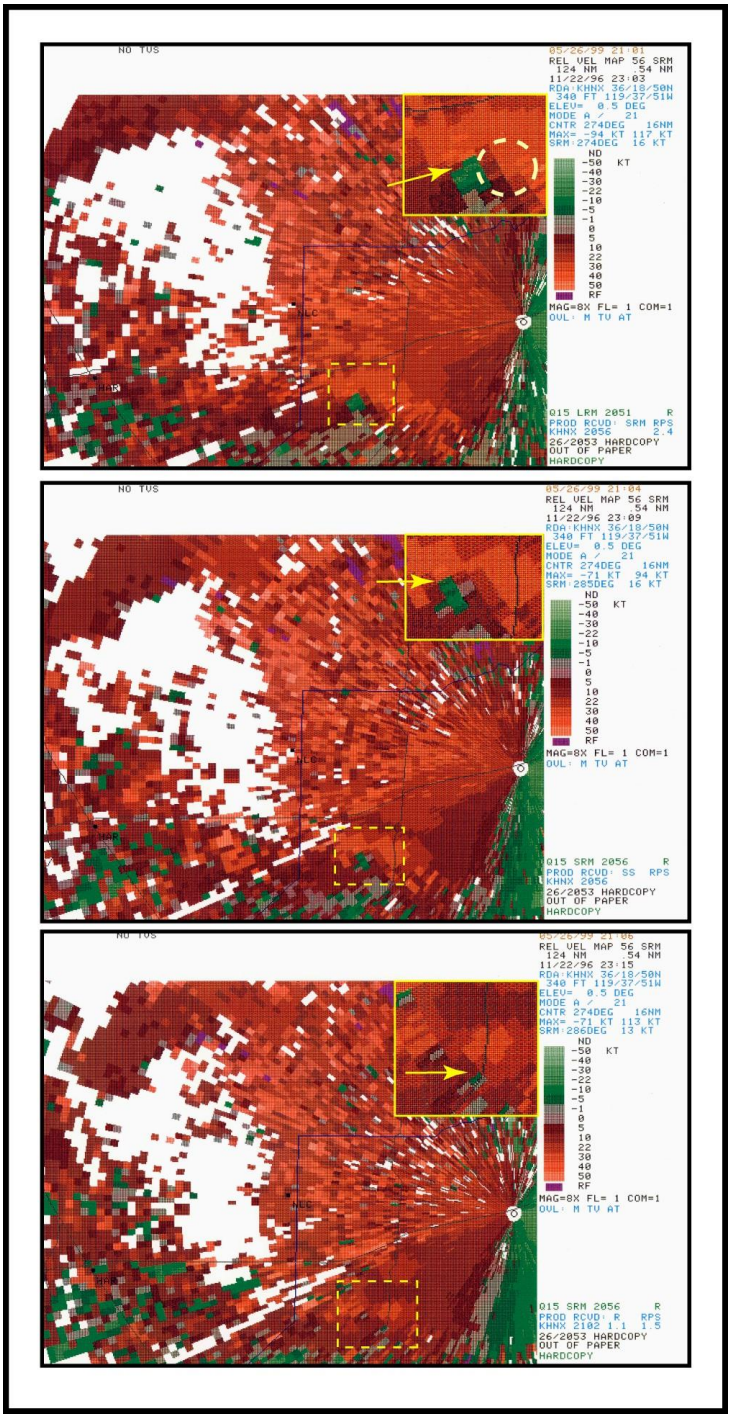

Fig. 5–17. The 0.5° KHNX WSR-88D storm-relative velocity images at 22:03 (top), 22:09 (middle), and 22:15 (bottom) UTC 22 November 1996.

SRV scans between 2303 and 2315 UTC showed that the TCS associated with the Lemoore Storm weakened and became more diffuse simultaneously with the tornado dissipation. Rotational velocity with the small scale vortex (Fig. 5–17, top image inset–yellow arrow) at 2303 UTC decreased to 30 knots (15.4 ms^{-1}), the diameter of the circulation increased by 0.5 nm (500 m) to 1.0 nm (2 km), and rotational shear fell to 15.4 X $10^{-3}\ s^{-1}$—indications that a tornado was now only possible (instead of likely) with this circulation (Fig. 5–3). The 0.5° elevation SRV scan shows that larger low-level mesocyclone was still evident (Fig. 5–17, top image inset–dashed pale yellow circle) but had weakened considerably as well since the gust front undercut the inflow jet. Rotational velocity decreased to 30 knots (15.4 ms^{-1}) over a wider area (~3 nm/6 km) resulting in only a minimal strength mesocyclone (5.1 X $10^{-3}\ s^{-1}$).

The TSC dissipated and was barely evident on the 2309 UTC 0.5° elevation SRV image (Fig. 5–17, middle image inset–yellow arrow) and was even more diffuse (1.5 nm/3 km). Rotational velocity was only 25 knots (12.9 ms^{-1}) and shear 8.6 X $10^{-3}\ s^{-1}$ indicating a minimal circulation (Fig. 5–3). At 2315 UTC, no circulations were evident on the 0.5° elevation SRV image (Fig. 5–17, bottom image inset–yellow arrow), the long-lived Lemoore supercell had dissipated.

6. Summary

The Lemoore Storm was a right-moving tornadic classic supercell that occurred on 22 November 1996. A mesocyclone-induced F0 and a subsequent F1 tornado were observed at the Lemoore Naval Air Station in the San Joaquin Valley of California that caused significant wind and hail damage. The Lemoore storm of November 1996 was a unique California event due to the close proximity of the storm to the WSR-88D radar at Hanford. Furthermore, because of the flat expanse of the San Joaquin Valley, the Doppler radar had an unobstructed view of the tornadic storm. These factors lead to an unprecedented quality of the low (0.5°) elevation radar scans for this storm. This study was the first to document a classic, right-moving supercell for which WSR-88D, high-resolution satellite and photographic evidence were available.

The severe storm developed ahead of a subsynoptic trough in a broad upward vertical motion field. Cyclonic isothermal vorticity advection (CIVA) contributed to the mid-tropospheric forcing for this quasi-geostrophic omega upward motion field associated with the post-frontal trough. Upper-tropospheric jet-streak-induced divergence also was associated with an augmented mid-tropospheric vertical motion field over the San Joaquin Valley. This occurred after the passage of a synoptic-scale cold front in a cold sector, low-buoyancy environment.

The Lemoore storm was the southernmost cell in a line of strong thunderstorms. The right-moving storm tracked into a region of locally higher SBCAPE and stronger deep-layer shear (due to the jet-streak) in the central San Joaquin Valley that led to explosive development of the storm during maximum heating hours. Just prior to tornadogenesis, the storm likely interacted with a local thermally generated solenoid field that likely contributed to enhanced low-level streamwise vorticity in the central San Joaquin Valley.

Values of convective and rotational parameters (i.e. BRN) associated with the Lemoore storm were within ranges observed with previous mesocyclone induced tornadic thunderstorms in California and elsewhere. Strong tropospheric flow normal to the Coast Range and Sierra Nevada caused the formation of mesoscale low pressure area in the northern Sacramento Valley and a surface lee-side trough that extended southward into the central San Joaquin Valley. The result was an increase in the strength of the low-level shear (0–1-km, 0–2-km) and deep-layer shear (0–6-km) in locales east of the trough axis. Not only was the shear within ranges of previous California tornadic thunderstorm case studies, but also within thresholds for weak tornadic storms observed outside of the state. Furthermore, the development of a low-level mesocyclone and tornado is suggested by the modified hodograph of the actual storm environment. The slight clockwise curved low-level hodograph in combination with storm movement

off the hodograph resulted in values of 0–1-km and 0–3-km SREH that concur with observations of mesocyclonic induced tornadoes outside of California.

Radar reflectivity and radial wind velocity signatures showed well-defined supercell structure was present during the nearly 1.5 hour lifespan of the Lemoore storm. The storm evolved on base-reflectivity images from a classic supercell with a 'kidney bean' type appearance, a hook echo, and a highly reflective (>68-dBZ) updraft core into a storm that resembled a high-precipitation (HP) supercell with strong returns across a wide swath of a more pronounced hook appendage and two highly reflective (68-dBZ) updraft cores during the F1 tornado event and just before dissipation. The (VIL) product showed that large hail was likely associated with these intense updrafts and especially with the updraft in the hook echo region where base-reflectivity scans detected returns of 71 dBZ. Furthermore, just before the formation of the first tornado, reflectivity cross-section scans indicated a BWER adjacent to a tilted updraft vault containing strong mid-level echo overhang.

SRV volume scans during the Lemoore storm's lifespan showed the presence of mid-level mesocyclone indicated by numerous detections of a deep circulation by the WSR-88D mesocyclone algorithm. SRV images at 0.5° elevation showed the development of a low-level mesocyclone that occurred simultaneously with the initiation of a RFD just prior the formation of the first tornado. Inbound radial velocity signatures associated well with the location of

the hook echo and continued to increase in speed due to downdraft accelerations within the RFD. The low-level mesocyclone then strengthened through the baroclinic generation of low-level vorticity and led to the occurrences of the tornado episodes. Two distinct circulations were evident on the SRV data embedded within the Lemoore storm during both tornado episodes. The larger (~1.75 nm/3.5 km), weaker (rotational shear 14.6 X $10^{-3}\ s^{-1}$) circulation was the low-level mesocyclone and the smaller (0.5 nm/1 km), intense (rotational shear 51.4 X $10^{-3}\ s^{-1}$) one was a TCS. The TCS evolved from small-scale downdrafts in the RFD that descended to near the surface and developed into an area of intense and increasingly rotational convergence. In this region of strong vertical shear is where the tornadoes occurred. The author believes this is the first documentation of a TCS in California.

7. Concluding remarks

This case study of the Lemoore storm included a detailed analysis of the synoptic, subsynoptic and dynamic controls in addition to a complete consideration of the buoyancy and shear information for the Lemoore storm environment. In addition, evolution of the satellite and radar structure of the Lemoore storm was deduced on the basis of analyses of high-resolution visible satellite imagery and KHNX WSR-88D radar information. From this information,

evidence of a subsynoptic focus in the San Joaquin Valley and of storm interaction with a solenoidal circulation/convergence zone was presented that would lead to expectations of the development of a severe storm. Due to the close proximity of the storm to the KHNX Doppler site, detailed reflectivity (i.e. BWER) and wind velocity (i.e. TCS) data of the Lemoore storm's structure yielded evidence that a tornado was also likely associated with the storm.

The controls on the Lemoore storm were also examined in the light of what is now known about the role of buoyancy and shear in the development of tornadic storms in general. Qualitative and quantitative aspects of the buoyancy and shear associated with the Lemoore storm were consistent with those observed in previous case studies of tornadic storms associated with low-topped supercells in California and elsewhere. The values of SBCAPE observed with this storm were higher than the values observed for other California severe storm events. Shear magnitudes were similar in extent for tornadic supercells observed both in California and elsewhere. The study also showed that the Lemoore storm generally fit the typical synoptic scale schematic pattern (SP) for Central Valley severe and tornadic storms in a low buoyancy, cold sector environment outlined by Monteverdi et. al. (2003). Finally, the development of this tornadic supercell underscored the significance of topographically induced low-level (0-1-km) and deep-layer (0–6-km) wind shear in contributing toward the

development of F1 and stronger mesocyclone-induced tornadoes in California's Central Valley and the usefulness of Doppler radar for identifying and analyzing such storms in California.

References

Andra, Jr., D. L., 1997: The origin and evolution of the WSR-88D mesocyclone recognition nomogram. *Preprints, 28th Conf. On Radar Meteorology*, Austin, TX, 364-365.

Atkins, N.T., and M.L. Weisman, 1998: The influence of Pre-existing boundaries on supercell evolution. *Preprints, 19th Conf. On Severe Local Storms*, Minneapolis, MN, 334-337.

Blier, W. and K. A. Batten, 1994: On the incidence of tornadoes in California *Wea. Forecasting* **9**, 301–315.

Bluestein, H. B. 1992: *Synoptic-Dynamic Meteorology in Middle Latitudes.* Vol. I. Oxford University Press, 431 pp.

_____, 1983: Surface meteorological observations in severe thunderstorms. Part II: Experiments with TOTO. *J. Atmos. Sci.,* **22,** 919-930.

Braun, S. A., and J. P. Monteverdi, 1991: An analysis of a mesocyclone-induced tornado occurrence in Northern California. *Wea. Forecasting*, **6**, 13–31.

Brooks, H. E., C. A. Doswell, and J. Cooper, 1994: On the environments of tornadic and nontornadic mesocyclones. *Wea. Forecasting*, **9**, 606-618.

_____, C. A. Doswell, and R. B. Wilhelmson, 1994: The role of mid-tropospheric winds in the evolution and maintenance of low-level mesocyclones. *Mon. Wea. Rev.,* **122,** 126-136.

Browning, K. A., 1986: Morphology and classification of middle-latitude thunderstorms. *Thunderstorm Morphology and Dynamics, Second Edition,* E. Kessler, Ed., University of Oklahoma Press, 133-153.

Bunkers M. J., B. A. Klimowski, J. W. Zeitler, R. L. Thompson, and M. L. Weisman 2000: Predicting supercell motion using a new hodograph technique. *Wea. Forecasting,* **15,** 61–79.

Burgess, D. W., R. J. Donaldson Jr, and P. R. Desrochers, 1993: Tornado detection/warning by radar. *The Tornado: Its Structure, Dynamics, Prediction and Hazards, Geophys. Monogr.*, Vol 79, Amer. Geophys. Union, 203-221.

Carbone, R. E., 1982: A severe frontal rainband. Part I: Stormwide hydrodynamic structure. *J. Atmos. Sci.,* **39,** 258–279.

_____, 1983: A severe frontal rainband. Part II: Tornado parent vortex circulation. *J. Atmos. Sci.,* **40,** 2639–2654.

Cooley, J., 1978: Cold Air Funnel clouds. *Mon. Wea. Rev.,* **106,** 1368–1372.

Crum, T.D., and R.L. Alberty, 1993: The WSR-88D and the WSR-88D Operational Support Facility. *Bull. Amer. Meteor. Soc.*, **74**, 1669-1687

Davies-Jones R. P., D. Burguess, and M. Foster, 1990: Test of helicity as a tornado forecast parameter. Preprints, *16th Conf. On Severe Local Storms,* Kananaskis Park, AB, Canada, Amer. Meteor. Soc., 588–592.

_____, and H. E. Brooks, 1993: Mesocyclogenesis from a theoretical perspective. *The Tornado: Its Structure, Dynamics, Prediction and Hazards, Geophys. Monogr.*, Vol 79, Amer. Geophys. Union, 105-114.

_____, 2000b: Can the hook echo instigate tornadogenesis barotropically? Preprints, *20th Conf. On Severe Local Storms*, Orlando, FL., Amer. Meteor. Soc., 269-272.

Davies, J. M., and R. H. Johns, 1993: Some wind and instability parameters associated with strong and violent tornadoes. Part I: Wind shear and helicity. *The Tornado: Its Structure, Dynamics,Prediction, and Hazards, Geophys. Monogr.*, Vol 79, Amer. Geophys. Union, 573–582.

Donaldson, R. J., Jr., 1990: Foundations of severe storm detection by radar. *Radar in Meteorology,* D. Atlas, Ed., Amer. Meteor. Soc., 115-121.

Doswell, C., 1987: The distinction between large-scale and mesoscale contribution to severe convection: A case study example. *Wea. Forecasting*, **2,** 17–31.

Doswell, C., D.V. Baker, and C.A. Liles 2002: Recognition of negative mesoscale factors for severe weather potential: A case study. *Wea. Forecasting*, **17,** 937-934.

Falk, K., and W. Parker, 1998: Rotational shear nomogram for tornadoes. *Preprints, 19th Conf. On Severe Local Storms*, Minneapolis, MN, 733-735.

Fujita, T. T., 1973: Proposed mechanism for tornado formation from rotating thunderstorms. Preprints, *8th Conf. on Severe Local Storms,* Denver, CO, Amer. Meteor. Soc., 191–196.

Garrett, R. A., and V. D. Rockney, 1962: Tornadoes in northeastern Kansas, May 19, 1960. *Mon. Wea Rev.*, **90,** 231-240.

Haglund, G. T., 1969: A study of the severe local storm of 16 April 1967. ESSA Tech. Memo. ERLTM-NSSL 44, 54 pp. [NTISPB188315]

Hales, J., 1985: Synoptic features associated with Los Angeles tornado occurrences. *Bull. Amer. Meteor. Soc.*, **66**, 657–662.

Holton, J. R., 1992: *An Introduction to Dynamic Meteorology*, 3rd editon. Academic Press, Inc, 511 pp.

Johns, R. H., and C. A. Doswell III, 1992: Severe local storms forecasting. *Wea. Forecasting,* **7,** 588–612.

_____, J. M. Davies, and P. W. Leftwich, 1993: Some wind and instability parameters associated with strong and violent tornadoes: 2. Variations in the combinations of wind and instability parameters. *The tornado: It's Structure, Dynamics, Prediction and Hazards, Geophys. Monogr.*, Vol. 79, Amer. Geophys. Union, 583–590.

Johnson, K. W., P. S. Ray, B. C. Johnson, and R. P. Davies-Jones, 1987: Observations related to the rotational dynamics of the 20 May 1977 tornadic storms. *Mon. Wea Rev.*, **115,** 2463–2478.

Klemp, J. B., and R. Rotunno, 1993: A study of the tornadic region within a supercell thunderstorm. *J. Appl. Sci.*, **40,** 359-377.

Krudzlo, R., 1998: The Lemoore Naval Air Station Classic Supercell Tornado of 22 November 1996. Western Region Tech. Attachment 98-07, 2 pp. [Available online at http://www.wrh.noaa.gov/wrhq/98TAs/9807/index.html]

Lipari, G. S. and J. P. Monteverdi, 2000: Convective and shear parameters associated with Northern and Central California tornadoes during the period 1990-1994. Preprints, *20th Conf. on Severe Local Storms,* Orlando, FL, Amer. Meteor. Soc., 518–521.

Lemon, L. R., and C. A. Doswell III, 1979, Severe thunderstorm evolution and mesocyclone structure as related to tornadogenesis. *Mon. Wea Rev.*, **107,** 1184–1197.

Maddox, R. A., L.R. Hoxit, and C.F. Chappell, 1980: A Study of tornadic thunderstorm interactions and thermal boundaries. *Mon. Wea Rev.,* **108,** 322-336.

Markowski, P. M., E. N. Rasmussen, and J. M. Straka, 1998: The occurrence of tornadoes in supercells interacting with boundaries during VORTEX-95. *Wea. Forecasting*, **13**, 852-859.

_____, and J. M. Straka, 2000: Some observations of rotating updrafts in a low-buoyancy, highly sheared environment. *Mon. Wea Rev.,* **128,** 449–461.

_____, 2002: Hook echoes and rear-flank downdrafts: A review. *Mon. Wea. Rev.*, **130**, 852-876.

_____, J. M. Straka, and E. N. Rasmussen, 2002: Direct surface thermodynamic observations within the rear-flank downdrafts of nontornadic and tornadic supercells. *Mon. Wea. Rev.*, **130**, 1692-1721.

McCaul, E. W., Jr., 1990: Simulations of convective storms in hurricane environments. Preprints, *16th Conf. on Severe Local Storms,* Kananaskis Park, AB, Canada, Amer. Meteor. Soc., 334–339.

_____, 1991: Buoyancy and shear characteristics of hurricane-tornado environments. *Mon. Wea Rev.*, **119,** 1954–1978.

Miller, R. C. 1972: Notes on the Analysis and Severe Storm Forecasting Procedures of the Air Force Global Forecast Center, Air Weather Service Technical Report 200 (Rev.), Air Force Service, Scott Air Force Base, IL, 190 pp.

Mitchell, E. D., and G. J. Stumpf, 1996: The 19 April 1995 Fort Worth/Dallas Tornado Event: Implications for Automated Vortex Recognition. *Preprints, 18th Conf. On Severe Local Storms*, San Francisco, CA, 574-576.

Moller, A. R. , C. A. Doswell, M. P. Foster, and G. R. Woodall, 1994: The operational recognition of supercell thunderstorm environments and storm structures. *Wea. Forecasting,* **9,** 327–347.

Monteverdi, J. P., S. A. Braun, and T.C. Trimble, 1988: Funnel Clouds in the San Joaquin Valley, California. *Mon. Wea. Rev. ,* **116,** 782–789.

_____, and J. Quadros, 1994: Convective and rotational parameters associated with three tornado episodes in Northern and Central California. *Wea. Forecasting*, **9,** 285–300.

_____, and S. Johnson, 1996: A supercell thunderstorm with hook echo in the San Joaquin Valley, California. *Wea. Forecasting,* **11,** 246–261.

_____, W. Blier, G. Stumpf, W. Pi, and K. Anderson, 2001: First WSR-88D documentation of an anticyclonic supercell with anticyclonic tornadoes: The Sunnyvale/Los Altos, California tornadoes of 4 May 1998, *Mon. Wea. Rev.*, **129,** 2805-2814.

_____, C. Doswell III, and G.S. Lipari, 2003: Shear parameter thresholds for forecasting tornadic thunderstorms in Northern and Central California. *Wea. Forecasting,* **18,** 357-370.

Parish, T. R., 1982: Barrier winds along the Sierra Nevada Mountains. *J. Appl. Meteor.*, **21,** 925–930.

Purdom, L. F., 1993: Satellite Observations of Tornadic Storms. *The Tornado: Its Structure, Dynamics,Prediction, and Hazards, Geophys. Monogr.*, Vol 79, Amer. Geophys. Union, 265–274.

Rasmussen, E. N., and D. O. Blanchard, 1998: A baseline climatology of sounding-derived supercell and tornado forecast parameters. *Wea. Forecasting,* **13,** 1148–1164.

_____, and J. M. Straka, 1996: Mobile Mesonet Observations of Tornadoes during VORTEX***.*** *Preprints, 18th Conf. On Severe Local Storms*, San Francisco, CA, 1-5.

_____, and J. M. Straka, 2000: Variations in Supercell Morphology. Part 1: Observations of the role of upper-level storm-relative flow. *Mon. Wea. Rev.,* **126,** 2406–2421.

Reed R., and W. Blier, 1986: A case study of comma cloud development the eastern Pacific. *Mon.Wea. Rev.*, **114,** 1681–1695.

Rotunno, R., and J. Klemp, 1982: The influence of the shear-induced vertical pressure gradient on thunderstorm motion. *Mon. Wea. Rev.,* **110,** 136–151.

_____, R., and J. Klemp, 1985: On the rotation and propagation of simulated supercell thunderstorms. *J. Atmos. Sci.* , **42,** 271–292.

_____, 1986: Tornadoes and tornadogenesis. *Mesoscale meteorology and Forecasting*, P. S. Ray Ed., 414-436

Smith, T.B., andV.A. Mirabella, 1972: Characteristics of California tornadoes. Report to the University of California Lawrence Livermore Laboratory by Meteorological Research Inc., 25 pp.

Staudenmaier, M. Jr., 1995: The 10 February 1994 Oroville Tornado A Case Study. NOAA Technical Memorandum. NWS WR-229.

Staudenmaier, M., and S. Cunningham, 1995: The Walnut Grove Tornado of 23 March 1995: An example of a Mini-Supercell. Western Region Tech. Attachment 95-28.

Straka, J. M., Wurman, J., and E. N. Rasmussen, 1996: Observations of the low-levels of tornadic storms using a portable X-band Doppler Radar. *Preprints, 18th Conf. On Severe Local Storms*, San Francisco, CA, 11-16.

Trenberth, K. E., 1978: On the interpretation of the diagnostic quasi-geostrophic omega Equation. *Mon. Wea. Rev.* **106,** 131-37.

U.S.D.C., 1996: Storm Data-California, Vol. 38, No 11. National Climatic Data Center, Asheville, NC 28801.

Weaver, R. L., 1962: Meteorology of hydrologically critical storms in California. Hydrologic Rep. No. 37, U.S.Weather Bureau, Hydrologic Services Division, Washington, DC, 207 pp.

Weisman, M. L., and J. B. Klemp, 1982: The dependence of numerically simulated convective storms on vertical wind shear and buoyancy. *Mon. Wea. Rev.,* **110,** 504–520.

_____, and J. B. Klemp, 1984: The structure and classification of numerically Simulated convective storms in directionally varying wind shears.*Mon. Wea. Rev.*, **112,** 2479–2498.

Appendix 1: Fujita Scale of tornado damage intensity (from Storm Data)

Class	% of All Tornadoes	Fujita Category	Wind Speed	Damage
Weak	69 %	F0	35–62 knots 40–72 mph	Light; small trees uprooted
		F1	63–97 knots 73–112 mph	Mod. trailer home damage
Strong	29%	F2	98–136 knots 113–157 mph	Considerable; roofs torn off houses
		F3	137–179 knots 158–206 mph	Severe: Cars lifted into air
Violent	2%	F4	180–226 knots 207–260 mph	Devastating; houses leveled
		F5	227–276 knots 261–318 mph	Incredible: total damage